

For Reference

NOT TO BE TAKEN FROM THIS ROOM

Ex LIBRIS
UNIVERSITATIS
ALBERTAENSIS





Digitized by the Internet Archive
in 2020 with funding from
University of Alberta Libraries

https://archive.org/details/Cross1979_0

THE UNIVERSITY OF ALBERTA

RELEASE FORM

NAME OF AUTHOR Robert Kenneth Cross

TITLE OF THESIS Application of Satellite Infra-Red Data In

..... The Derivation of Sea-Surface Temperatures

..... In the Canadian Arctic

DEGREE FOR WHICH THESIS WAS PRESENTED Master of Science

YEAR THIS DEGREE GRANTED 1979

Permission is hereby granted to THE UNIVERSITY OF
ALBERTA LIBRARY to reproduce single copies of this
thesis and to lend or sell such copies for private,
scholarly or scientific research purposes only.

The author reserves other publication rights, and
neither the thesis nor extensive extracts from it may
be printed or otherwise reproduced without the author's
written permission.

THE UNIVERSITY OF ALBERTA

APPLICATION OF SATELLITE INFRA-RED DATA IN
THE DERIVATION OF SEA-SURFACE TEMPERATURES
IN THE CANADIAN ARCTIC

by



ROBERT KENNETH CROSS

A THESIS

SUBMITTED TO THE FACULTY OF GRADUATE STUDIES AND RESEARCH
IN PARTIAL FULFILMENT OF THE REQUIREMENTS FOR THE DEGREE
OF MASTER OF SCIENCE

IN

METEOROLOGY

DEPARTMENT OF GEOGRAPHY

EDMONTON, ALBERTA

FALL, 1979

72F-42

THE UNIVERSITY OF ALBERTA
FACULTY OF GRADUATE STUDIES AND RESEARCH

The undersigned certify that they have read, and recommend to the Faculty of Graduate Studies and Research, for acceptance, a thesis entitled "Application of Satellite Infra-Red Data in the Derivation of Sea-Surface Temperatures in the Canadian Arctic", submitted by Robert Kenneth Cross in partial fulfilment of the requirements for the degree of Master of Science in Meteorology.

ABSTRACT

Digitized infra-red scanning radiometer data from the NOAA-5 satellite were used to deduce sea and ice temperatures and horizontal temperature gradients in the Western Canadian Arctic during July and August, 1977. The area studied comprises much of the Beaufort Sea, the contiguous Arctic coastal regions and Banks Island. The digitized images are converted into two-dimensional arrays of histograms of the distributions of relative infra-red radiances received from a corresponding array of surface elements. Based on the assumption that the entries in each histogram are normally distributed about an appropriate mean value, the surface temperatures are derived.

The investigation was carried out in three stages:

(1) The effect on the resolution of the histogram analysis technique through changes in geodetic grid (array) size was considered first. The optimum grid area size required to produce surface temperature distributions accurate to 1°C is approximately one-half degree square. The averaging of consecutive digital elements does not appreciably change the analysis in regions where data are of high resolution.

(2) The above results were then applied to single orbit studies of surface temperatures and their horizontal gradients. Temperatures over multi-year pack ice are generally below 0°C and quite uniform, while over first-year pack ice the regime is some 1° to 2°C warmer and somewhat more variable. Over multi-year ice, temperature gradients of 1.0 - $1.5^{\circ}\text{C}/^{\circ}$ latitude are found to separate ice concentrations of greater and less than $6/10$; the locus of maximum gradient is found to separate

open water from ice concentrations greater than 1/10. Over first-year ice correlations are much less reliable. Layers of cloud, islands and coastlines frequently complicate the analysis.

(3) Finally, composite histograms were used to filter out cloudiness. In practice a three-day compositing period has been found to be effective in reducing errors due to the presence of cloud. Processing the coldest appropriate mode in the distributions is an effective means of minimizing land-form "contamination". Approximately one-half of all arrays affected by coastlines are recovered using the above modal processing method.

The effects of atmospheric attenuation on the temperatures derived from the IR imagery are also considered; the computed temperatures are found, in the mean, to be less than one degree lower than those measured by conventional means.

The case studies revealed a complex surface temperature regime in the Beaufort Sea. Ice movement, surface currents and upwelling episodes are identifiable, as are the effects of strong insolation on ice melt and surface warming.

ACKNOWLEDGEMENTS

I wish to express my gratitude to my departmental supervisor, Dr. E.R. Reinelt, for having suggested the topic on which this study was based, and for contributing his time and unique editorial skill in the preparation of the final draft. His enthusiasm was a constant source of inspiration. In addition, I would like to thank Dr. K.D. Hage and Dr. W. Adams for their willingness to serve on the examining committee.

Sincere thanks are due Mr. Peter Hof and his staff at the University of Alberta Satellite Laboratory. The assistance of Mr. D. Oracheski, especially his useful advice and work on satellite image reproduction, is gratefully appreciated, as is the computer programming of Mr. B. Greaves.

I wish to express my thanks to the staff of the Cartography Section, Department of Geography, for their advice and assistance in the drafting and reduction of the figures and photographs.

The cooperation of the staff of the Arctic Weather Center, Edmonton, is appreciated.

This study was conducted while on leave from the Atmospheric Environment Service, Environment Canada.

TABLE OF CONTENTS

	PAGE
ABSTRACT	iv
ACKNOWLEDGEMENTS	vi
TABLE OF CONTENTS	vii
LIST OF TABLES	x
LIST OF FIGURES	xi
CHAPTER	
I Satellite Meteorology and Its Usefulness in the Study of the Arctic	1
1.1 Introduction	1
1.2 Physical Rationale	2
1.3 Utility of Satellites in the Arctic	5
II A Model for Computing Surface Temperatures in the Arctic	12
2.1 Introduction	12
2.2 The Data	12
2.2.1 Internal Calibration	13
2.2.2 External Calibration	14
2.2.3 Mapping	15
2.2.4 Analysis of Histograms	17
2.3 The Experiments	18
III Refining the Surface Temperature Model	19
3.1 Introduction	19
3.2 Grid Size Optimization	19
3.3 Averaging of Digital Values	25
3.4 External Calibration	30
3.5 Temperature Gradients	31

CHAPTER		PAGE
IV	Sea-Surface Temperatures and Their Horizontal Gradients	34
4.1	Introduction	34
4.2	Case Study 1, July 27, 1977	35
4.2.1	Synoptic Situation	35
4.2.2	Verification	35
4.3	Case Study 2, July 28, 1977	39
4.3.1	Synoptic Situation	39
4.3.2	Verification	39
4.4	Case Study 3, August 14, 1977	43
4.4.1	Synoptic Situation	43
4.4.2	Verification	43
4.5	Discussion	46
4.5.1	Surface Temperatures	46
4.5.2	Temperature Gradients	46
V	On the Use of Composite Histograms in Deriving Sea-Surface Temperatures	48
5.1	Introduction	48
5.2	Formation of a Composite Temperature Analysis	49
5.3	Case 1, July 05-08, 1977	50
5.3.1	Synoptic Situation	50
5.3.2	Building the Composite Chart	50
5.3.3	Verification	55
5.3.4	Statistical Summary	59
5.4	Case 2, July 27-31, 1977	61
5.4.1	Synoptic Situation	61
5.4.2	Verification	61
5.4.3	Statistical Summary	70
5.5	Case 3, August 13-16, 1977	72
5.5.1	Synoptic Situation	72
5.5.2	Verification	72
5.5.3	Statistical Summary	83
5.6	Information in the Composite Analyses ...	85
5.7	Compositing - Statistical Summary	85
5.8	External Calibration	89

CHAPTER		PAGE
VI	Summary of Results	91
	6.1 Introduction	91
	6.1.1 Optimum Grid Size	91
	6.1.2 Daton Averaging	92
	6.1.3 Ice Conditions	92
	6.1.4 External Calibration	92
	6.1.5 Cloud Filtering	93
	6.1.6 Resolution Near Coastlines	93
	6.2 A Study of the Beaufort Sea	94
	6.3 Suggestions for Future Studies	95
REFERENCES	96
APPENDIX		
A	Histogram Compilation Routine	99
B	Internal Calibration of the Radiometer	113
C	External Calibration of Data	116
D	Sample Output for Histogram Analysis Program .	119
E	Ice Nomenclature	121
F	Ice Information Overlays	124

LIST OF TABLES

TABLE		PAGE
3.1	Statistical summary of histograms shown in Figures 3.5a, 3.5b.	27
3.2	Ground-truth information versus satellite-derived temperatures, August 14, 1977.	30
4.1	Ground-truth information versus satellite-derived temperatures, July 27, 1977.	38
4.2	Ground-truth information versus satellite-derived temperatures, July 28, 1977.	41
5.1	Statistical summary of compositing, Case 1, July 5-8, 1977.	60
5.2	Compositing over land- or water- covered areas, Case 1.	61
5.3	Ground-truth information versus satellite-derived temperatures, Case 2, July 27-31, 1977.	70
5.4	Statistical summary of compositing, Case 2, July 27-31, 1977.	71
5.5	Compositing over land- or water- covered areas, Case 2.	71
5.6	Ground-truth information versus satellite-derived temperatures, Case 3, August 13-16, 1977.	82
5.7	Statistical summary of compositing, Case 3, August 13-16, 1977.	84
5.8	Compositing over land- or water- covered areas, Case 3.	83
5.9	Statistical summary of all compositing cases.	87
A.1	Histogram compilation program.	100
A.2	Sample list of parameters for HIST.	111
A.3	Sample output for HIST, Orbit 4718.	112
B.1	Sample calibration points for NOAA-5, Orbit 9433.	114
D.1	Square-by-square temperature retrievals, low resolution grid, Orbit 4222, July 5, 1977.	120

LIST OF FIGURES

FIGURE		PAGE
1.1	Atmospheric Environment Service radiation measuring sites for Northern Canada.	3
1.2	Visible image, obtained by NOAA-5 satellite, August 14, 1977, Orbit 4718.	6
1.3	Infra-red (IR) image, obtained by NOAA-5, August 14, 1977, Orbit 4718.	7
1.4	Ten-day composite minimum brightness (CMB) chart derived from ESSA-9 digitized brightness data for the period 24 May - 2 June 1970.	9
3.1	Map of study areas.	20
3.2a	Isotherm analysis: July 5, 1977, Orbit 4222. Low resolution grid.	22
3.2b	Isotherm analysis: July 5, 1977, Orbit 4222. High resolution grid.	22
3.3	IR image, July 5, 1977, Orbit 4222.	23
3.4	Relative frequency versus temperature, showing effect of change of bin size.	24
3.5	Relative frequency versus temperature. (a) High gradient bin (b) Low gradient bin	26
3.6a	Isotherm analysis: August 14, 1977, Orbit 4718. All datons used.	28
3.6b	Isotherm analysis: August 14, 1977, Orbit 4718. Averaging of two datons.	28
3.6c	Isotherm analysis: August 14, 1977, Orbit 4718. Averaging of three datons.	29
3.7	Representation of grid for temperature gradient calculation.	32
4.1a	Isotherm analysis: July 27, 1977, Orbit 4495.	36
4.1b	Temperature gradient analysis: July 27, 1977, Orbit 4495.	36

FIGURE		PAGE
4.2a	Visible image, July 27, 1977, Orbit 4495.	37
4.2b	IR image, July 27, 1977, Orbit 4495.	37
4.3a	Isotherm analysis: July 28, 1977, Orbit 4507.	40
4.3b	Temperature gradient analysis: July 28, 1977, Orbit 4507.	40
4.4a	Visible image, July 28, 1977, Orbit 4508.	42
4.4b	IR image, July 28, 1977, Orbit 4507.	42
4.5a	Isotherm analysis: August 14, 1977, Orbit 4718.	44
4.5b	Temperature gradient analysis: August 14, 1977, Orbit 4718.	44
5.1	BAB surface map: July 5, 1977, 1800 GMT.	51
5.2	BAB surface map: July 6, 1977, 1800 GMT.	51
5.3	BAB surface map: July 7, 1977, 1800 GMT.	52
5.4	BAB surface map: July 8, 1977, 1800 GMT.	52
5.5	Isotherm analysis: July 5, 1977, Orbit 4222.	53
5.6	Composite isotherm analysis: July 5-6, 1977, Orbits 4222 and 4235.	53
5.7	Composite isotherm analysis: July 5-7, 1977, Orbits 4222, 4235 and 4247.	54
5.8	Composite isotherm analysis: July 5-8, 1977, Orbits 4222, 4235, 4247 and 4259.	54
5.9	Composite isotherm analysis: July 6-8, 1977, Orbits 4235, 4247 and 4259.	56
5.10a	Visible image, July 6, 1977, Orbit 4235.	57
5.10b	IR image, July 6, 1977, Orbit 4235.	57
5.11	IR image, July 7, 1977, Orbit 4247.	58
5.12	BAB surface map: July 27, 1977, 1800 GMT.	62
5.13	BAB surface map: July 28, 1977, 1800 GMT.	62

FIGURE		PAGE
5.14	BAB surface map: July 29, 1977, 1800 GMT.	63
5.15	BAB surface map: July 30, 1977, 1800 GMT.	63
5.16	BAB surface map: July 31, 1977, 1800 GMT.	64
5.17	Composite isotherm analysis: July 27-29, 1977, Orbits 4495, 4507 and 4519.	64
5.18	Composite isotherm analysis: July 28-30, 1977, Orbits 4507, 4519 and 4532.	65
5.19	Composite isotherm analysis: July 29-31, 1977, Orbits 4519, 4532 and 4544.	65
5.20a	Visible image, July 29, 1977, Orbit 4520.	67
5.20b	IR image, July 29, 1977, Orbit 4520.	67
5.21a	IR image, July 30, 1977, Orbit 4532.	68
5.21b	Visible image, July 30, 1977, Orbit 4533.	68
5.22	BAB surface map: August 13, 1977, 1800 GMT.	73
5.23	BAB surface map: August 14, 1977, 1800 GMT.	73
5.24	BAB surface map: August 15, 1977, 1800 GMT.	74
5.25	BAB surface map: August 16, 1977, 1800 GMT.	74
5.26	Composite isotherm analysis: August 13-15, 1977, Orbits 4705, 4717 and 4730.	75
5.27	Composite isotherm analysis: August 13-15, 1977, Orbits 4706, 4718 and 4731.	75
5.28	Composite isotherm analysis: August 14-16, 1977, Orbits 4717, 4730 and 4742.	76
5.29	Composite isotherm analysis: August 14-16, 1977, Orbits 4718, 4731 and 4743.	76
5.30a	IR image, August 13, 1977, Orbit 4705.	78
5.30b	Visible image, August 13, 1977, Orbit 4706.	78
5.31	IR image, August 14, 1977, Orbit 4717.	79

FIGURE		PAGE
5.32a	Visible image, August 15, 1977, Orbit 4731.	81
5.32b	IR image, August 15, 1977, Orbit 4731.	81
5.33	Surface water currents in the Arctic as summarized by Collin (1963).	86
5.34	Compositing summary, all cases (a) Mean recovery versus compositing period. (b) Mean of mean standard deviation versus compositing period.	88
5.35	Ground-truth versus satellite-derived temperature, all cases.	90
B.1	IR response curve for scanning radiometer.	113
C.1	Depiction of data zenith angle calculation.	117
F.1	Overlay 1: Mean ice conditions for week ending July 29, 1977.	124
F.2	Overlay 2: Mean ice conditions for week ending August 12, 1977.	125
F.3	Overlay 3: Mean ice conditions for week ending July 8, 1977.	126

CHAPTER I
SATELLITE METEOROLOGY AND ITS USEFULNESS
IN THE STUDY OF THE ARCTIC

1.1 Introduction

In recent years an increased interest has been expressed in the Arctic, by commercial and environmental interests alike. To enhance man's understanding of the polar regions it is essential to obtain accurate knowledge of spatial and temporal distributions of meteorological and oceanographic parameters. Despite the importance of obtaining such information, the remoteness of the Arctic and Antarctic regions has until recent times hampered most research efforts. In the following are set forth the exigencies for determining the sea-surface temperature and sea-ice distributions of the Arctic, and how the current generation of polar-orbiting meteorological satellites serves as a practical means of acquiring this information.

1.2 Physical Rationale

Accurate determination of the surface temperature field over the Arctic promises to benefit various meteorological concerns. The oceans act as major heat sources and sinks for the atmosphere, through heat and moisture transfer. The seas bordering ice-infested seas in

polar regions are important heat exchange and cyclogenetic areas. Sea temperature and its horizontal gradient are often indicators of, or are associated with, upwelling zones, ocean current dynamics and marine life.

The effect of the sea-ice cover in polar regions on weather and climate on both global and local scales should be more intensively investigated as recent technological advances make such research effective. The surface albedo, (i.e., the fraction of solar radiation reflected back to space) is probably the single most important regional factor affecting the heat and mass budgets of the Arctic Basin in summer (Maykut and Untersteiner, 1971). This parameter is almost totally a function of the presence or absence of sea ice and its type and concentration. Ice is the major factor that controls the exchange of heat and momentum between atmosphere and ocean during the polar winter. One should systematically observe the location and extent of pack ice and related features in order to monitor the seasonal patterns of surface heat exchange over the polar oceans.

With reference to the radiation budget of the Arctic Basin, there are problems inherent to this region that merit consideration. In terms of radiation components of the heat balance, equation 1.1, measurements have been made since the early 1960's at the meteorological stations shown in Figure 1.1.

$$R = I(1 - A) + L_{IN} - L_{OUT} \quad (1.1)$$

where R = net radiation
 I = incoming solar radiation (direct and diffuse)
 A = albedo
 L_{IN} = incoming long-wave radiation
 L_{OUT} = outgoing long-wave radiation

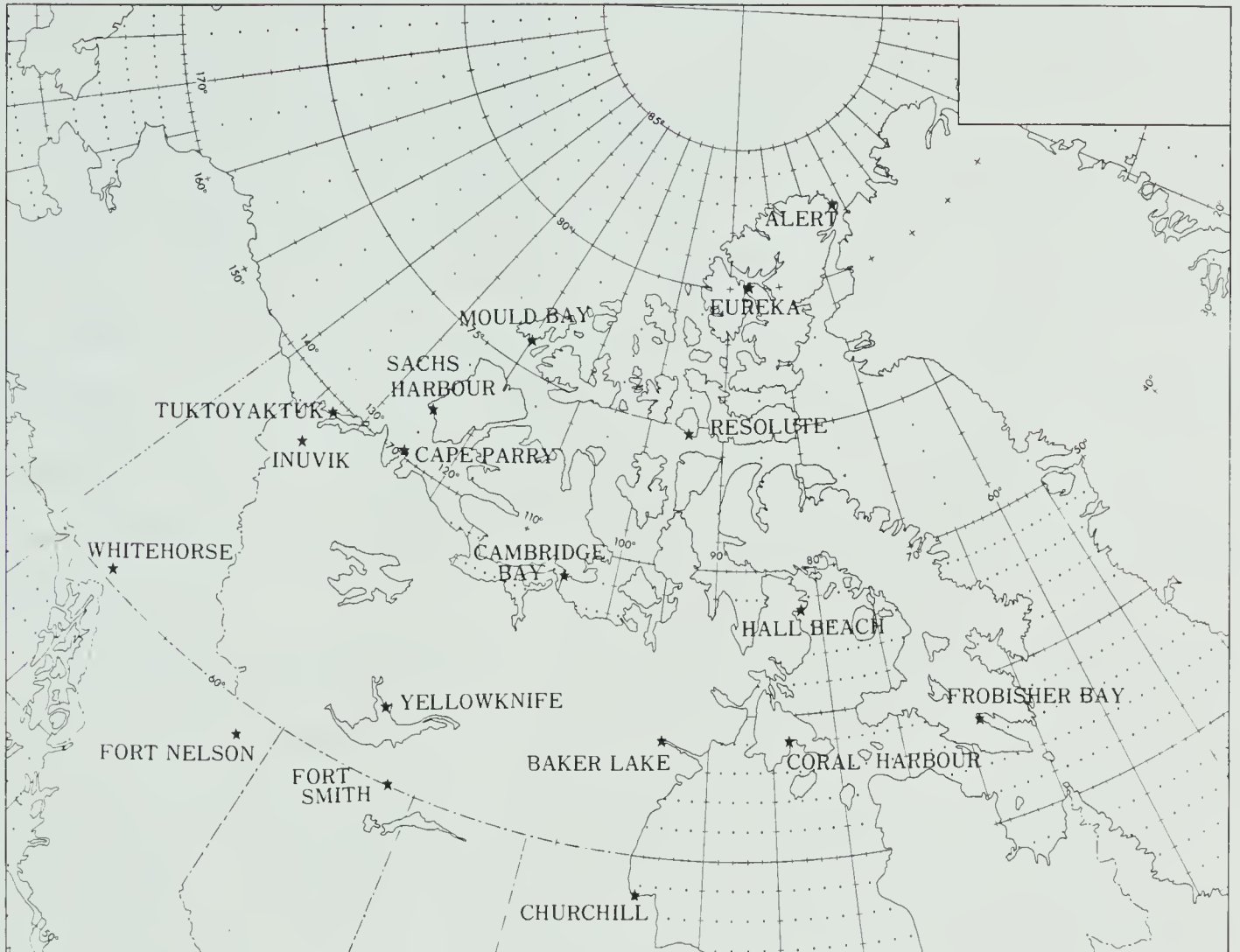


FIGURE 1.1: Atmospheric Environment Service radiation measuring sites for Northern Canada.

Both direct and diffuse radiation are measured at these locations. In winter, large areas are snowcovered; the little radiation received is reflected rather than absorbed. In summer, when snow and ice melt only in certain regions and at different rates, albedos measured at these stations may not be representative of a large area. The net radiation is thus affected in an unpredictable manner.

Infra-red (IR), or long-wave radiation fluxes are not routinely measured. Upward IR radiation can be estimated from surface temperatures and other surface characteristics such as mean ice distributions; downward IR radiation may be computed from conventionally-collected upper atmospheric temperature and humidity measurements. Few estimates have been published related to fields of radiation fluxes over Northern Canada (Walker, 1977).

In terms of heat exchange in the Arctic, the evaporation from snow, water and ice surfaces is an essential consideration. Estimates of evaporation in high latitudes are probably unreliable (Vowinckel and Orvig, 1976). The small-scale variability, caused by differences in types of terrain or the presence of sea or ice, is always present in heat budget calculations. An accurate estimate of evaporation requires reliable values for surface winds and air and sea-surface temperatures.

The estimate of net radiation and its variation with latitude is crucial in determining the magnitude of the associated driving force for large-scale atmospheric and oceanographic circulations. Early studies have generally been faced with the difficulty of computing radiation transfer in a cloudy atmosphere, and the lack of adequate observations of temperature, moisture and cloudiness. In these respects the polar-orbiting satellite is particularly useful over

areas of the world where conventional meteorological observations are very sparse or non-existent.

1.3 Utility of Satellites in the Arctic

Since the launching of the first meteorological satellite two decades ago, many researchers have undertaken the tasks discussed above, and much progress has been achieved. The many techniques that have evolved in the applications of satellite information to meteorological problems may be categorized rather broadly as being either qualitative or quantitative in nature. A brief overview of some of these techniques, in particular those related to Arctic studies, is presented below.

Much of the early work in satellite meteorology involved the development of photo-interpretive techniques, whereby a qualitative assessment of the satellite picture, or image, is made. Examples of the familiar "grey-shade" satellite images are shown in Figures 1.2 and 1.3.

The interpretation of cloud types and formations is well summarized in a World Meteorological Organization Technical Publication, No. 124 (Anderson, 1973). The successful application of such techniques is only achieved by skilled analysts who are familiar with the geography and meteorology of the particular area of interest. A major problem in the usage of either the visible or IR imagery for Arctic studies is the proper differentiation between clouds and snow or sea-ice, whose reflectances and temperatures may often be comparable. Characteristic differences in form, tone and texture, and, in particular, persistence of movement (of clouds) are the major interpretive tools. In addition,

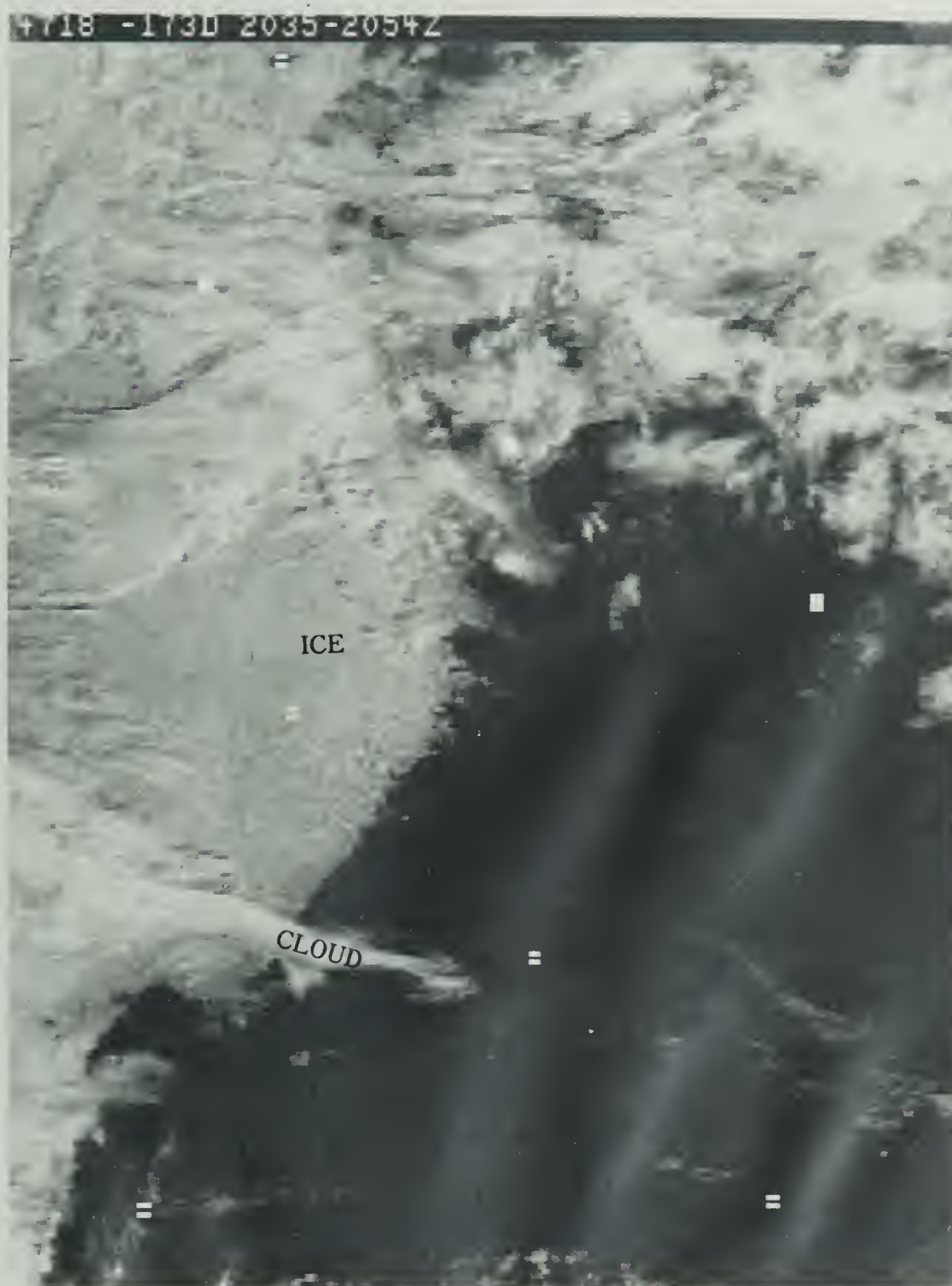


FIGURE 1.2 Visible image, obtained by NOAA-5 satellite, August 14, 1977, Orbit 4718.

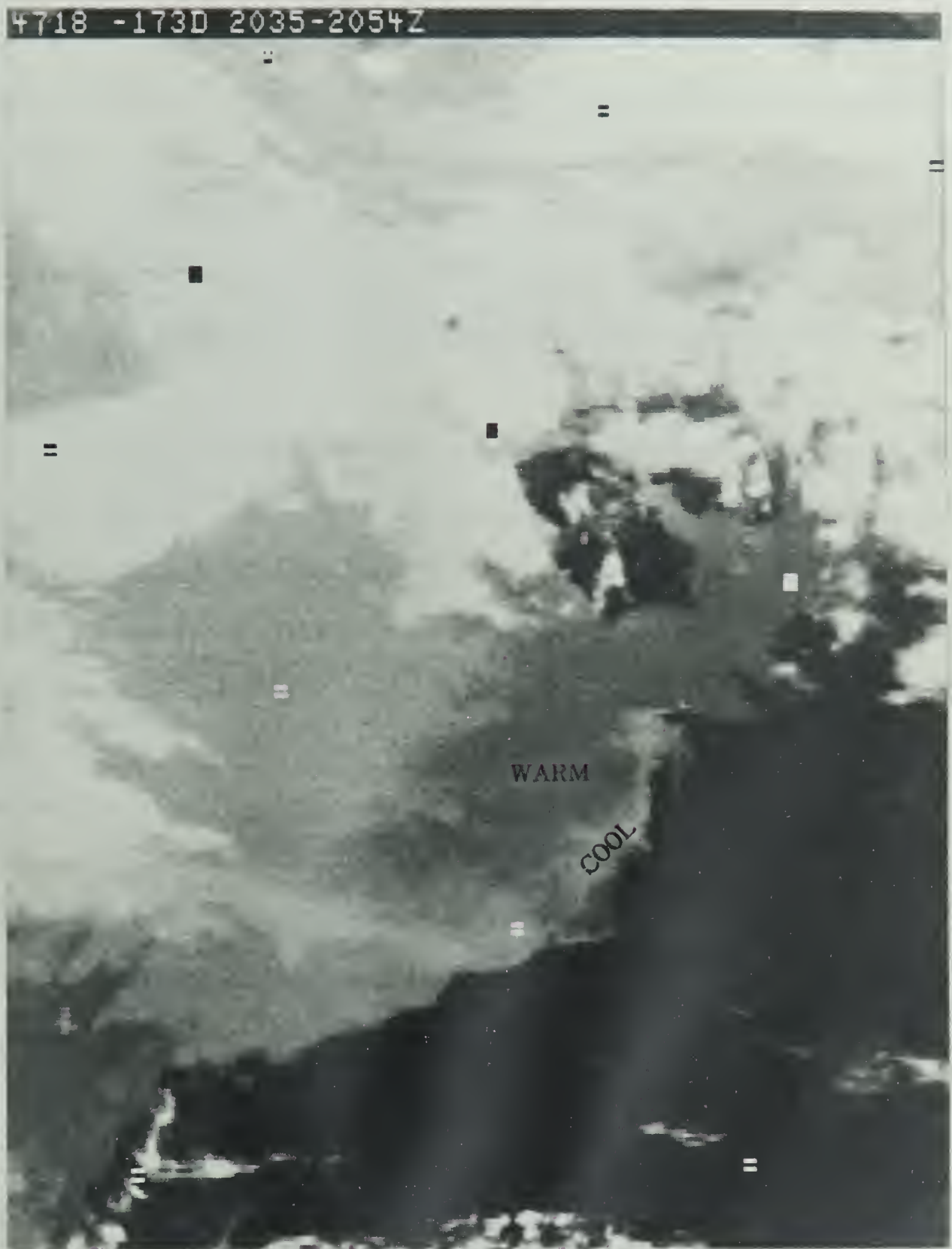


Figure 1.3 Infra-red (IR) image, obtained by NOAA-5, August 14, 1977, Orbit 4718.

clouds may cross coastlines, be partially transparent, or, under proper illumination conditions, cast shadows. Even when clouds are thin, however, there may remain the difficulty of differentiating between the grey shade resulting from thin cloud over open water, and that of thin or patchy ice on water. Unless there is a large expanse of known ice-free water nearby to serve as a reference, it may be virtually impossible to distinguish between clouds and ice or snow from one picture alone.

In terms of IR image interpretation, an "enhancement" process is often employed to emphasize temperature contrasts. The grey shades comprising an image typically represent a temperature range of over one hundred degrees. Through computer manipulation of the satellite data, the available shades may be applied to a specified thermal window of say, twenty degrees. The increased contrast over the range of interest facilitates differentiation of thermal conditions. The enhancement process may also be applied to visible satellite data to aid in the separation of land-water boundaries and cloud types.

In view of the sporadic nature of clouds in comparison with the major snow and ice fields in polar regions, the development of composite satellite data charts is a logical extension of photo-interpretive work. By saving the minimum brightness value at a specific location over a number of orbits, a composite chart of the minimum brightness, or CMB chart, is obtained for an appropriate area. A compositing period of five to ten days has been successfully employed in the Arctic (McClain et al., 1967). Figure 1.4 is an example of such a chart. In general, extremely persistent cloudiness will appear as tenuous or irregular

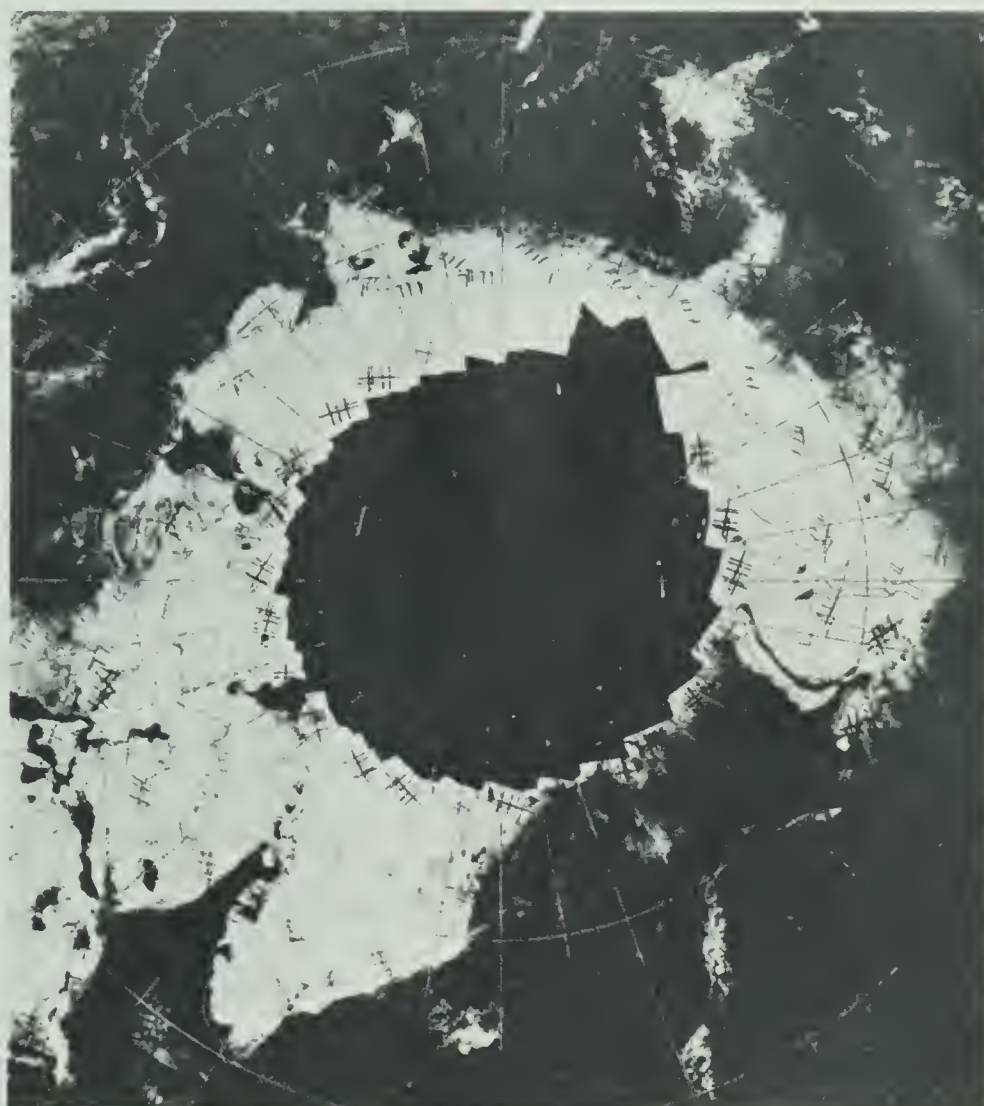


FIGURE 1.4 Ten-day composite minimum brightness (CMB) chart derived from ESSA-9 digitized brightness data for the period 24 May - 2 June 1970. The Greenland ice cap is readily identifiable on the lower left corner (from McClain and Baliles, 1970).

areas of lower brightness than the ice pack, especially for short compositing periods. Certain problems are inherent to the CMB chart, such as, (1) inability to deal with extremely persistent cloudiness, transient ice features and short-term melting or freezing; (2) position inaccuracies in data location; and (3) resolution of fine-scale detail, since the minimum brightness value will generally be the mean value from an array of data spots, or pixels, representing an area several kilometers across. In terms of the second problem, small changes in the geometric orientation of the satellite may cause finite and unpredictable errors in location of data with respect to the Earth. With reference to the third problem, subjective input can often aid in the visual interpretation of the CMB information.

A similar approach may be employed with regards the compositing of IR information. The highest temperature is retained at a specific location in the construction of composite maximum temperature (CMT) charts (McClain, 1978). The problems inherent to this procedure are in effect similar in nature to those encountered in the production of CMB charts.

The processing of satellite data in the form of composite charts provides a more quantitative measure of the information available in satellite imagery. The trend in recent years has been in this direction. Among the first to apply a simple statistical analysis to IR data were Smith et al. (1970), in the determination of sea-surface temperature over the Pacific Ocean. Histograms of radiative temperatures were collected for large geodetic areas, whereby surface temperatures were extracted from calculations of the standard deviation and mean in each

distribution. In the Arctic, 32 by 32 arrays of infra-red data have been collected and analysed to discriminate between different sea-ice ages and concentrations, and land, water and clouds (LeSchack, 1975), again making use of simple statistical techniques.

In the latter case, the spatial resolution of the IR data is a maximum of one kilometer. The data collected by the Satellite Laboratory at the University of Alberta have a maximum resolution of about eight kilometers. The question arises as to whether or not a reliable determination of the surface temperature fields in the Arctic can be achieved through processing of this lower resolution data. To this end a simple statistical technique is applied to histograms of the IR satellite data available. Cloud interference is a major concern, and an effort is made to reduce this problem.

CHAPTER II

A MODEL FOR COMPUTING SURFACE TEMPERATURES

IN THE ARCTIC

2.1 Introduction

With respect to the computation of surface temperature distributions from satellite IR data, some familiarity with the operation of the NOAA polar satellite system is helpful. A comprehensive description of system hardware and orbital characteristics is available elsewhere (Fortuna and Hambrick, 1974; Green, 1977) and is not included here. However, in the computational approach developed herein, a discussion of certain satellite characteristics is necessary.

2.2 The Data

The data received from the Scanning Radiometer (SR) of NOAA-5 by the University of Alberta are in the form of an analog signal. This signal is then digitized as a series of values ranging from zero to 255 with, in the case of IR data, the lower temperatures indicated by higher digital values.

In the compilation of histograms the data are subjected to processing: (1) a calibration from digital value to radiative temperature; and, (2) a mapping process, whereby data are located relative

to a predetermined geodetic mesh or grid. The histograms may then be compiled and subsequently analysed to determine the appropriate surface temperature for each geodetic area. These processes are now described in turn.

2.2.1 Internal Calibration

Before the satellite is launched, the radiometer is calibrated against a blackbody, and a "response curve" of temperature versus radiance is generated. In flight, the radiometer's response will also depend on its internal operating temperature; this will be a function of solar angle and distance and can be predicted and measured.

Part of the signal transmitted back to Earth during each scan is a "calibration pulse", available in digital form. Using nine such pulses (taken from three scans at the beginning of an appropriate sequence, three near the middle, and three near the end) ten data values are extracted from each of the six calibration levels or "steps" comprising the calibration pulse. The mean values for each level in each scan are then averaged over the nine scans to give a mean value of data versus corresponding blackbody temperature. Thus a set of six calibration points is generated (Greaves, 1979). The extraction of the points in this manner reduces fluctuations associated with the random error component of the SR.

At this point a curve-fitting procedure is employed to determine the temperature, to the nearest degree, of a particular datum value (See Appendix B).

Using output generated by the above internal calibration, the standard deviation of data values for a target temperature of zero degrees is, in practice, about 1.0 digital units. This can be taken as a measure of the noise present in the digitized IR data.

The response of the SR is such that it is linear with input energy, but not with target temperature, since radiative energy is proportional to the fourth power of temperature. The accepted accuracy is about $\pm 2^{\circ}\text{C}$ at the warm end (300 K) of possible values, and only about $\pm 8^{\circ}\text{C}$ at the cold end (185 K) (Schwalb, 1972); at target temperatures of zero degrees (0°C) this error is about $\pm 3^{\circ}\text{C}$.

2.2.2 External Calibration

External data calibration is necessary to take into account errors not attributable to the satellite system. The most important of these is atmospheric attenuation of the IR radiation between the target and the radiometer by gases such as water vapour and carbon dioxide. This effect will generally cause the radiances measured to be less than the actual radiances since usually the absorption and re-emission by these gases is at a temperature lower than the earth's surface.

Atmospheric profile and scan angle affect the amount of attenuation. Near the horizons (as "seen" by the satellite) the effect can be marked and is known as "limb-darkening". Since the mirror in the SR instrument rotates at a constant angular rate, the geometric resolution of the ground field of view decreases as the distance from the subsatellite point increases; an image produced from these data will appear fore-shortened near the horizons. Such data are of dubious quality in a

quantitative application.

For small scan angles, gaseous absorption and attenuation will generally be minimal, and are likely negligible, within the measuring error of the SR (Barnes, 1972). Thus, to a fair approximation, the IR sensor measures the actual blackbody radiance emanating from the earth target.

With the preceding remarks in mind, the following external corrections are available in the computational scheme. Data analysed may be restricted to only those regions within a local zenith angle of 65° or less, to exclude low-resolution data. Assuming atmospheric effects to be uniform over the relevant area, a routine which compares conventionally-measured surface temperatures ("ground-truth" data) to that obtained from the mean value of satellite scan-data comprising an area approximately one-half a latitude degree square, centred at the ground-truth datum location, is available. In making such a comparison one must assume the data in the histogram to be normally distributed about a single mean value and also that ground-truth data errors are small and contain no bias. Furthermore, the sky in the vicinity of the surface measurement must be essentially cloud-free (See Appendix C).

In the absence of reliable ground-truth data, an area of an ice-water mixture in a cloudless region will typically be very near 0°C , and may be used as an external calibration reference.

2.2.3 Mapping

With the data properly calibrated, it remains to locate the data with respect to some pre-determined grid. In effect, one of two

distinct processes is normally employed in "locating" satellite data. The raw data may be "gridded"; that is, a geodetic grid is overlaid upon the data as required; the specific grid used will be a function of the satellite orbit. In the output of data for a specific, pre-determined region, the data are "mapped" onto that particular region. In the location of data for this study a previously devised scan-by-scan "gridding" program (Green, 1977) is adapted such that the "mapping", or placing of data into appropriate geodetic areas, or "bins" may subsequently be achieved. A listing of this program is given in Appendix A.

The question logically becomes "What is the proper size for the bins?", considering the assumptions which must be adhered to in subsequent computations of surface temperatures. To calculate the surface temperature from a histogram, the collected values must be normally distributed about an appropriate single mean value. It is presumed that each element in the distribution represents an earth target area which is very small relative to the total bin area, yet the total bin area must be small enough to allow the mean value calculated to be representative of the total bin area.

To give insight into the specific problem, consider the following. With each scan of earth, the SR "sees" a strip about eight kilometers wide at the subsatellite point; for every scan close to one thousand digital elements, or "datons", are produced. Thus near this point three datons are produced for every eight kilometers of scan. (Near the horizons this multiplicity decreases.) Thus a one by one degree latitude area contains roughly six hundred datons. Since sensor resolution is only eight kilometers at the subpoint, it would appear

sensible to average three neighbouring datons, reducing the population in the area to about two hundred, a number still more than adequate to produce representative histograms. However, is the mean value obtained from such a distribution relevant for the entire area? The answer to this question must presumably be obtained in a semi-empirical manner.

2.2.4 Analysis of Histograms

In the analysis of the compiled histograms, an appropriate modal temperature, with a frequency of at least 0.1 is obtained from each distribution. The modal value must be within reasonable climatological limits, and have the specified frequency, or else the distribution is likely too flat or too cloud-contaminated to be representative. All data within three degrees of the mode are used in calculations of mean and standard deviation. The three-degree window is felt to be consistent with the suspected reliability of the SR's response. In practice, using cloud-free data, the standard deviation values are generally between 1.0° and 1.5°C (See Appendix D for sample output); the value of 1.5°C was chosen as the "cut-off" value for the sharpness required in determining the acceptance or rejection of the mean value for the bin in question.

Using N values in the histogram representation of the data will reduce random errors (noise and sensor) by a factor of $N^{\frac{1}{2}}$; thus the computed means are well within an accuracy of $\pm 1^\circ\text{C}$, allowing the drawing of isotherms at that interval.

2.3 The Experiments

In the design of experiments performed in this research, several questions posed in preceding sections are pursued:

1. What is an optimum geodetic grid size?
2. What effects does averaging of datons produce?
3. Can IR data be processed to detect differences in sea-ice concentrations as well as sea-surface temperature?
4. How important is atmospheric attenuation?
5. Can clouds be filtered in some reliable manner?
6. Can coastal areas be included in analyses?

These questions are considered in turn in the following experiments, conducted using digitized IR scanning radiometer data obtained from NOAA-5 for the period July-August, 1977, over an area comprising much of the Beaufort Sea, Banks Island and the Northern Canadian mainland coast.

The first experiment considers effects of resolution of the histogram analysis technique through changes in geodetic grid size. It also examines the effect, both mathematical and physical, of averaging together consecutive datons.

In the second experiment the results of the first are applied to three case studies of sea-surface temperatures and incorporated into an analysis of horizontal temperature gradients.

Finally, the questions of the effects of cloud "contamination" and land intrusions on the sea-surface temperature analyses are examined. The feasibility of compositing the histogram data over a number of days is studied, and a modal scanning method, which screens out generally warmer land temperatures in coastal areas, is tried.

In all experiments the need for, or lack of external calibration is studied. Finally, conclusions are drawn from the experimentation as a single entity.

CHAPTER III

REFINING THE SURFACE TEMPERATURE MODEL

3.1 Introduction

In this chapter several essential considerations in the development of the surface temperature retrieval model are examined. The study areas used are shown in Figure 3.1. The smaller area is basically employed in case studies of single-orbit sea-surface temperature and horizontal temperature gradient analyses, while experiments in cloud filtering employ the full outlined area.

Since the Beaufort Sea lies in a region beset by substantial cloudiness and fog during the summer months, the satellite data are taken from passes over the study area which occurred near or just after local noon, to minimize the effect of low cloud and fog near coastlines. Once-daily information is collected as near as possible to the same local time so that analyses may be more consistently compared on a day-to-day basis.

3.2 Grid Size Optimization

The mathematical restrictions previously discussed are of prime importance in the determination of an optimum grid size. In addition,

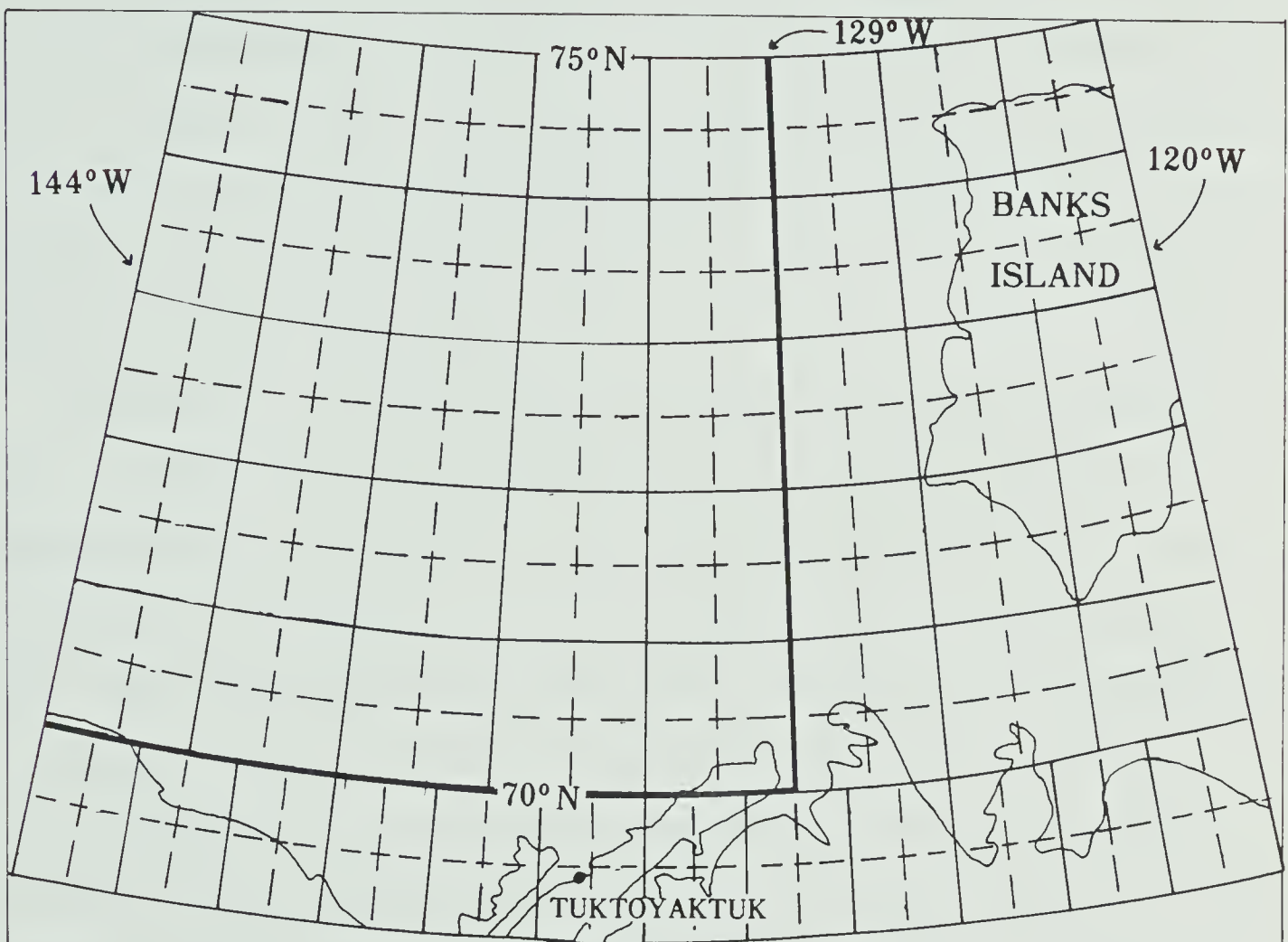


FIGURE 3.1 Map of study areas. Single orbit studies employ the smaller region. Low resolution bins are delineated by solid outline, while the addition of the dashed outline depicts the high resolution bins.

the proper mesh should reproduce the detail identifiable on the conventional grey-shade imagery.

The original grid size investigated employs a latitude increment of one degree, and a longitude increment of two degrees to the south of latitude seventy degrees, and three degrees to the north. A sample of the corresponding isotherm analysis, taken from Orbit 4222, July 5, 1977, is shown in Figure 3.2a. By reducing the dimensions of the grid by a factor of two, the corresponding analysis in Figure 3.2b is produced. The square by square temperature retrievals are shown in Appendix D for the former case.

The manner in which the subjective isotherms are drawn requires that a value plotted for a square where a coastline intersects be representative of the centre of the water-covered portion only, if the plotted value is a climatologically reasonable one for the particular area. Values plotted for land-locked areas are ignored in the analysis.

A portion of the IR image for Orbit 4222 is displayed in Figure 3.3. Considering the detail reproduced near Banks Island, as well as for the cloud band in the central Beaufort Sea in Figure 3.2b, as compared with the detail identifiable in Figure 3.2a, the use of the finer mesh appears warranted.

Sample histograms for the above data are shown in Figure 3.4 for the large grid and the four corresponding areas for the smaller grid. Generally the number of datons contained by the larger grid is about 150-175, and about 35-45 for the smaller mesh. (An averaging of three neighbouring datons is employed.)

While examination of these histograms illustrates how the assumption of uniformity of temperature in a square may easily be violated

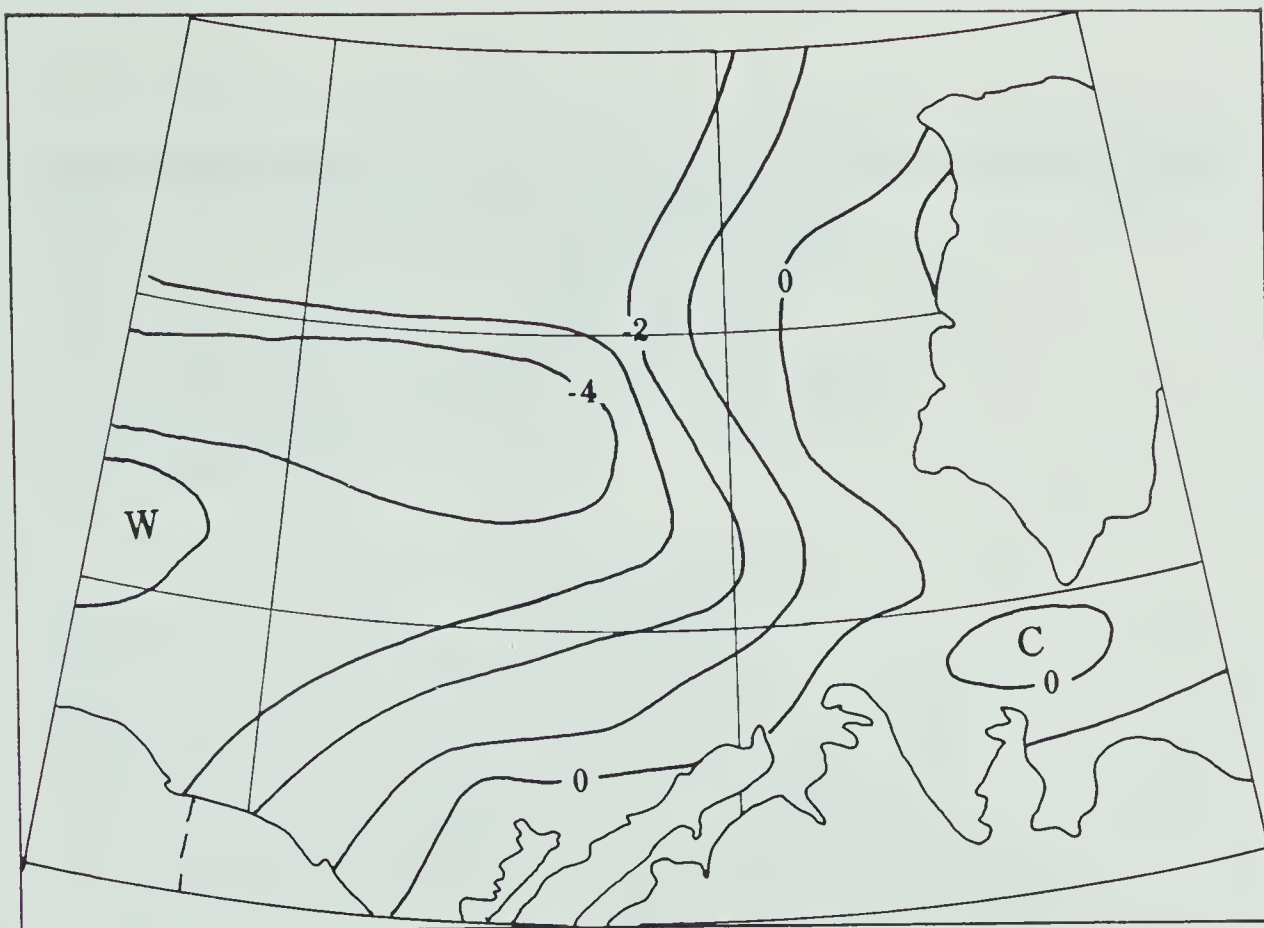


FIGURE 3.2a Isotherm analysis: July 5, 1977, Orbit 4222. Low resolution grid.

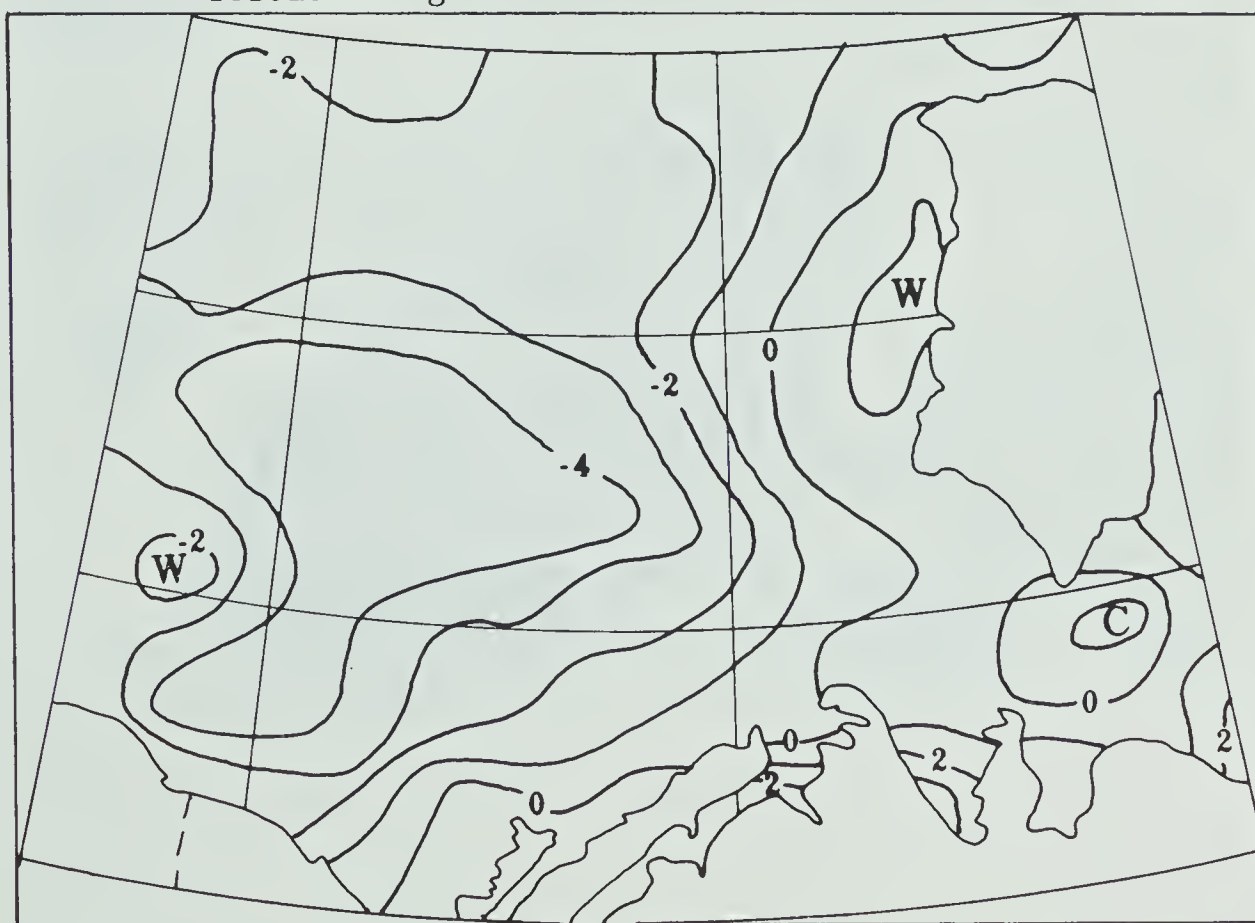


FIGURE 3.2b Isotherm analysis: July 5, 1977, Orbit 4222. High resolution grid.

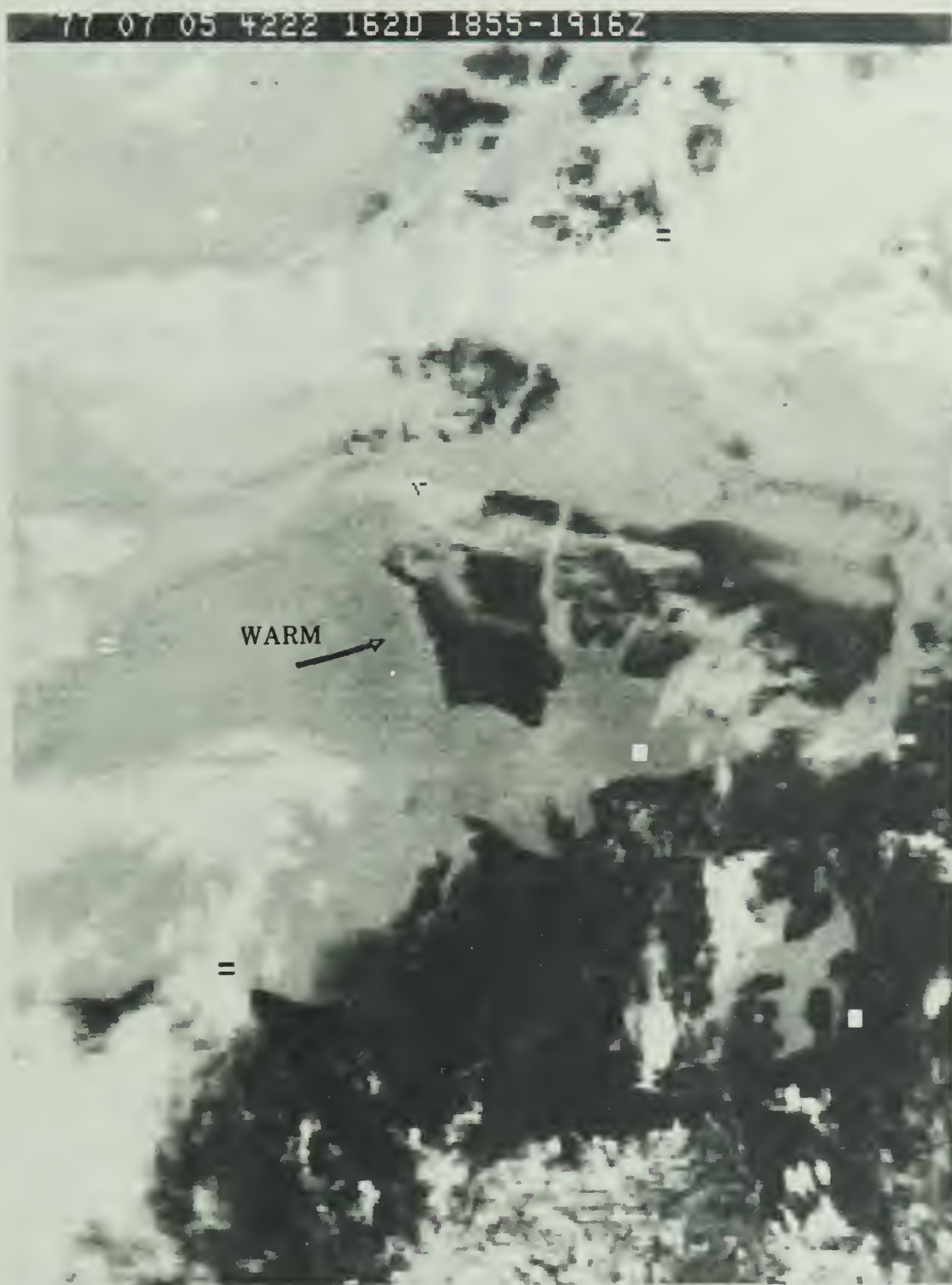


FIGURE 3.3 IR image, July 5, 1977, Orbit 4222.

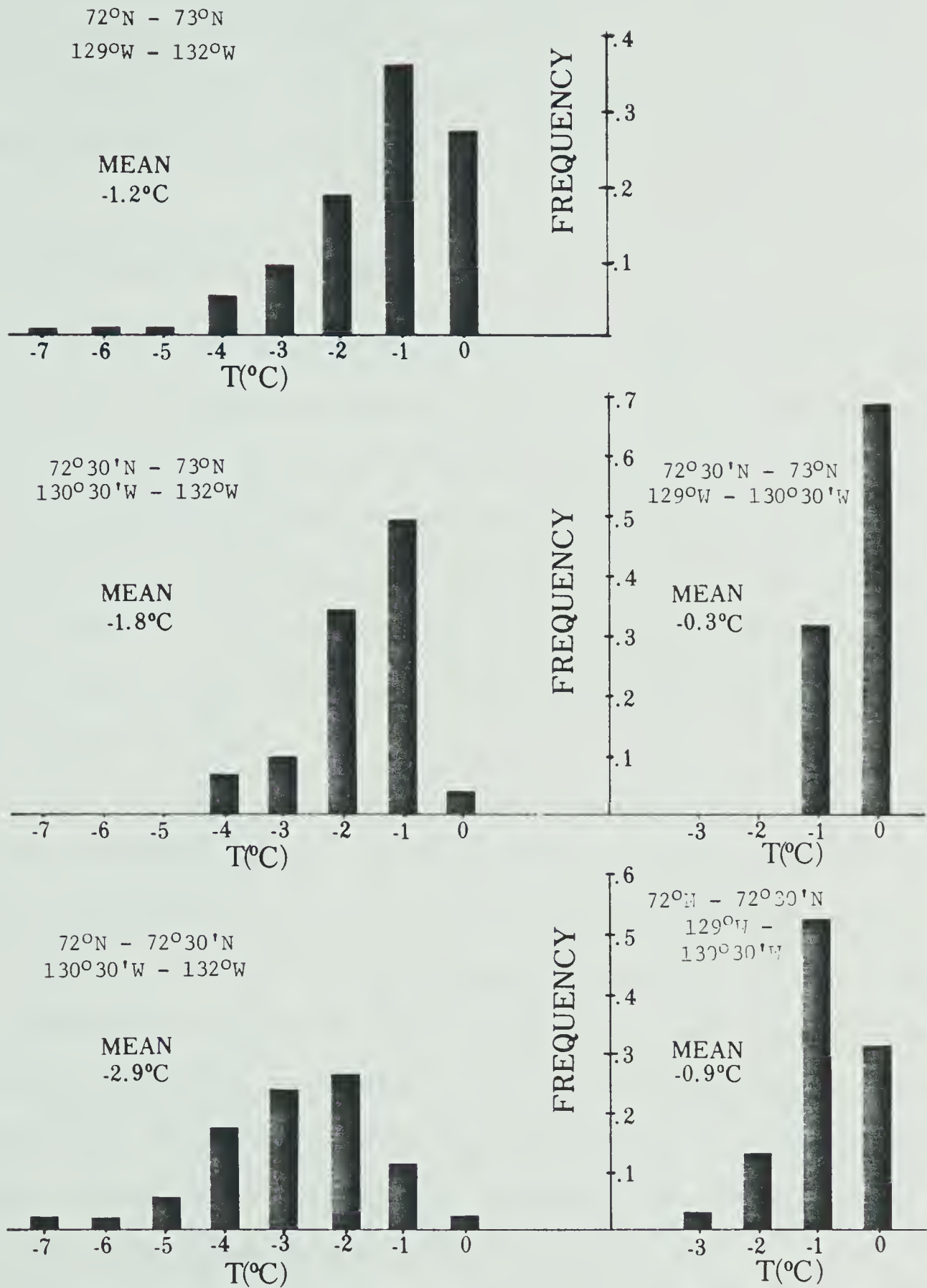


FIGURE 3.4 Relative frequency versus temperature, showing effect of change of bin size. Data taken from July 5, 1977, Orbit 4222.

for the large grid, a reduction in grid size beyond that of the smaller grid will invalidate the specification that daton size be small relative to bin size. The smaller grid size used here is adopted for use in subsequent experiments.

3.3 Averaging of Digital Values

If the number of entries in a histogram is reduced by the averaging of a specified number of consecutive datons before being entered into the frequency table, the shape of the distribution will change. If relative frequency is plotted versus temperature, the area under the distribution will remain constant. However, the distribution will become sharper as the number of consecutive datons averaged increases, provided the curve is a normal one. Skew distributions may behave in a less predictable manner.

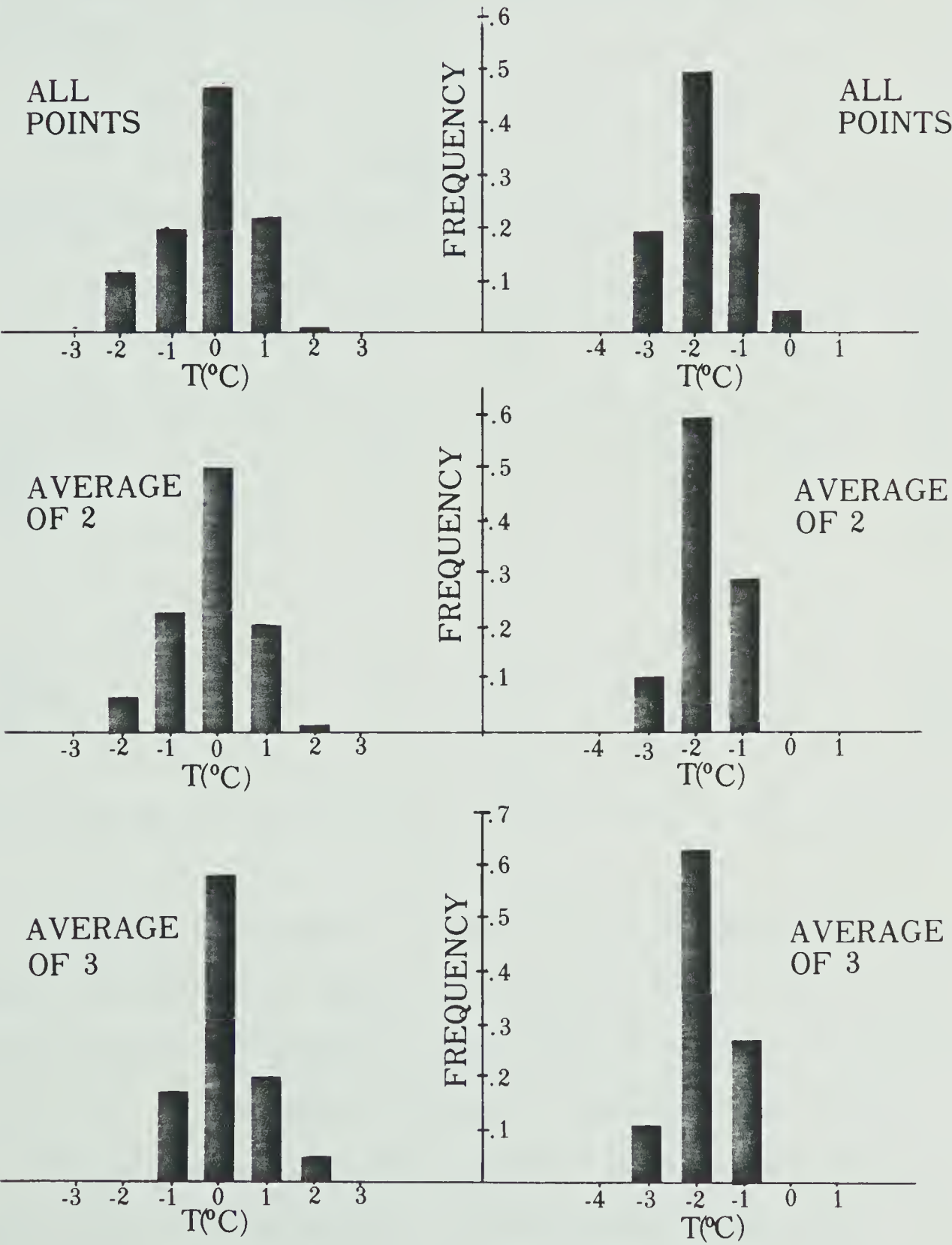
Sample distributions of IR data taken from Orbit 4718, August 14, 1977 are displayed in Figure 3.5a for a bin in a high temperature gradient region, and for a bin in a low temperature gradient region, in Figure 3.5b. The effect of averaging neighbouring datons is apparent. As the amount of averaging increases, skewness is removed from the low temperature end of the distribution, while modes are sharpened as well. In particular, the distribution in the high-gradient case is noticeably changed. The normality assumption is evidently not well-satisfied in such areas, even though the mode is well-defined.

The summary of the averaging effect in this particular case is shown in Table 3.1. The calculated mean changes very little in a low gradient bin, but noticeably otherwise. The standard error is a

FIGURE 3.5 Relative frequency versus temperature. Effect of averaging on distribution shape.

(a) High Gradient Bin
72°30'N - 73°N
138°W - 139°30'W

(b) Low Gradient Bin
73°30'N - 74°N
138°W - 139°30'W



reasonably stable statistic, in spite of the averaging, in both situations. From a statistical viewpoint the averaging of three datons does not affect the temperatures retrieved in a low gradient area; the real effect of this process in a high gradient area may only be identified by examining the actual surface temperature distributions.

TABLE 3.1

Statistical Summary of Histograms Shown in Figures 3.5a, 3.5b (Orbit 4718)

	Averaging	Pop'n	Mode (°C)	Mean (°C)	Std. Dev. (°C)	Std. Error (°C)
High Gradient Area	1	118	0	-.2	1.0	.092
	2	59	0	-.1	.9	.117
	3	40	0	.1	.7	.111
Low Gradient Area	1	111	-2	-1.8	.8	.076
	2	54	-2	-1.8	.6	.082
	3	37	-2	-1.8	.6	.099

The temperature analyses for August 14, using different averaging amounts, are depicted in Figures 3.6a, 3.6b and 3.6c. Values in the southeast section are missing in Figure 3.6a; in this area the sharpness criterion of 1.5° may not have been met. Otherwise, even in high temperature gradient areas, the averaging of three datons, with the general effects of simultaneously smoothing and sharpening the distributions, appears to be a reasonable procedure to adopt for

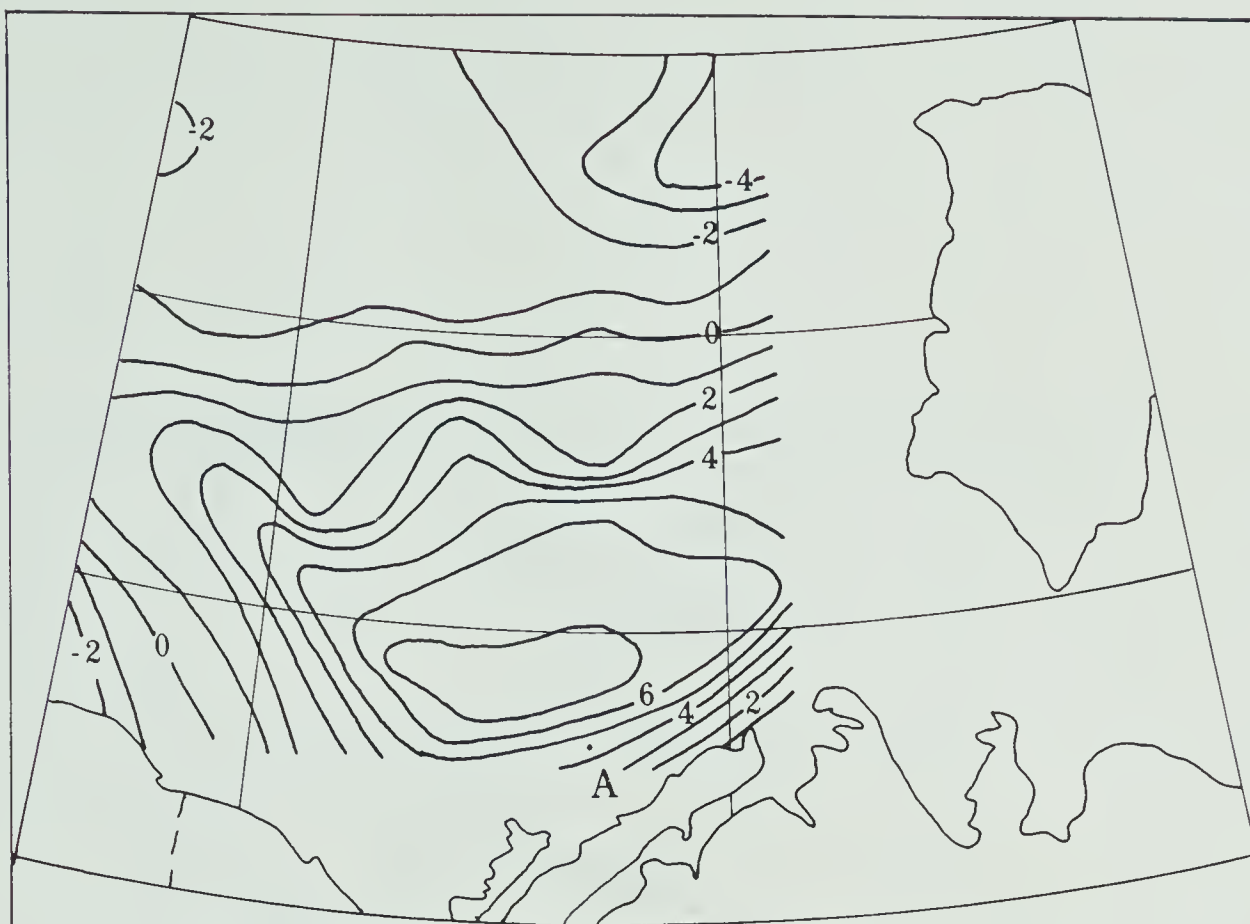


FIGURE 3.6a Isotherm analysis: August 14, 1977, Orbit 4718.
All datons used.

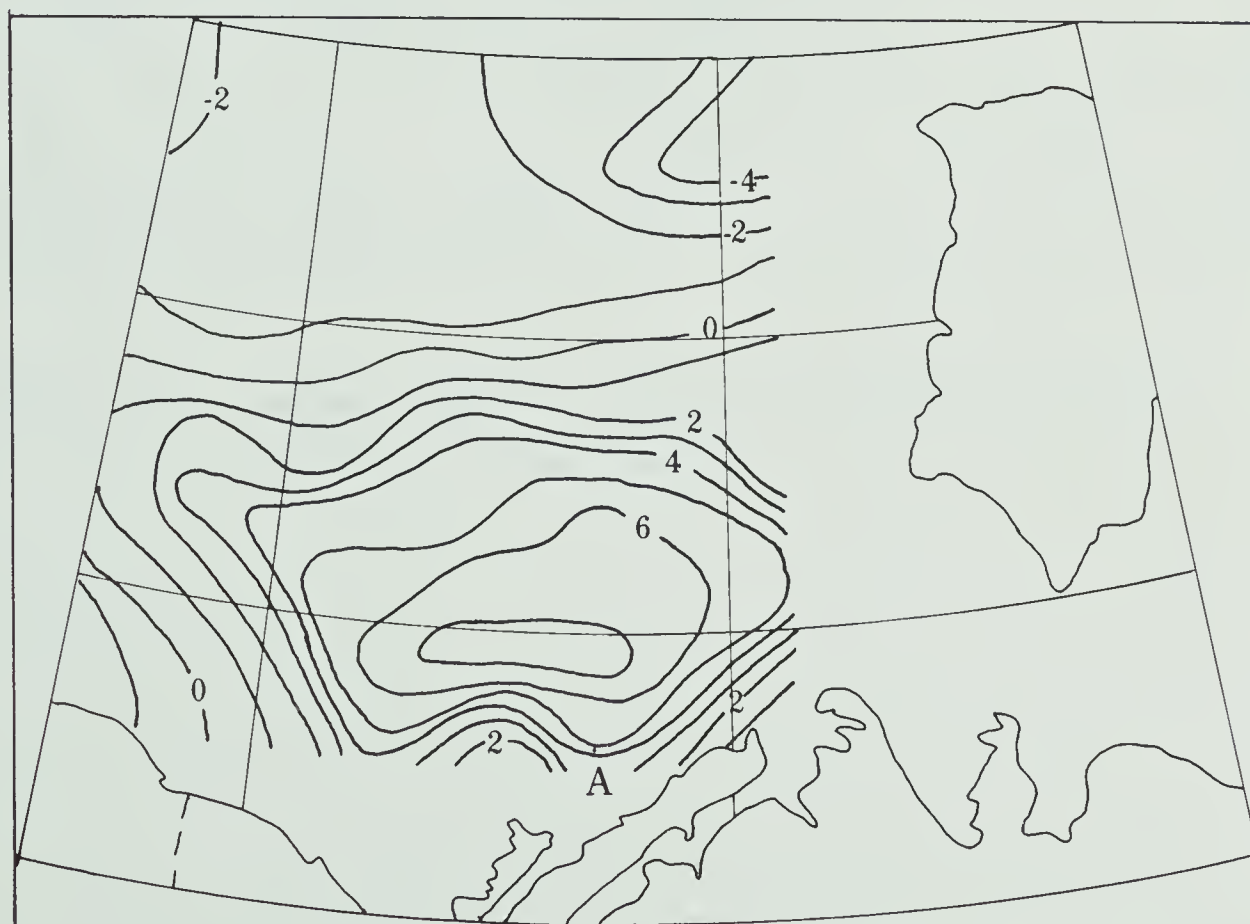


FIGURE 3.6b Isotherm analysis: August 14, 1977, Orbit 4718.
Averaging of two datons.

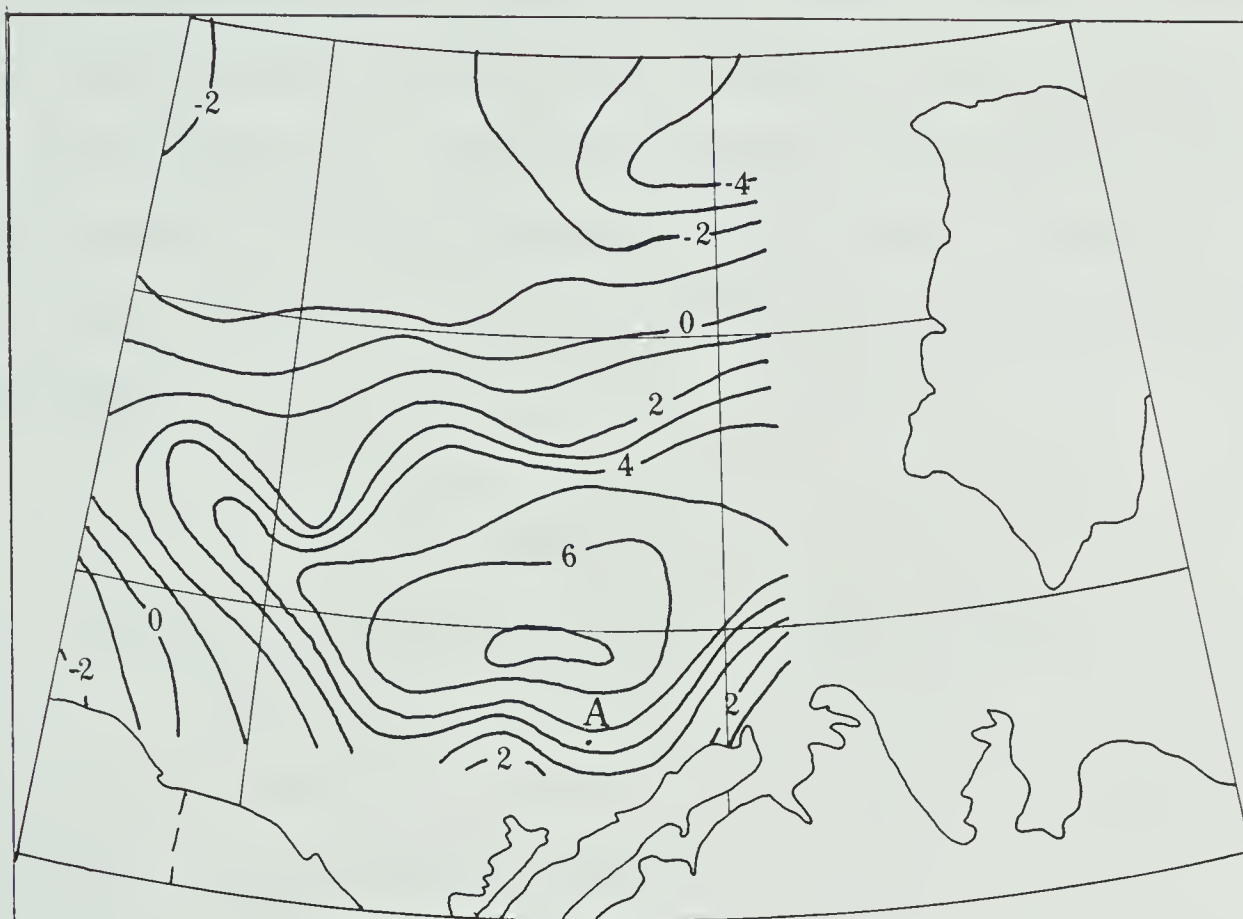


FIGURE 3.6c Isotherm analysis: August 14, 1977, Orbit 4718.
Averaging of three datons.

subsequent work, especially where data obtained at small zenith angles relative to the satellite are concerned.

3.4 External Calibration

A check on atmospheric effects for the August 14 data is appropriate. The location of ground truth information is shown on Figures 3.6a, 3.6b and 3.6c (point A). The satellite passed nearly directly overhead point A in Orbit 4718, and atmospheric effects might be expected to be fairly small. Table 3.2 summarizes the satellite-calculated surface temperatures.

TABLE 3.2

Ground-Truth Information Versus Satellite-Derived
Temperatures, August 14, 1977, Orbit 4718

Ground-truth				
Location: 70°09'N 132°48'W, 1800 GMT				
Temperature: 5.2°C				
Weather: Clear Sky				
	Pts. Avg'd	Pop'n	Temp (°C)	Std. Dev. (°C)
Satellite- Computed Temperature	1	91	4.8	1.70
	2	63	4.3	1.70
	3	49	4.6	1.74

Ideally, ground-truth information should be incorporated into each temperature analysis as a final correction; however, this is not always

possible. There may be excessive cloudiness in the vicinity of the ground-truth datum location, the temperature in the appropriate area may not be sufficiently uniform, or else no measurement may even be available.

3.5 Temperature Gradients

In the absence of suitable ground-truth data, the comparison of surface temperature patterns to ice conditions is necessarily a relative one. No reliable correlation between a particular ice state and temperature value may be made, although in some cases the correction required may be fairly small, as shown above.

One way to circumvent this situation is to produce, from the temperature distribution, a temperature gradient analysis. The physical rationale in the comparison of temperature gradients to ice conditions is as follows: over the major ice surface, the temperature gradient should be fairly small and reasonably uniform; towards the edge of the ice pack the gradients will increase as the ice concentration values change more rapidly; finally, over open water and ice-free areas, the gradients will decrease and behave in a more haphazard manner. (A partial glossary of ice types, concentrations and other relevant nomenclature is given in Appendix E.)

If atmospheric attenuation is presumed constant over the relevant area, the temperature gradients should give a reliable measure of ice information, and also of the resolving capability of the histogram analysis technique.

The temperature gradients are derived as follows: given the sea-surface temperatures for each square in a ten by ten geodetic array, an eight by eight array of gradients may be computed. Figure 3.7 shows the grid representation used in the derivation of equation 3.1.

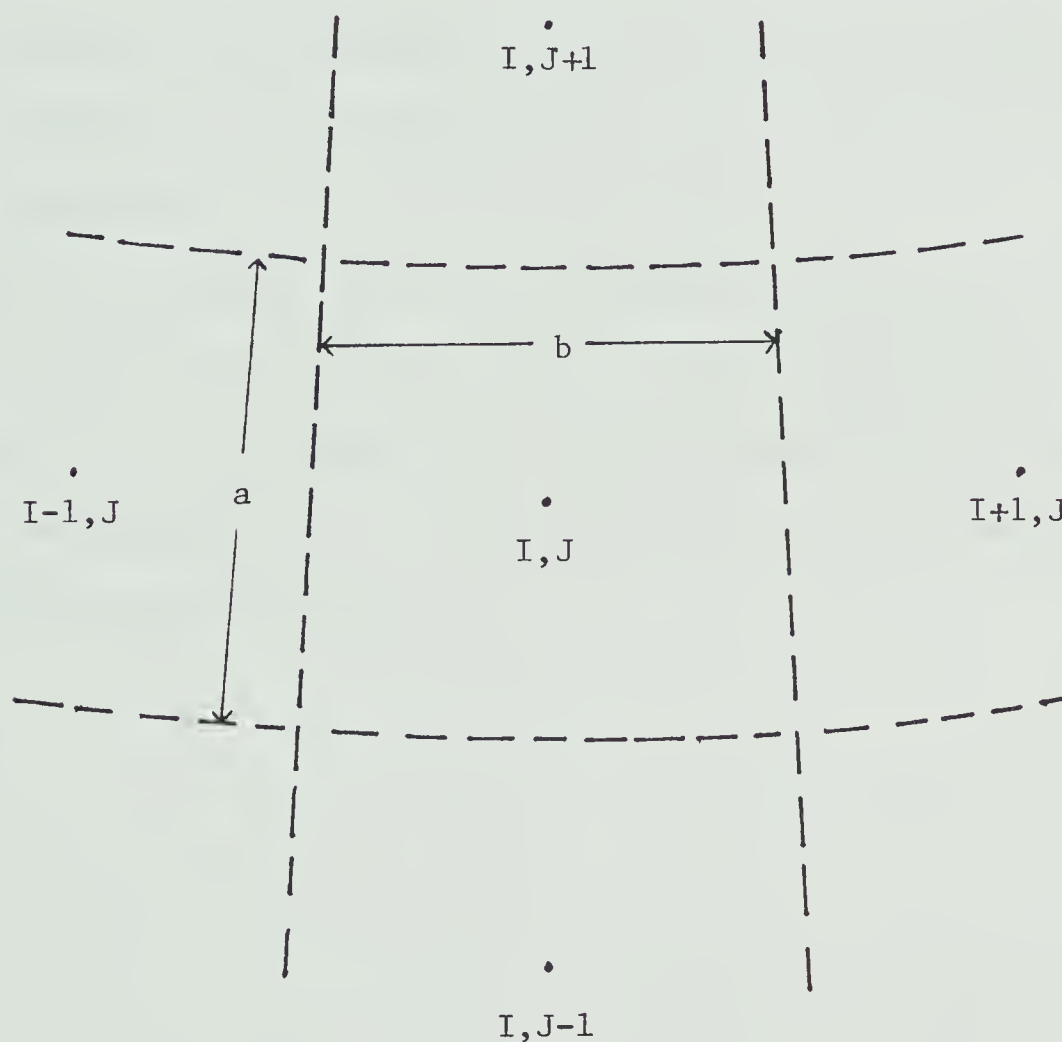


FIGURE 3.7 Representation of grid for temperature gradient calculation.

$$\text{GRADIENT (I,J)} = \left[(\text{DX(I,J)})^2 + (\text{DY(I,J)})^2 \right]^{\frac{1}{2}} \quad (3.1)$$

where $\text{DX(I,J)} = (\text{SST(I+1,J)} - \text{SST(I-1,J)}) / (2 \cdot b \cdot \text{cosine of latitude of point (I,J)})$

$\text{DY(I,J)} = (\text{SST(I,J+1)} - \text{SST(I,J-1)}) / (2 \cdot a)$

and SST(I,J) = sea-surface temperature at location (I,J)
 a = latitude increment
 b = longitude increment

The gradients are expressed in degrees Celsius per latitude degree ($^{\circ}\text{C}/^{\circ}\text{L}$), and may be recorded directly onto the same grid map used for surface temperatures.

With the temperature retrieval technique developed to a functional state, it remains to be tested on actual cases. Three such cases are considered in the following chapter, using the appropriate geodetic mesh and averaging scheme, in the computation of surface temperatures and their horizontal gradients.

CHAPTER IV

SEA-SURFACE TEMPERATURES AND THEIR HORIZONTAL GRADIENTS

4.1 Introduction

In the study of three cases involving sea-surface temperature and temperature gradient analyses, a discussion of physical characteristics identifiable from the analyses is appropriate. In addition, a verification of the information produced in each analysis is necessary as well. The verification data consist of the appropriate satellite imagery, charts of mean weekly ice conditions produced by Environment Canada and, when available, ground-truth temperature data. In the verification of horizontal gradients the ice information provides the only true comparative test.

The Atmospheric Environment Service operated, in the summer months of 1977, a forecast office - the Beaufort Advance Base (BAB) - at Tuktoyaktuk. This office had access to meteorological reports from drill sites and nearby ships that enabled forecasters to perform more detailed in situ analyses than were possible elsewhere. These maps were used in these studies as the synoptic background. Since some overlap is involved with case studies done in Chapter V, all synoptic charts are grouped in that chapter.

4.2 Case Study 1, July 27, 1977

4.2.1 Synoptic Situation

On this date a high-pressure cell dominated the surface circulation as shown in Figure 5.12. This circulation produced mainly clear skies over the study area.

4.2.2 Verification

Figure 4.1a displays the surface temperature field using IR data from Orbit 4495; Figure 4.1b depicts the corresponding temperature gradient analysis. Using the ice information for July 29 (given in Appendix F, Overlay 1), note that, in Figure 4.1a, temperatures below 0°C correspond with very close pack or greater multi-year ice conditions, while temperatures between 0°C and 2°C generally outline regions of first-year and multi-year ice from 1/10 to 6/10 concentration.

The relevant satellite images are shown in Figures 4.2a and 4.2b for Orbit 4495. Relative temperature features correspond fairly well with the isothermal analysis. The warm (dark) tongue of water at point A on the IR image is well-marked on the isotherm analysis, as is the belt of first year ice to the immediate northeast (B). The general outline of the ice edge from the visible image is also well-marked on the isotherm analysis.

Table 4.1 summarizes the external effects for Orbit 4495, using the report at location A on Figure 4.1a. While fog was reported both early and late in the day, clear skies prevailed in this area at the time of the satellite pass. The temperature "analysed" by the

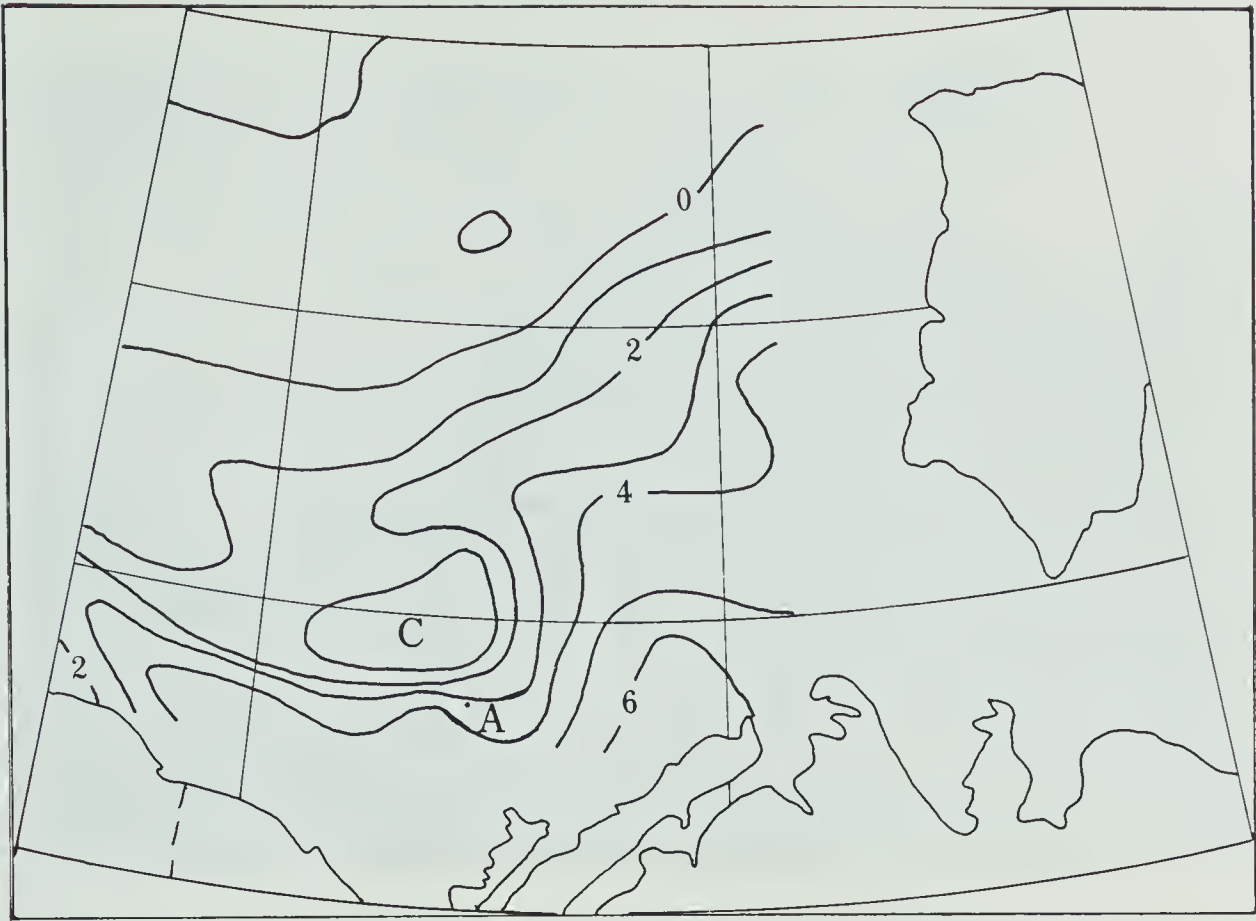


FIGURE 4.1a. Isotherm analysis: July 27, 1977, Orbit 4495.

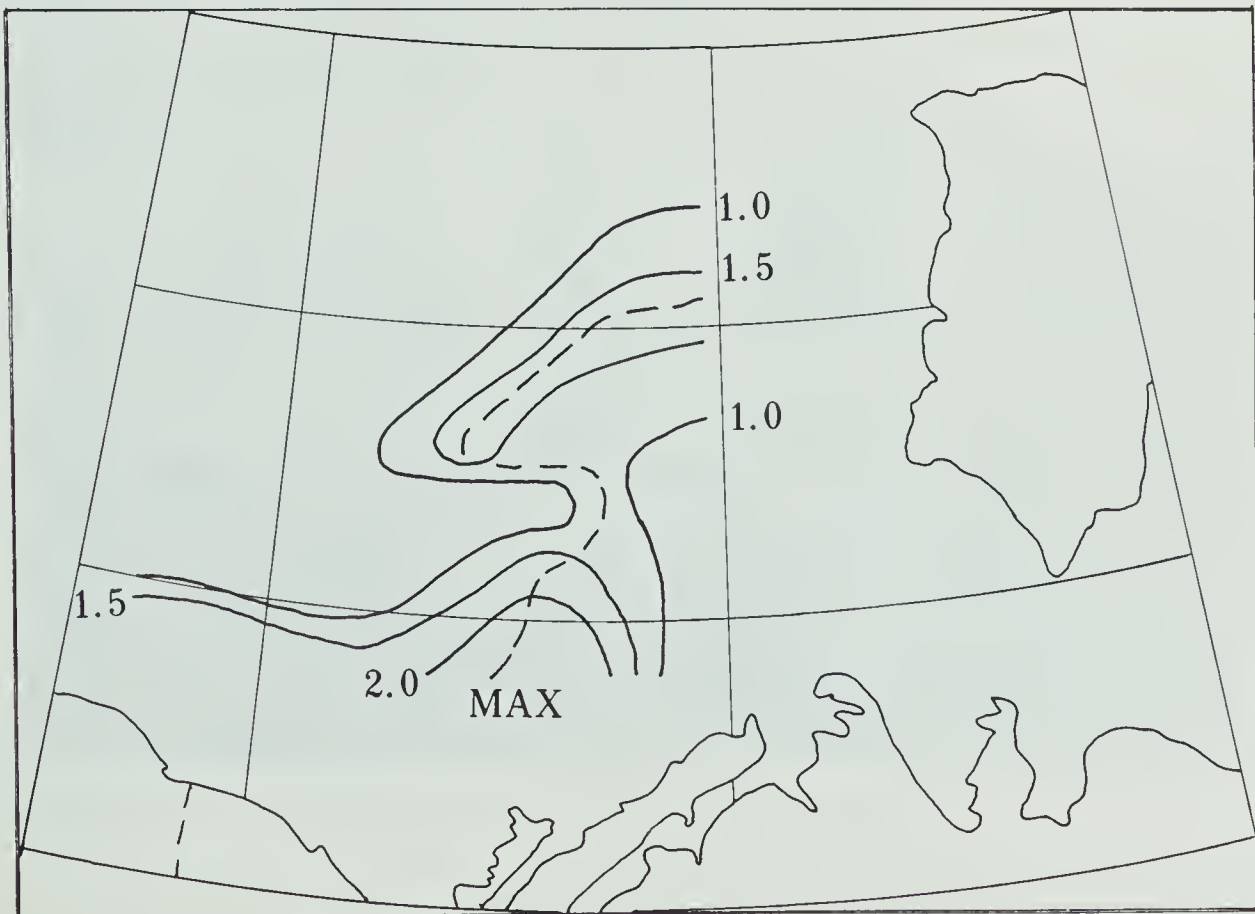


FIGURE 4.1b Temperature gradient analysis: July 27, 1977, Orbit 4495.

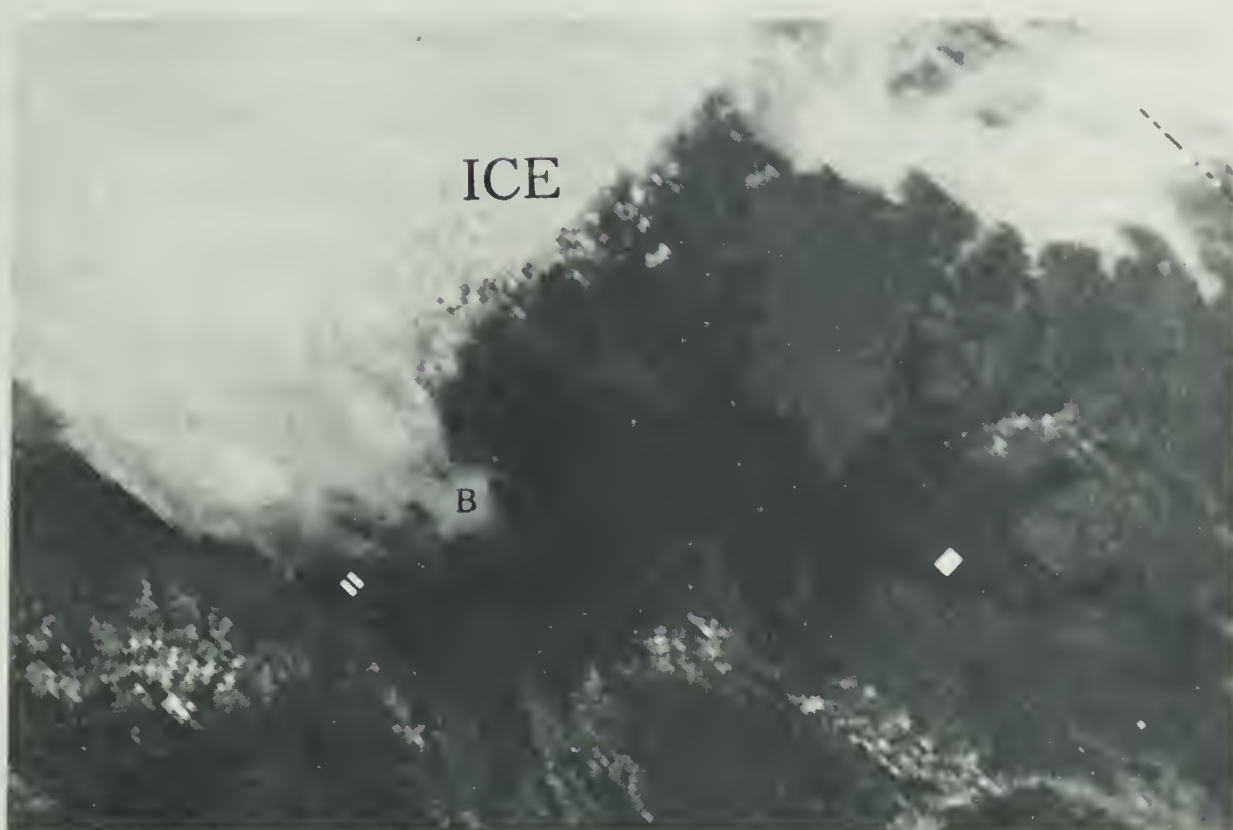


FIGURE 4.2a Visible image, July 27, 1977, Orbit 4495.

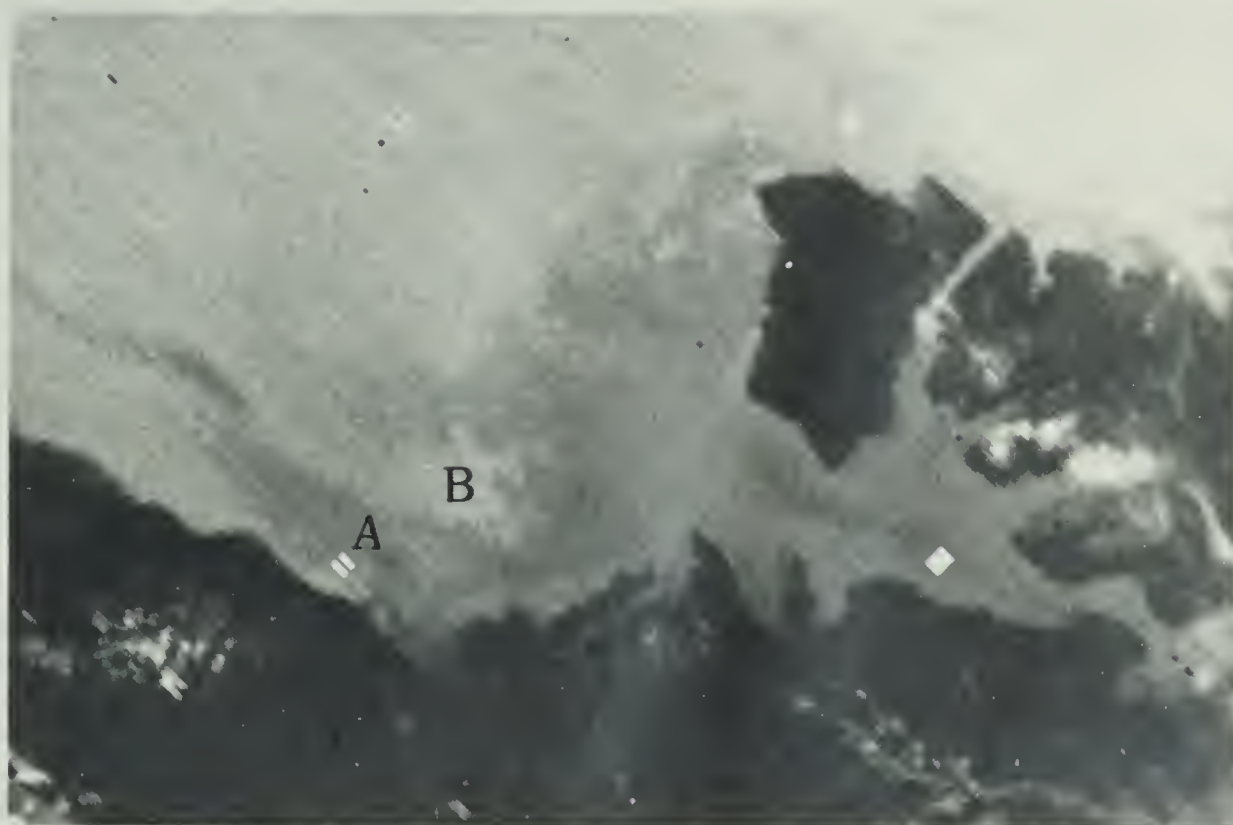


FIGURE 4.2b IR image, July 27, 1977, Orbit 4495.

subjectively drawn isotherms is between 3°C and 4°C while the computed temperature is 3.2°C. This agreement may be coincidental; however, point A is situated in a high-gradient area, where the histogram analysis technique might be expected to perform poorly. Since temperatures near the ice edge appear quite reasonable, it is unlikely that there is two degrees worth of attenuation in this case. The discrepancy may lie in the fact that the ground-truth measurement represents a specific point, not an area.

TABLE 4.1

Ground-Truth Information Versus Satellite-Derived
Temperatures, July 27, 1977, Orbit 4495.

Location: 70°23'N 135°06'W			
Time (GMT)	Temp (°C)	Weather	Computed Temp./ Std. Dev. (°C)
1200	5	Fog	3.2 / 2.04
2400	6	Fog	

The scanning routine employed to determine modal temperatures bears elaboration. A "cold-mode" scanning is used, whereby the first mode encountered starting from a temperature of -3°C is analysed for mean and dispersion. In general, a bias towards cold values is expected when surface temperatures are recorded; however, the agreement between subjectively and objectively determined surface temperatures in a high-gradient region suggests the bias may be fairly small, and temperatures

along the ice edge appear physically reasonable, as noted above. In the next chapter the value of the "cold-mode" scanning as opposed to "warm-mode" scanning will be further demonstrated.

In comparing Figure 4.1b, the temperature gradient analysis, to the appropriate ice data, the best correlations are evident in the northeast region, where the multi-year ice edge is well-defined, and not irregularly-shaped. Here a temperature gradient of $1^{\circ}\text{C}/^{\circ}\text{L}$ forms a reasonable boundary between close and open pack ice. In this same region the locus of maximum gradient corresponds well with the separation of open water areas and very open pack ice. In the southwest areas, the $1^{\circ}\text{C}/^{\circ}\text{L}$ line offers a similar but less convincing delineation to that found above.

Owing to a strong temperature gradient in open water areas in southern regions, the locus of maximum gradient appears to be of little value in a comparative study.

4.3 Case Study 2, July 28, 1977

4.3.1 Synoptic Situation

Generally clear conditions continue to dominate the study area on July 28, in spite of a low pressure area which formed in the southern Beaufort Sea, as depicted in Figure 5.13.

4.3.2 Verification

Infra-red data from Orbit 4507, July 28 were used to derive the surface temperature and temperature gradient analyses shown in Figures 4.3a and 4.3b.

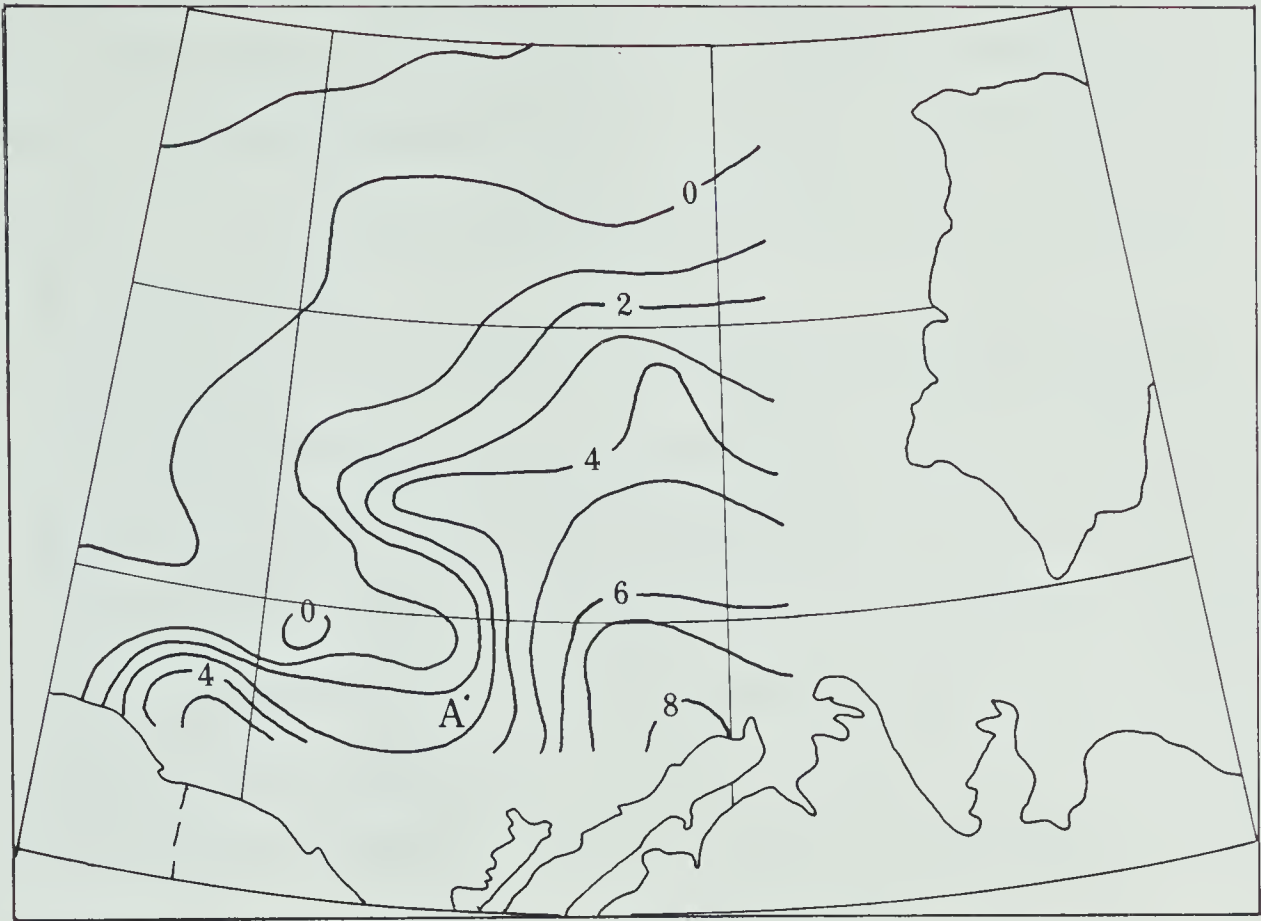


FIGURE 4.3a Isotherm analysis: July 28, 1977, Orbit 4507.

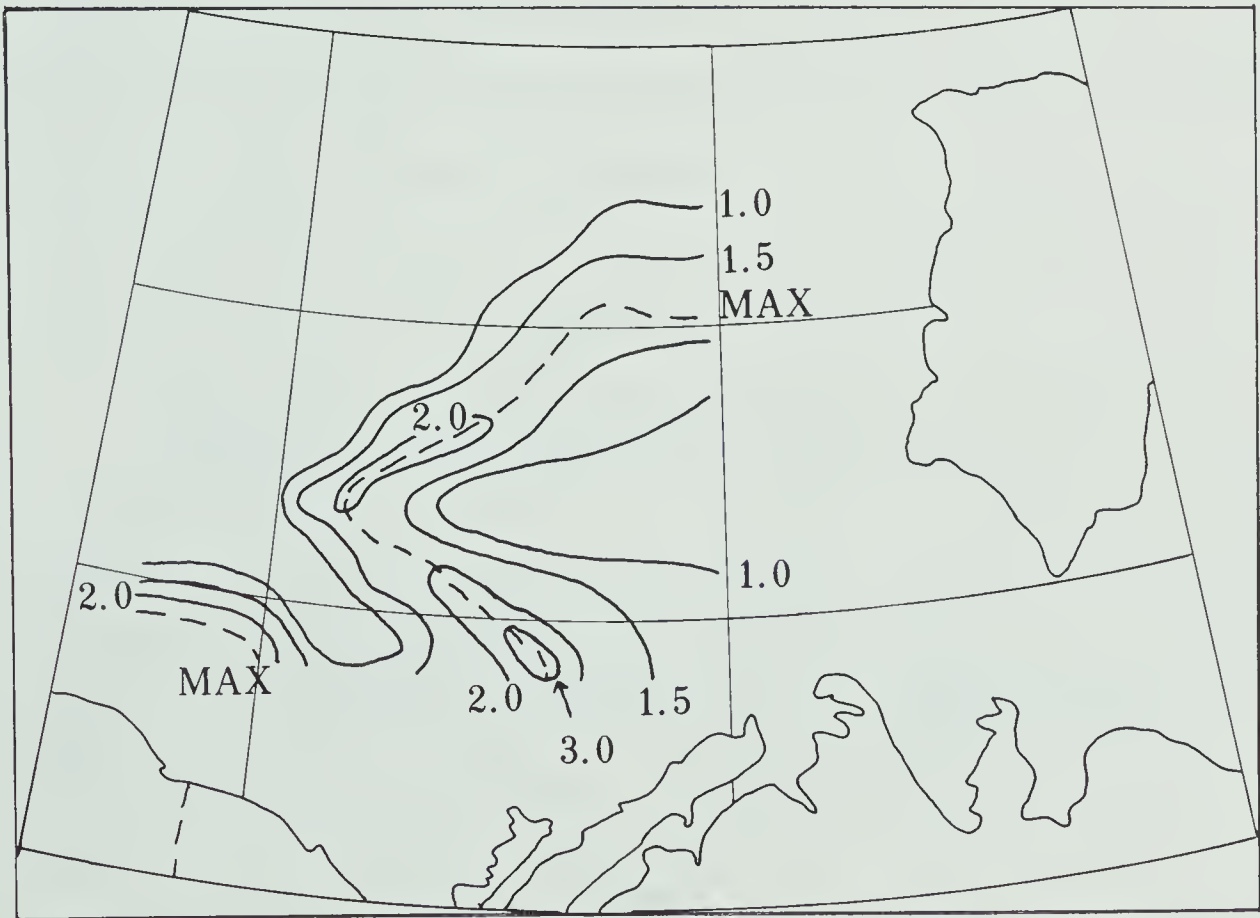


FIGURE 4.3b Temperature gradient analysis: July 28, 1977, Orbit 4507.

In terms of the ice conditions for July 29 (Overlay 1), the open water - very open pack ice separation is reasonably marked by the 2°C isotherm, as was the case for July 27. However, the delineation of multi-year ice conditions using the 0°C isotherm is not as marked as for the previous day.

Due to satellite data transmission problems on July 28, the available imagery provides only relevant visible data for Orbit 4508 and IR data for Orbit 4507; these are displayed in Figures 4.4a and 4.4b, respectively. The gross features in these images are reproduced faithfully in Figure 4.3a. Examination of the images shows a band of cloud over the southern portion of the study area; it is possible that changes in the orientation of the zero degree isotherm from that analysed from Orbit 4495 may be due to unequal insolation at the surface, affecting freezing and melting of puddles atop the ice.

Table 4.2 summarizes the ground-truth data as compared to the satellite-derived surface temperatures; point A on Figure 4.3a shows the location of the surface-based data.

TABLE 4.2

Ground-Truth Information Versus Satellite-Derived
Temperatures, July 28, 1977, Orbit 4507.

Location: 70°23'N 135°06'W			
Time (GMT)	Temp (°C)	Weather	Computed Temp./ Std. Dev. (°C)
1800	8	4/10 high cloud	3.7 / 0.65

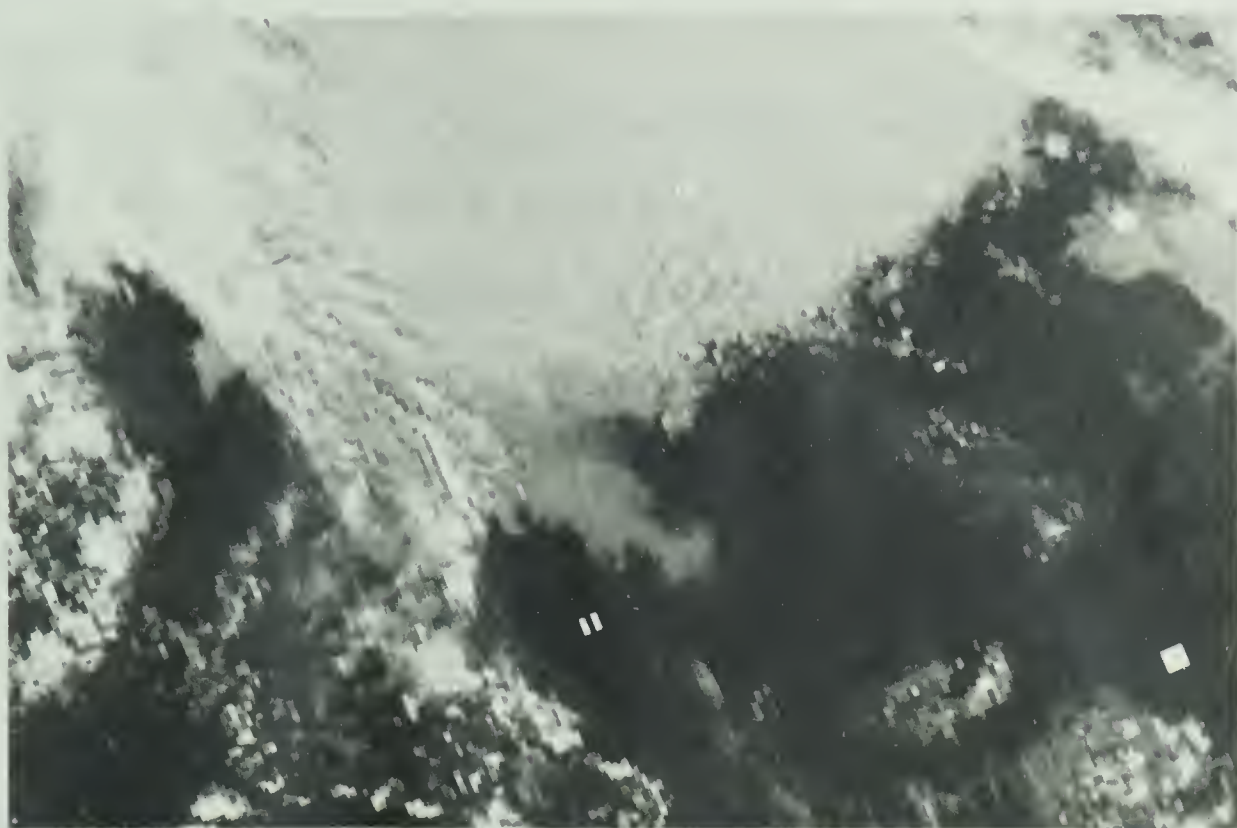


FIGURE 4.4a Visible image, July 28, 1977, Orbit 4508.

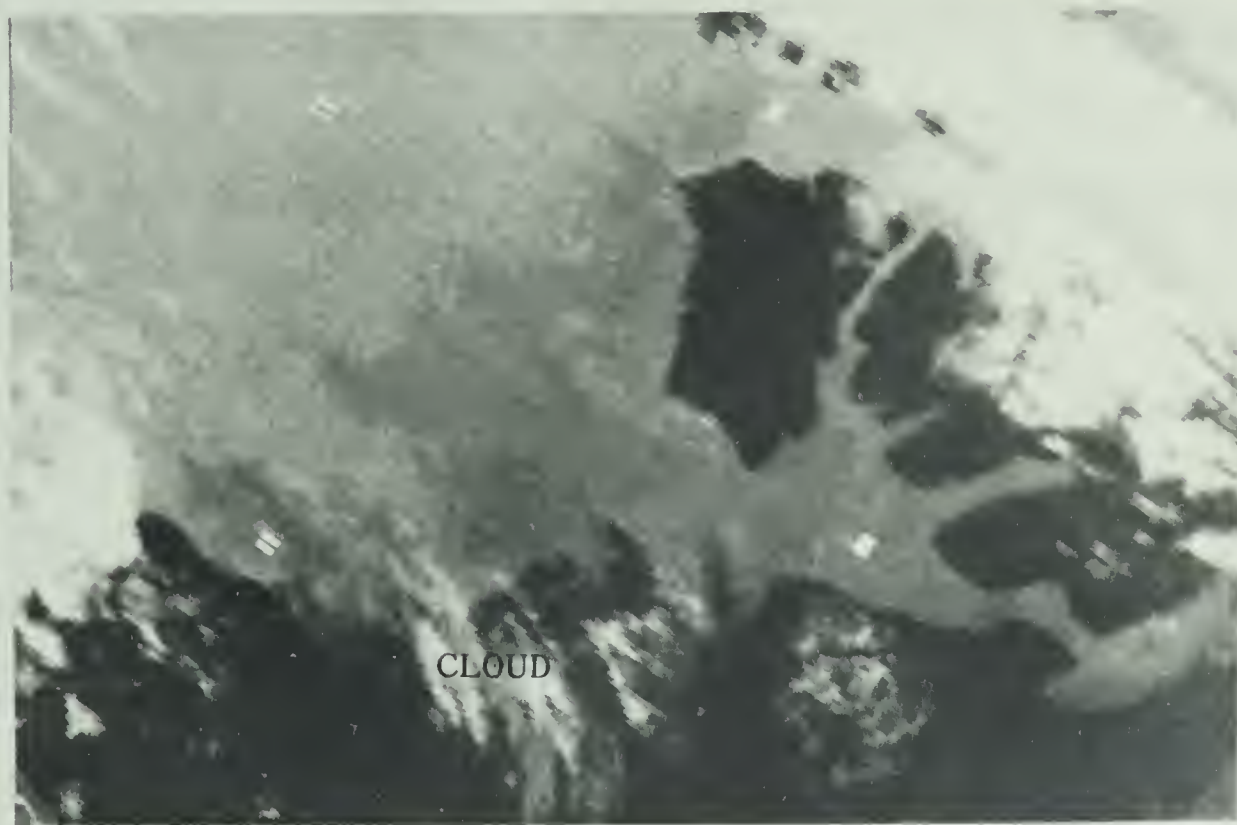


FIGURE 4.4b IR image, July 28, 1977, Orbit 4507.

A temperature of about 3°C is indicated on Figure 4.3a; the discrepancy may be due to cloud contamination, or factors mentioned in the previous case.

With reference to the temperature gradient analysis, Figure 4.3b, the locus of maximum gradient again separates open water from very open pack ice in the northeast portion of the study area. The $1^{\circ}\text{C}/^{\circ}\text{L}$ line separates close and open pack ice in this region. In other areas the $1^{\circ}\text{C}/^{\circ}\text{L}$ line is not a reliable one in making correlations; however, most areas in the southwest study area with ice concentrations of 7/10 or greater are below this gradient value.

4.4 Case Study 3, August 14, 1977

4.4.1 Synoptic Situation

The general synoptic situation for August 14 is not as favourable for clear skies as were the previous two cases. The presence of a weak low near the Yukon-Alaska border poses a potential cloud-contamination problem in this area, as displayed in Figure 5.23.

4.4.2 Verification

The relevant ice information is contained in Overlay 2, for the week ending August 12, 1977. The derived surface temperature and temperature gradient analyses, for Orbit 4718, are shown in Figure 4.5a and 4.5b, respectively.

Judging by the isotherm pattern produced in Figure 4.5a, the extreme northeast and southwest study regions may be too cloud-contaminated to be of use in making comparisons. The best correlations

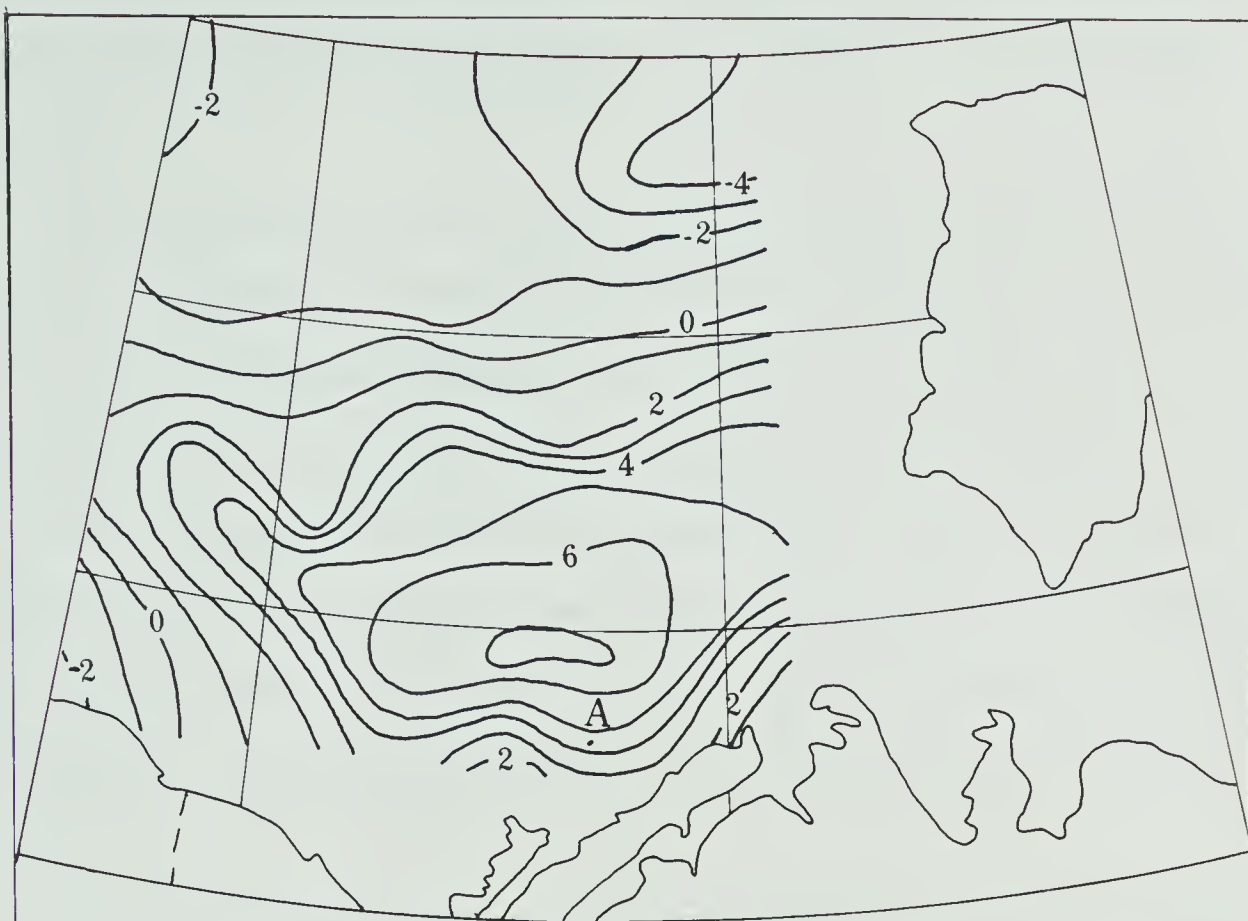


FIGURE 4.5a Isotherm analysis: August 14, 1977, Orbit 4718.

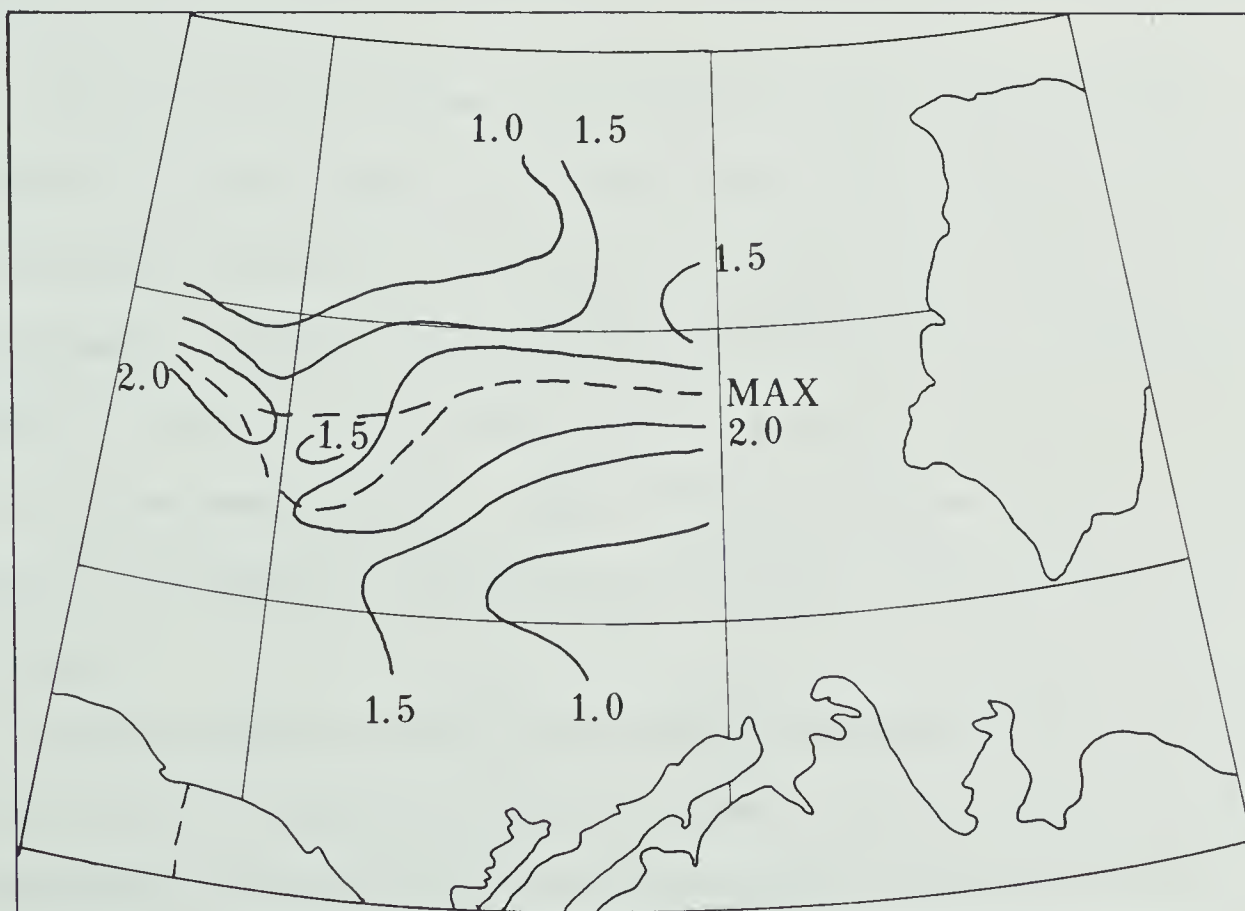


FIGURE 4.5b Temperature gradient analysis: August 14, 1977, Orbit 4718.

are the 1°C isotherm separating open water and very open pack ice areas, and the -1°C isotherm separating close and open pack multi-year ice.

The relevant satellite images are displayed in Figures 1.2 and 1.3. The cloudiness discussed above is identifiable in these images. Along the ice edge there appear to be wave-like features which are represented as temperature minima in Figure 4.5a; these may be areas of recent melting not depicted on the ice chart. The warm area in the south central region matches the corresponding area on the analysis, and the cool area along the Arctic Coast east of Tuktoyaktuk is also detectable; a further examination of this region will be done in Chapter V.

The comparison of ground-truth information to satellite-derived temperatures was done in Chapter III. The discrepancy is apparently less than one degree.

The correlations between ice conditions and the temperature gradient analysis, Figure 4.5b, are somewhat different for Case 3. The maximum gradient locus in all but extreme eastern areas (due to cloudiness) separates open water from very open pack ice conditions. However, a gradient of $1.5^{\circ}\text{C}/^{\circ}\text{L}$ seems more reliable here as a separation of close and open pack ice. (Note that some gradient values in eastern sections are missing, and any correlations made there are likely unreliable.)

It is evident that there is a secondary maximum which correlates better with ice conditions than the primary maximum. When looking for correlations, it may be that the first maximum encountered is the relevant one, as the progression towards lower ice concentrations is made.

4.5 Discussion

4.5.1 Surface Temperatures

Judging from the few situations examined here, the histogram analysis technique is reliable enough to permit a brief discussion of identifiable surface characteristics of the Beaufort Sea.

Multi-year ice surfaces are generally of temperatures below 0°C . Temperatures over first-year ice are somewhat higher and more variable, depending on local insolation conditions. This observation is sensible since first-year ice is typically thinner than the older ice and may thus be more subject to flooding and, due to an inherently thinner snow cover, to surface melting. Typically, sea ice forms at between -1°C and -2°C , depending on the salt content of the water. The salt largely separates upon freezing, and subsequent melting of this nearly-fresh water will be at near 0°C . Thus large puddles atop first-year ice at temperatures of 0° to 2°C are quite possible, with large daily fluctuations, depending on solar heating inhomogeneities. Thus in a season such as the Arctic summer, the 0°C isotherm, as derived above, may be of little use in terms of reliable correlations, over first-year ice especially.

4.5.2 Temperature Gradients

The use of temperature gradients to delineate ice concentrations shows that only gross correlations are possible, and likely only in terms of multi-year ice conditions. One problem inherent to these comparative studies is the large concentration difference present in the reported regions of very open pack ice thru open pack ice. The

ice conditions were grouped in this manner to simplify the verification procedure somewhat. Depending on local conditions and the ice observer, the concentration change may be gradual or dramatic. This condition may explain why different gradient values work for different days. Despite this shortcoming the temperature gradient method of depicting general ice conditions has merit.

CHAPTER V
ON THE USE OF COMPOSITE HISTOGRAMS IN
DERIVING SEA-SURFACE TEMPERATURES

5.1 Introduction

Surface temperatures have now been mapped for the Beaufort Sea in predominantly clear sky conditions, away from coastlines. The final questions posed in Chapter II are now examined in more detail.

5. Can clouds be filtered in some reliable manner?
6. Can coastal areas be included in analyses?

The results of Chapter IV indicate that CMT charts discussed earlier may not be viable over the ten-day interval used elsewhere, since the surface temperatures have been found to change rapidly under conditions of strong solar heating. Similarly, the maximum temperature in a square intersected by land will typically not be representative of the adjacent water temperature in summer.

The following computational procedure is proposed. Data are accumulated in appropriate bins over a number of consecutive days. These "composite" histograms are subsequently analysed for the appropriate information. Over a (short) period of time, the surface temperature in each bin is assumed constant; only very persistent cloudiness at a temperature very near the true surface temperature will substantially affect the analysis. By using data obtained from near

mid-day orbits, a large separation of modes representing land from sea should be possible. The use of the "cold-mode" scanning technique should allow retrieval of sea temperatures where both modes are present in the distribution.

The basic problem may now be formulated as follows: How many days of data may be composited to achieve maximum cloud filtering and minimum surface temperature changes?

5.2 Formation of a Composite Temperature Analysis

In the development of the compositing technique, the effect of addition of data on a daily basis is examined; the progressive screening of clouds may be subjectively studied in the format of the first of three case studies.

A more objective assessment of the compositing technique would be desirable. There are 208 bins subject to analysis in the study area, of which 84 are either partially or completely land-covered. By determining the fraction of areas for which an acceptable mean value is derived, a "recovery efficiency" is obtained. Areas over land or with obvious low-cloud contamination present are included in this calculation; however, the same land areas are present in each analysis, and clouds should have a generally decreasing effect on this determination, as the compositing interval increases. Thus the recovery efficiency should be a reliable relative measure of the compositing technique.

5.3 Case 1, July 05-08, 1977

5.3.1 Synoptic Situation

The synoptic information for the relevant period, displayed in Figures 5.1 to 5.4, illustrates that generally fair weather prevailed over the study area during this period. On July 5 a north to south ridge of high pressure extended through 120°W, while a weak low was situated near 71°N, 141°W. On July 6 a surface high pressure cell was situated over Victoria Island, with a trough of low pressure along the northern Alaska coast to Tuktoyaktuk. The high migrated to the central study area by July 7, and then to the western section of the study area on the 8th, allowing a moderate northwesterly flow to develop over Banks Island and adjacent waters.

Cloud contamination effects should not be a major concern in this case (except possibly on July 8) since mainly clear skies or transient cloud affected the area. Thus relatively few days' data should be required to remove cloud effects.

5.3.2 Building the Composite Chart

The effect on the surface temperature field of accumulating data is apparent when Figures 5.5 to 5.8 are examined. The cloudiness present on July 5, and again when a composite of data from July 5 and 6 is produced, is apparently eliminated when the third day is added in Figure 5.7. Structures of note which persist in all three Figures are the cold area at the south tip of Banks Island, and the warm area just to the west of the island. If the data from July 8 are added into the three-day composite chart, producing the four-day composite, Figure

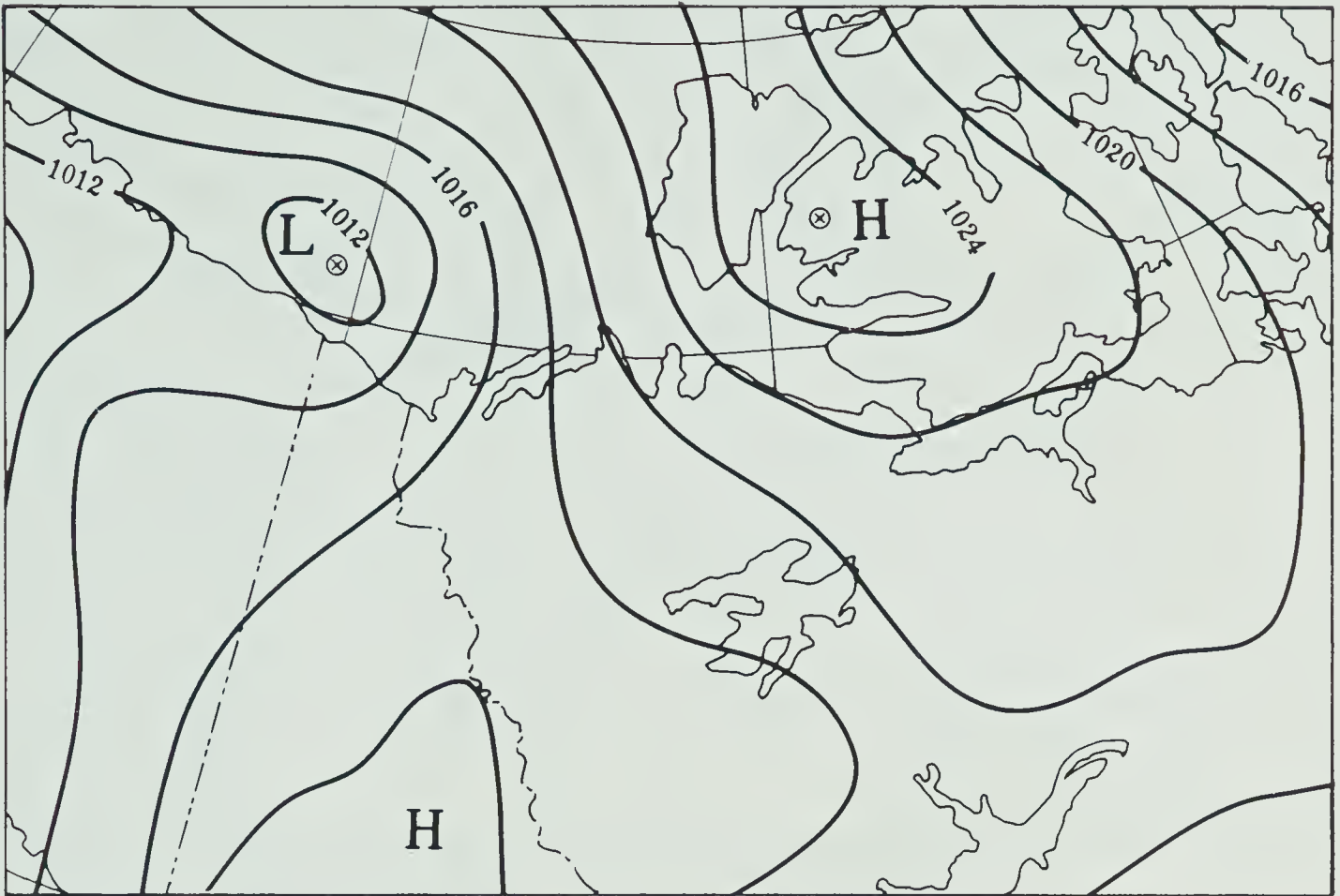


FIGURE 5.1 BAB surface map: July 5, 1977, 1800 GMT.

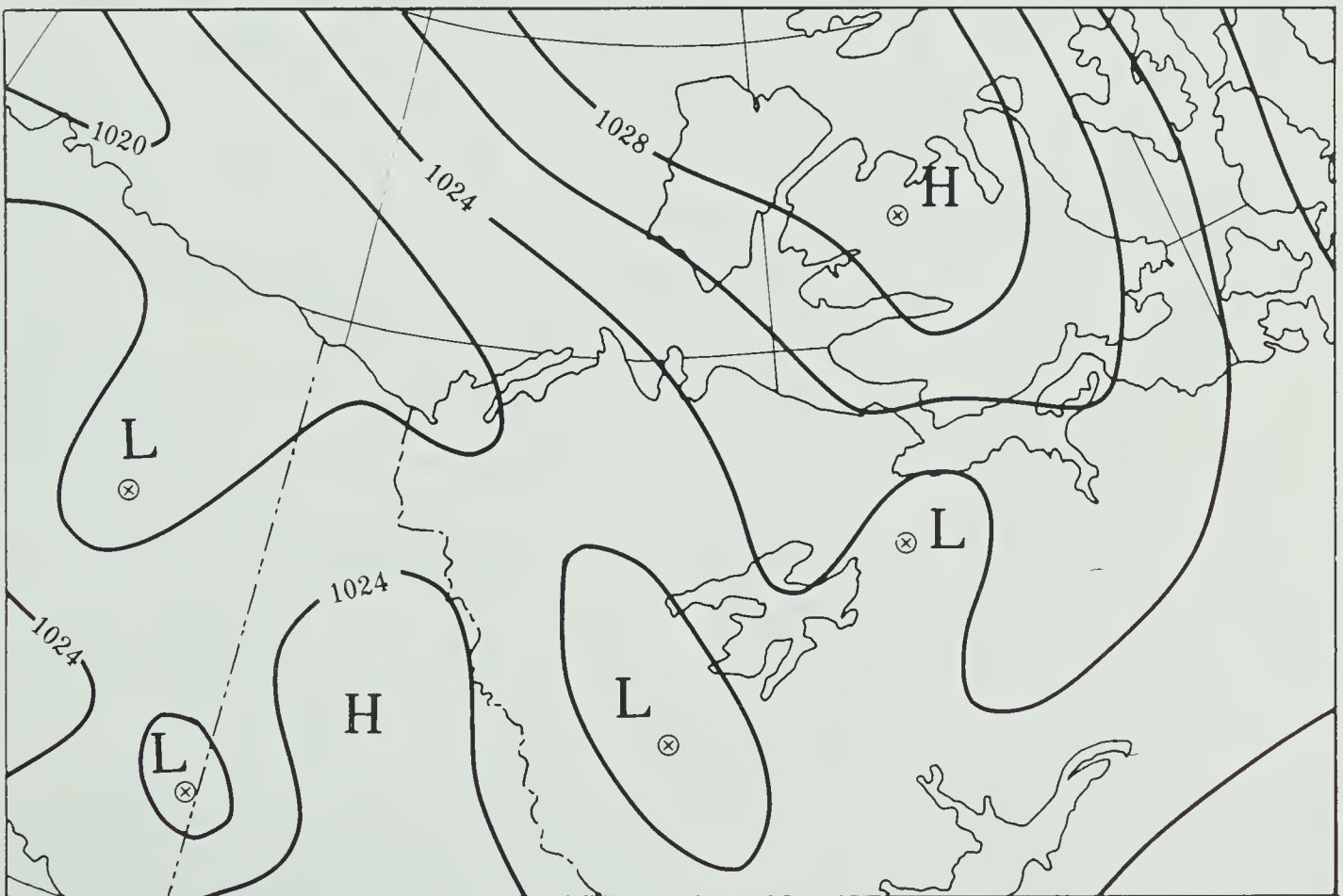


FIGURE 5.2 BAB surface map: July 6, 1977, 1800 GMT.

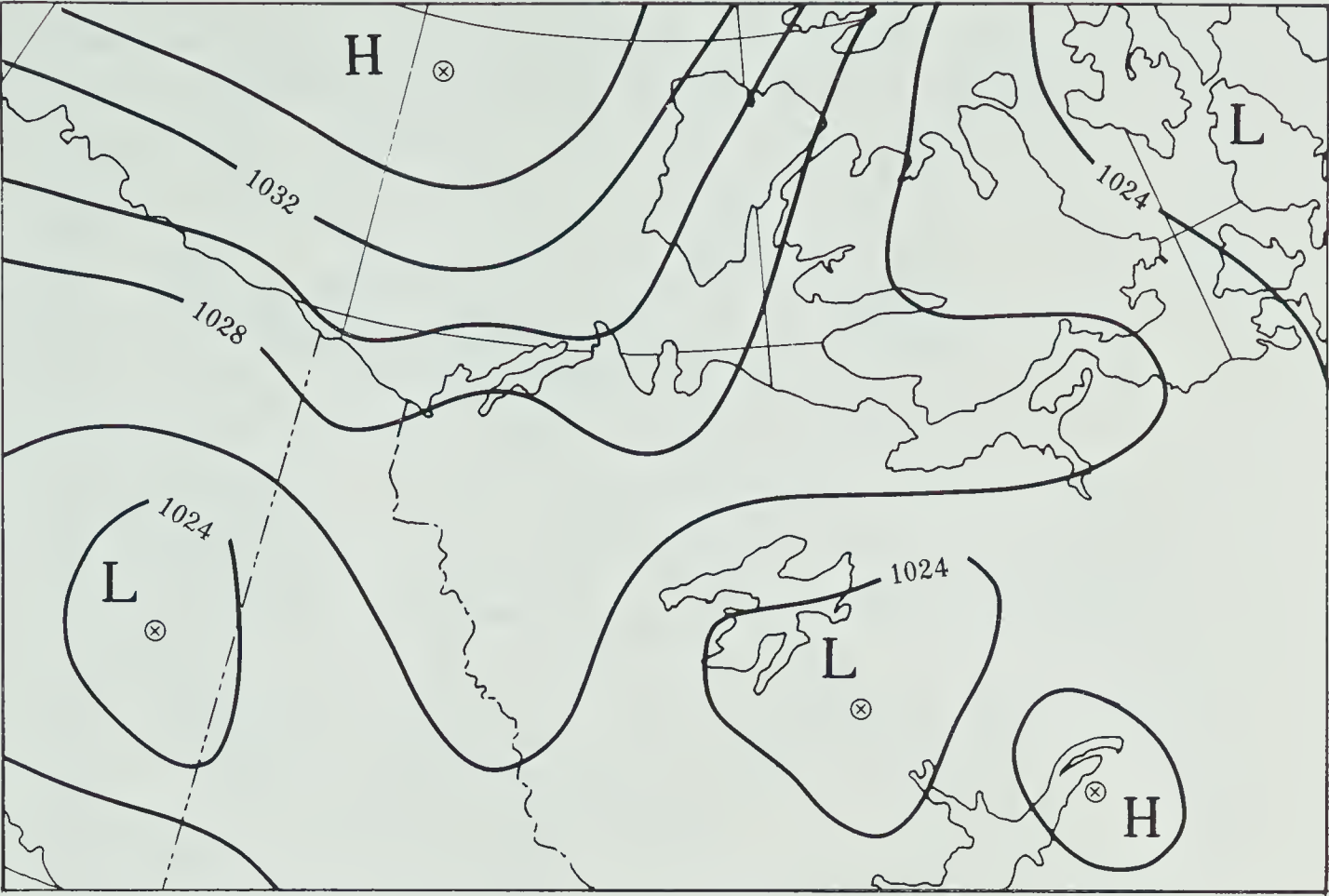


FIGURE 5.3 BAB surface map: July 7, 1977, 1800 GMT.

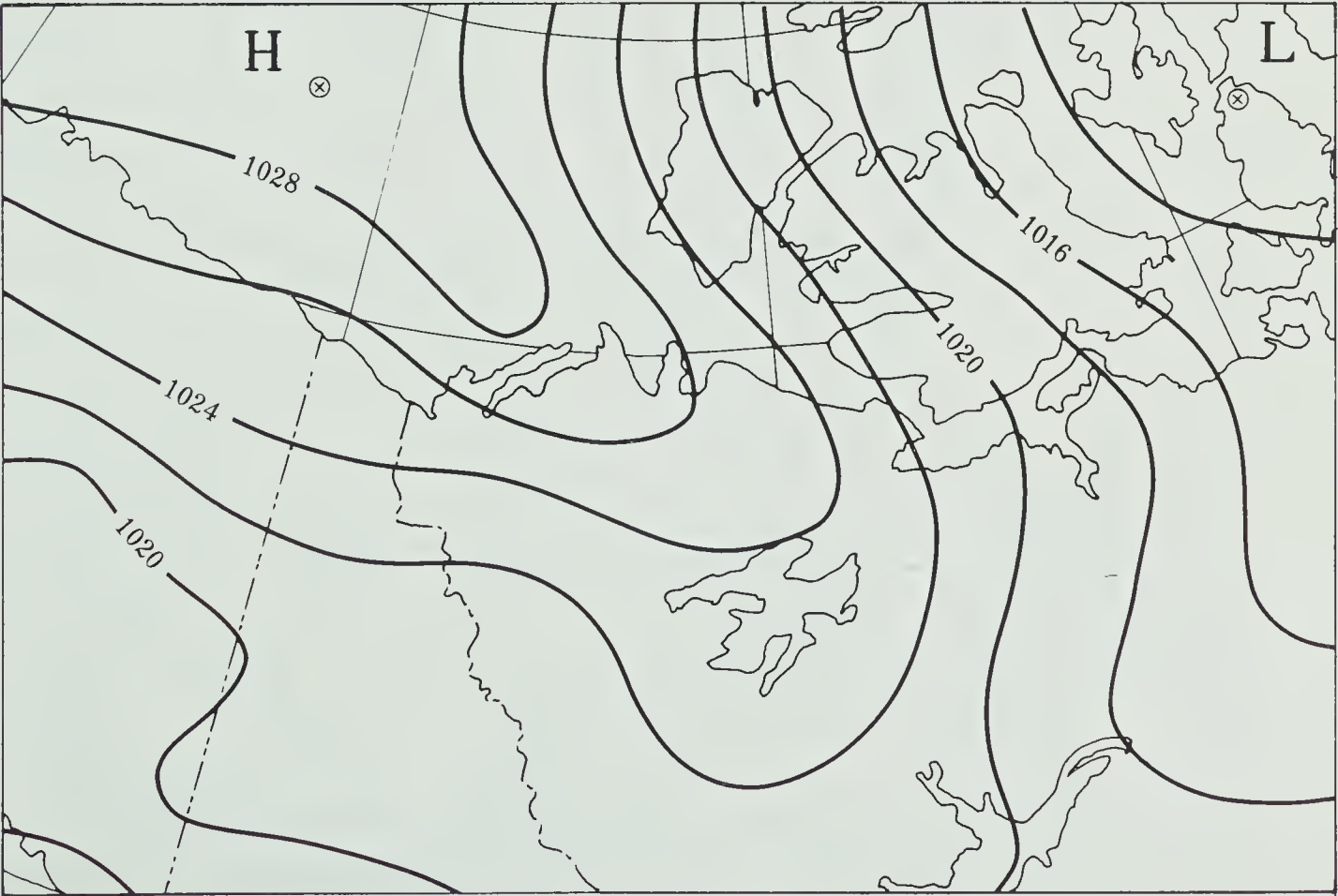


FIGURE 5.4 BAB Surface map: July 8, 1977, 1800 GMT.

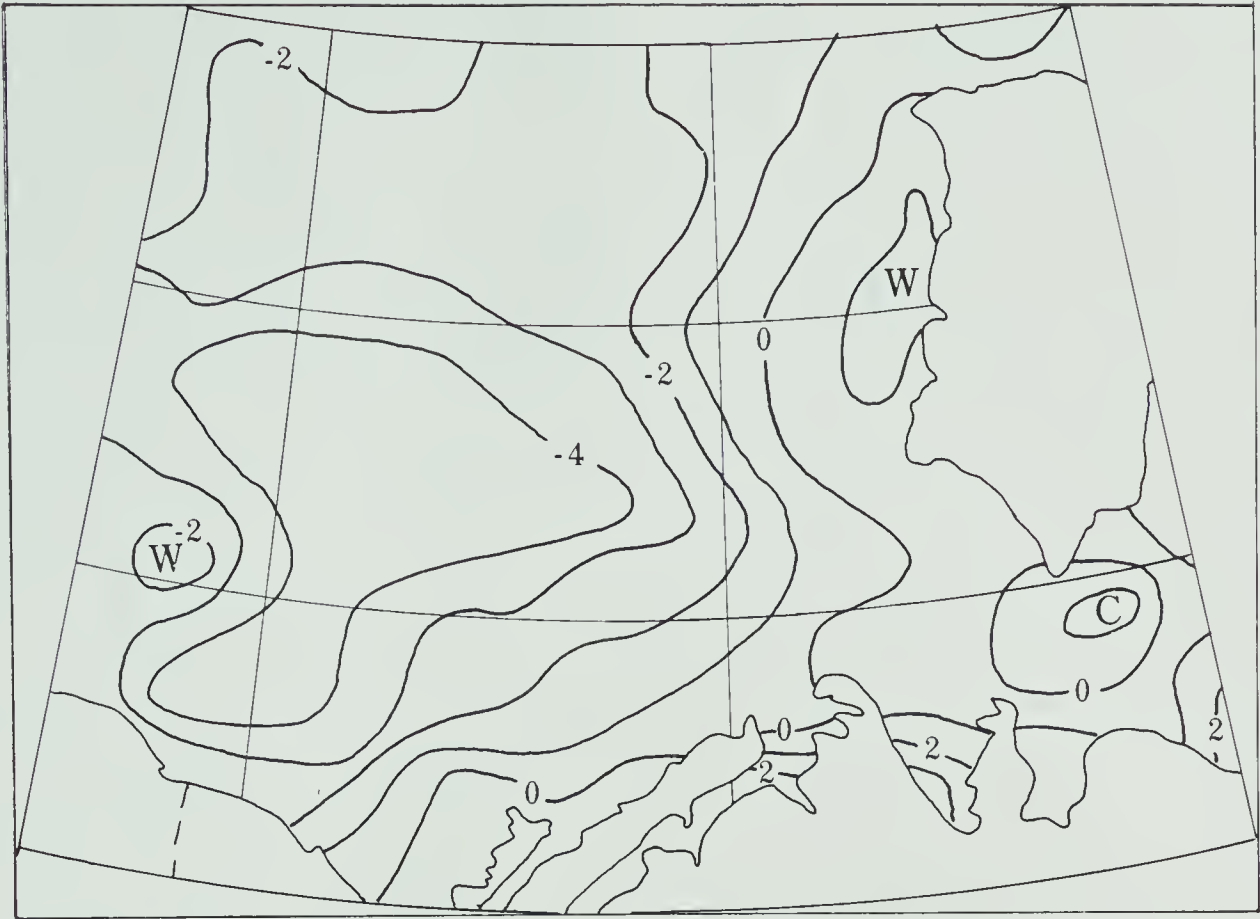


FIGURE 5.5 Isotherm analysis: July 5, 1977, Orbit 4222.

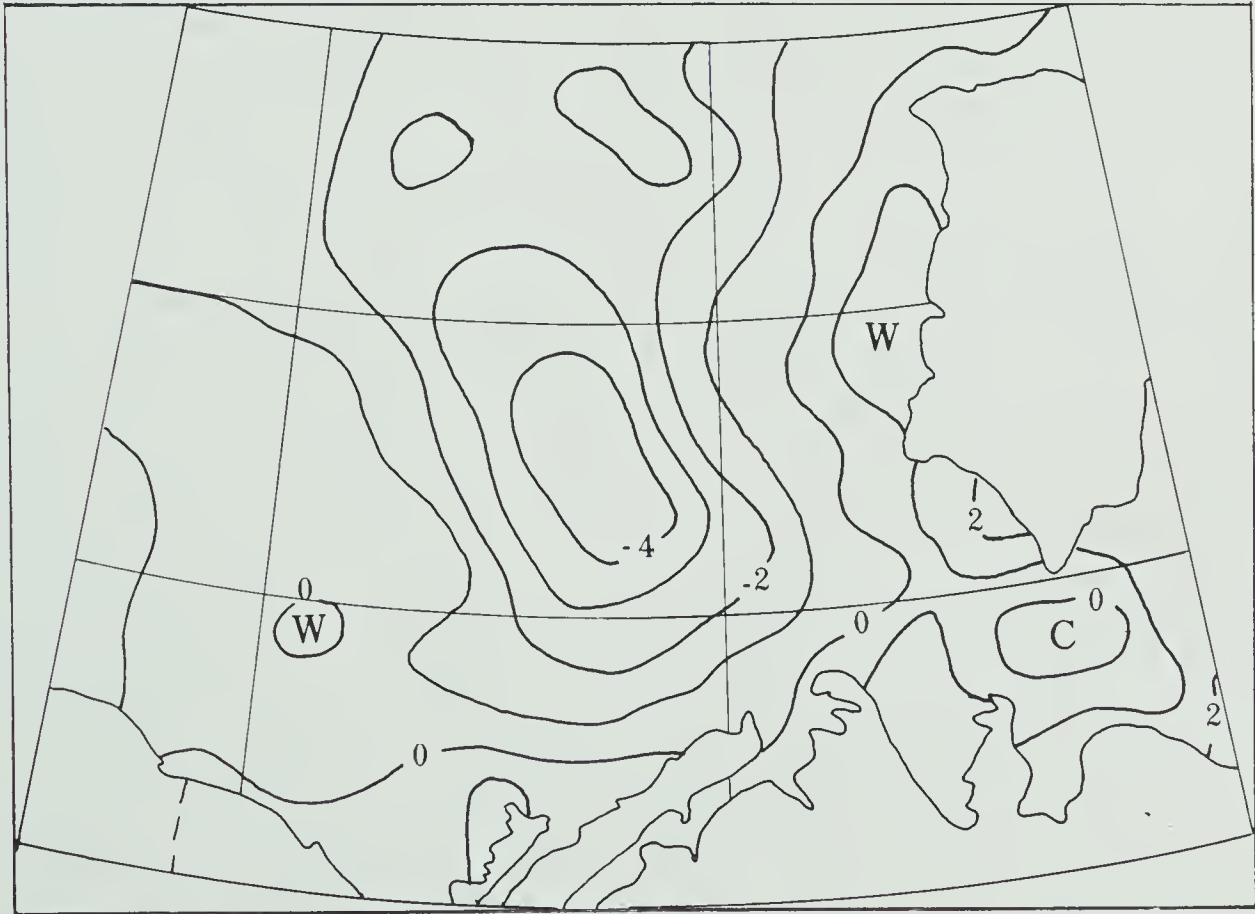


FIGURE 5.6 Composite isotherm analysis: July 5-6, 1977, Orbits 4222 and 4235.

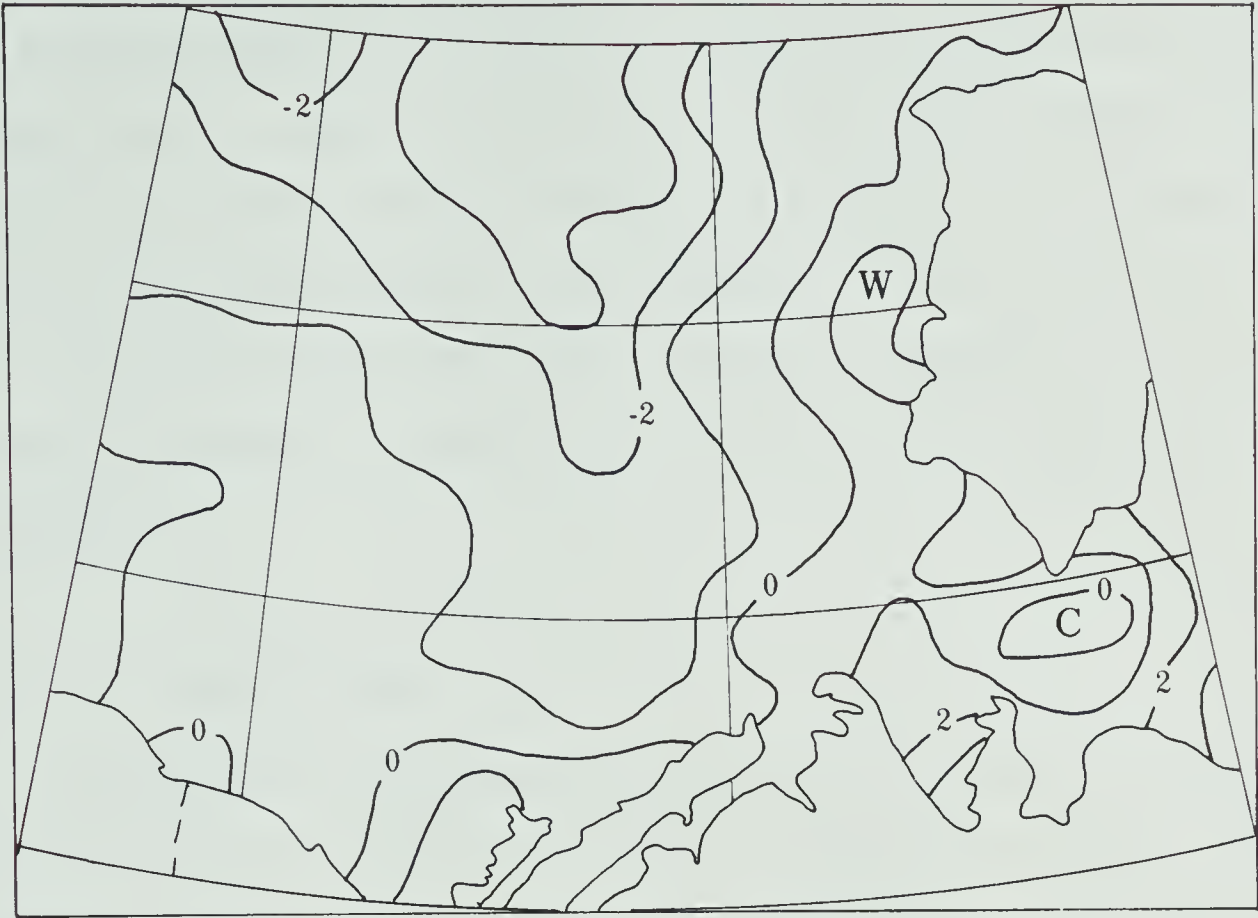


FIGURE 5.7 Composite isotherm analysis: July 5-7, 1977, Orbits 4222, 4235 and 4247.



FIGURE 5.8 Composite isotherm analysis: July 5-8, 1977, Orbits 4222, 4235, 4247 and 4259.

5.8, further cloud filtering effects are found to be minor. However, the three-day composite for July 6-8, Figure 5.9, displays identifiable changes from the similar composite for July 5-7. The cold area south of Banks Island has shrunk, a 2°C isotherm is present near Tuktoyaktuk, and the coastal bay adjacent to the Amundsen Gulf has warmed appreciably. All changes are probably the result of insolation effects. From this cursory examination, a three-day compositing interval yields worthwhile information.

5.3.3 Verification

The relevant ice information in Appendix F (Overlay 3) is representative of mean conditions for the week ending July 8, 1977. With reference to Figures 5.7 and 5.9, the -1°C isotherm on each composite, running generally north to south in the central study area, matches quite well the close pack versus open pack ice boundary. In southern areas the zero degree isotherm provides a similar correlation. The ice island south of Banks Island is reproduced on both composites.

The IR data for this study are taken from Orbits 4222, 4235, 4247 and 4259 of NOAA-5; since much cloud covered the study area on July 8, images for Orbit 4259 are not displayed. Figure 5.11 displays the image for Orbit 4247 on July 7; examination of this Figure and Figure 3.3 shows the relatively warm areas just west of Banks Island that are identifiable on the composite analyses. The area analysed between 0°C and -1°C northwest of Tuktoyaktuk appears as small dark spots on Figure 5.10a, the visible image for Orbit 4235. The same area is not readily detectable on the corresponding IR image, Figure 5.10b. This region



FIGURE 5.9 Composite isotherm analysis: July 6-8, 1977, Orbits 4235, 4247 and 4259.

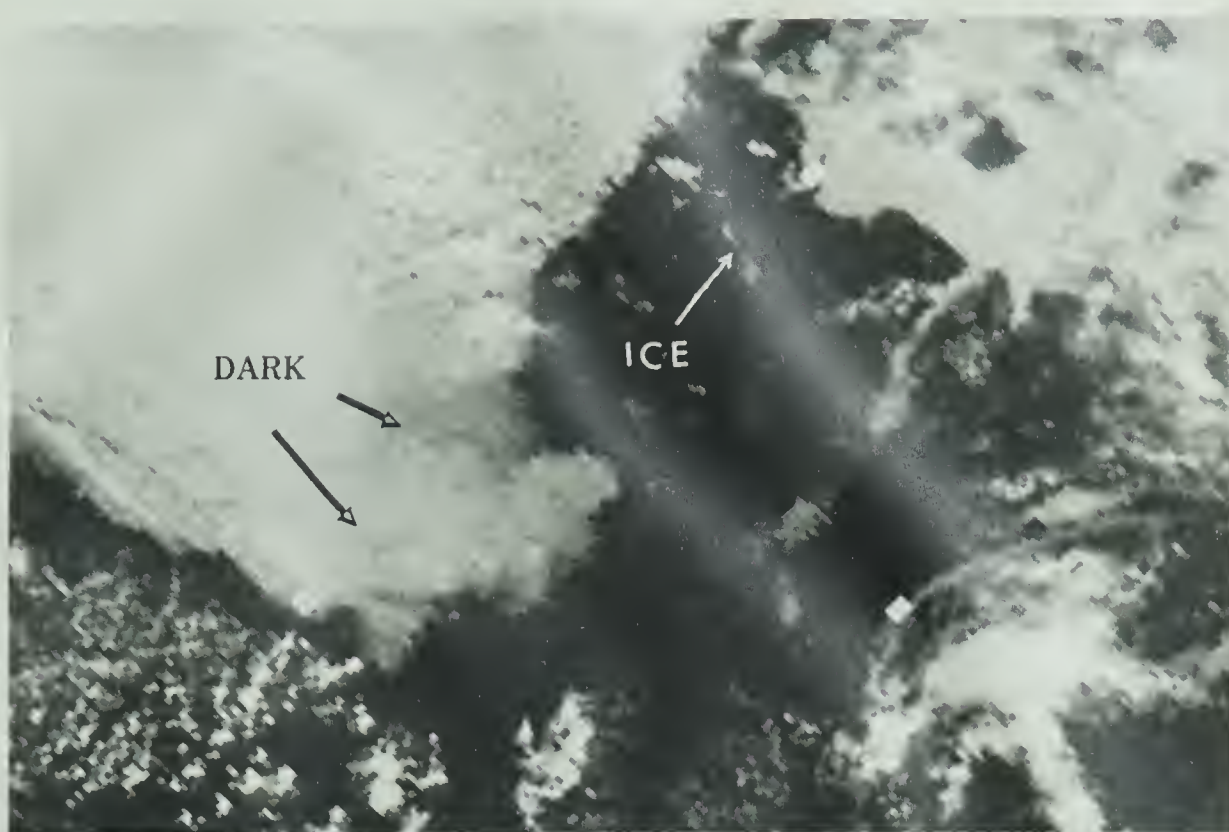


FIGURE 5.10a Visible image, July 6, 1977, Orbit 4235.

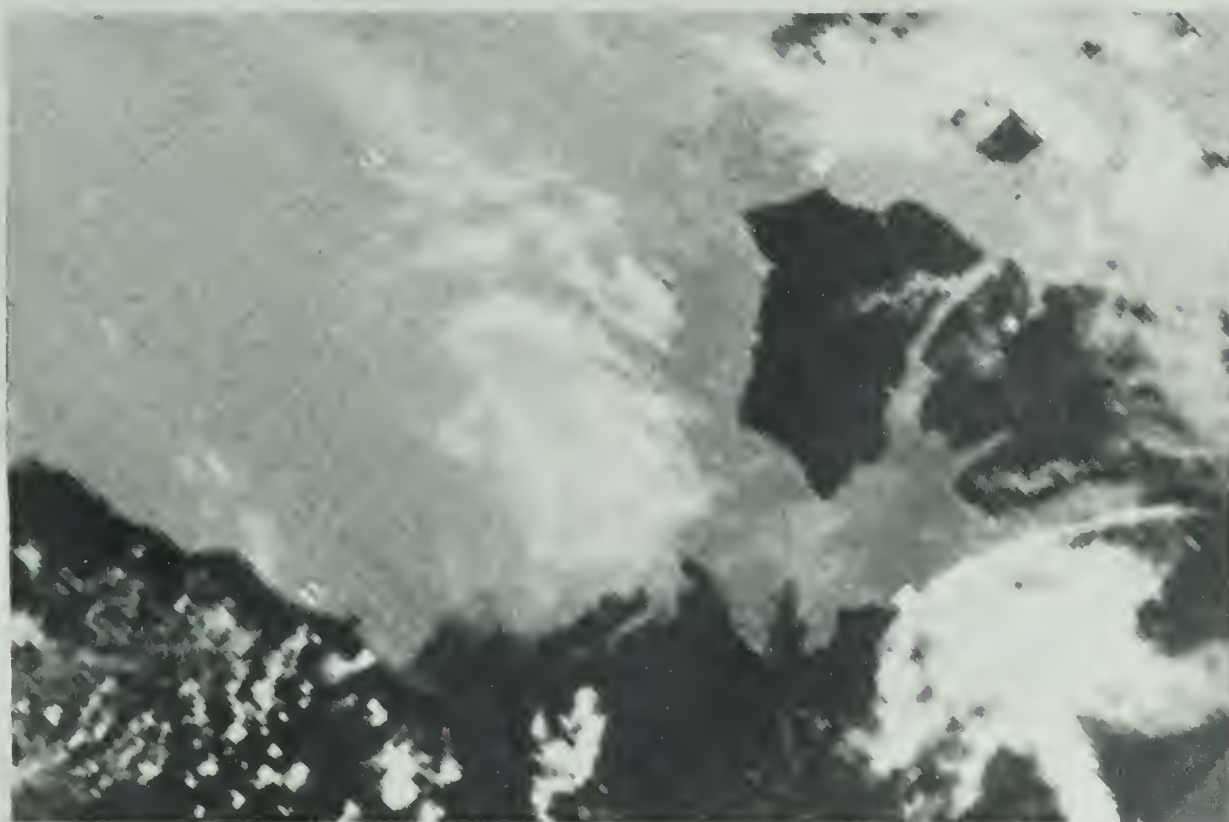


FIGURE 5.10b IR image, July 6, 1977, Orbit 4235.

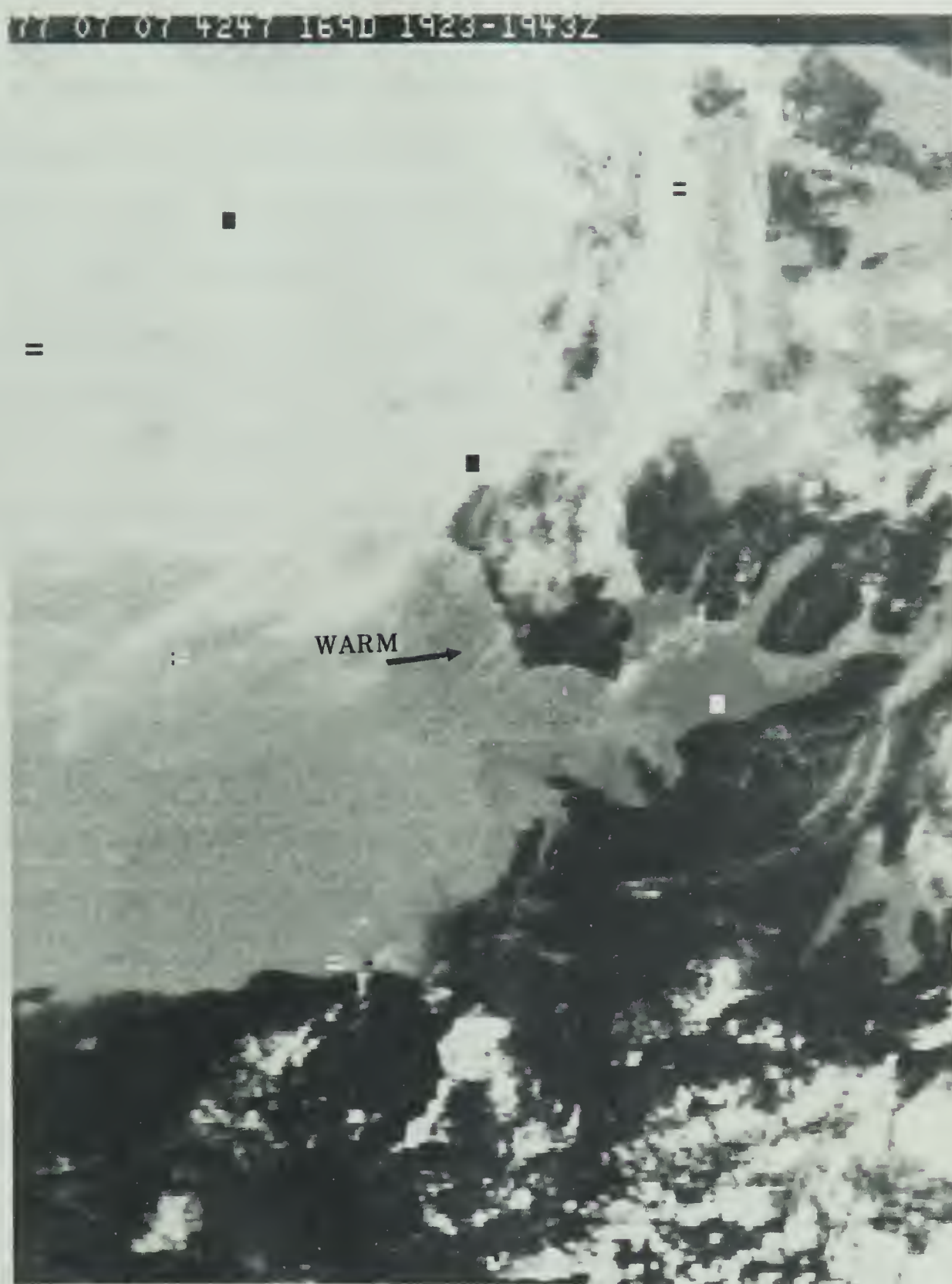


FIGURE 5.11 IR image, July 7, 1977, Orbit 4247.

is presumably one where puddles have formed on a large expanse of first-year ice.

Examination of Figure 5.10a also reveals shore-fast ice along the northern west coast of Banks Island; these areas are identifiable on Figures 5.7 and 5.9 as temperature minima.

It remains to check absolute temperature values produced by the composite analyses with ground-truth measurements. Unfortunately, no data are available for this particular case. However, since correlations with ice conditions found here match reasonably well those described in Chapter IV, the attenuation effect is likely fairly small.

5.3.4 Statistical Summary

In terms of recovery efficiency and mean values of standard deviations computed in the analyses, the effect of different compositing intervals is shown in Table 5.1. All combinations possible in a four-day period are included; that is, four one-day analyses, three two-day analyses, and so on.

The fluctuations in number of areas recovered and in mean standard deviation (for all areas where a mode was computed), are greatly reduced as the compositing interval increases.

The maximum recovery efficiency occurs for a three-day interval; the detail obscured due to cloud on, for example, the two day composite, Figure 5.6, suggests a two-day interval may suffer in this respect in spite of a high and relatively stable recovery efficiency. This revelation suggests that a simpler compositing technique, where it would be necessary merely to check the current days's data as an "update" to the previously obtained temperature, may not be feasible.

TABLE 5.1
Statistical Summary of Compositing
Case 1, July 5-8, 1977.

# Days of Data	1	2	3	4
Areas Recovered (/208)	162 165 173 15	170 151 165	167 164	163
Recovery Efficiency (%)	61.9	77.9	79.6	78.4
Mean Std. Dev. (M.S.D.) (°C)	.99 1.03 .99 1.29	1.20 1.11 1.04	1.19 1.12	1.19
Mean of M.S.D. . (°C)	1.08	1.12	1.16	1.19

The contention that resolution of the sea temperature regime for regions intersected by land may be obtained is verified by examination of any of the composite analyses. Table 5.2 summarizes the recovery of water- (or ice-) only areas and all other areas for Case 1. About 90% of water-only areas are recovered while close to 60% of land-contaminated areas are also recovered using the cold-mode scanning method.

TABLE 5.2
Compositing Over Land- or Water- Covered Areas,
Case 1.

Interval	Number Recovered		
	Water Only (/124)	Other (/84)	All (/208)
July 05 - 08	115	49	164
July 06 - 08	112	55	167
July 05 - 08	115	48	163

5.4 Case 2, July 27-31, 1977

5.4.1 Synoptic Situation

The synoptic situation for the final days of July, 1977 is displayed in Figures 5.12 to 5.16. Generally, high pressure dominated the northern Beaufort Sea during this period, while on July 28, 30 and 31 a weak low center or trough of low pressure lay near 70°N, 138°W.

5.4.2 Verification

The three relevant three-day composites for this study are displayed in Figures 5.17, 5.18 and 5.19, from data taken from Orbits 4495, 4507, 4519, 4532 and 4544 of NOAA-5. Overlay 2 from Appendix F contains the pertinent ice information, showing that the ice belt in the southern Beaufort Sea is identifiable on all three composite analyses. In Figure 5.17, temperatures between 0°C and 1°C delineate very open, and open pack ice concentrations in the northeast areas. Changes appear to be occurring in this area as the above correlation is not evident on the

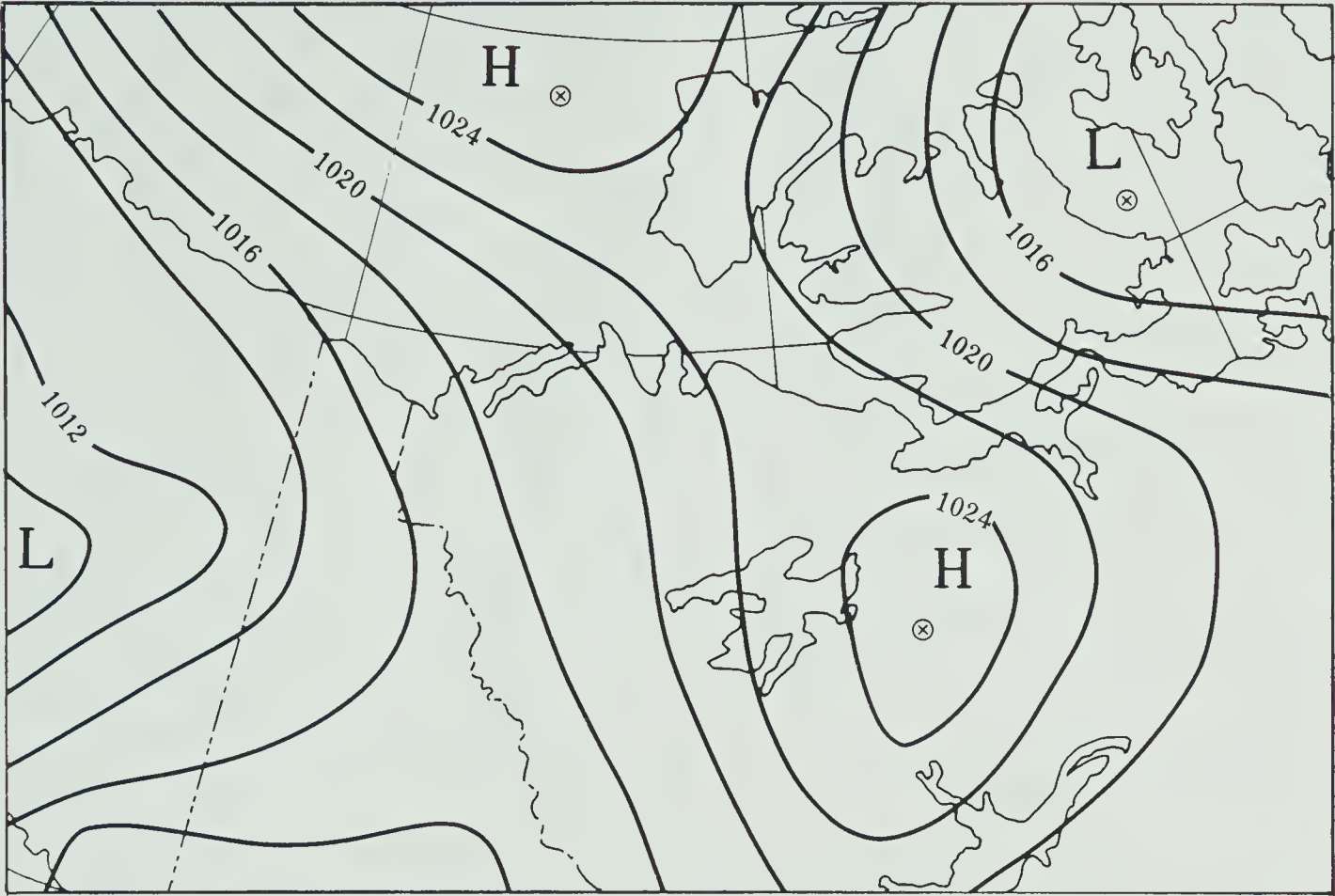


FIGURE 5.12 BAB surface map: July 27, 1977, 1800 GMT.

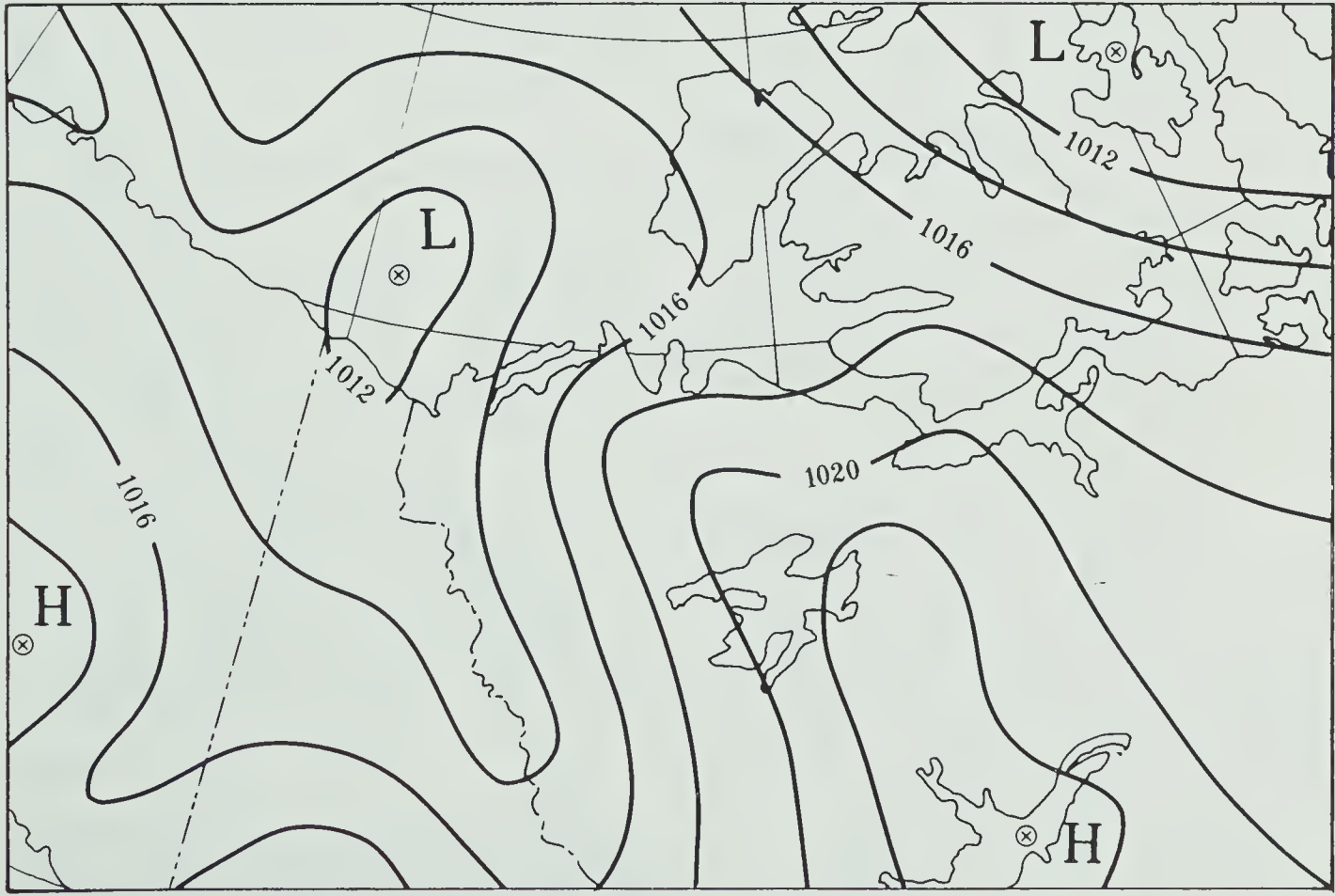


FIGURE 5.13 BAB surface map: July 28, 1977, 1800 GMT.

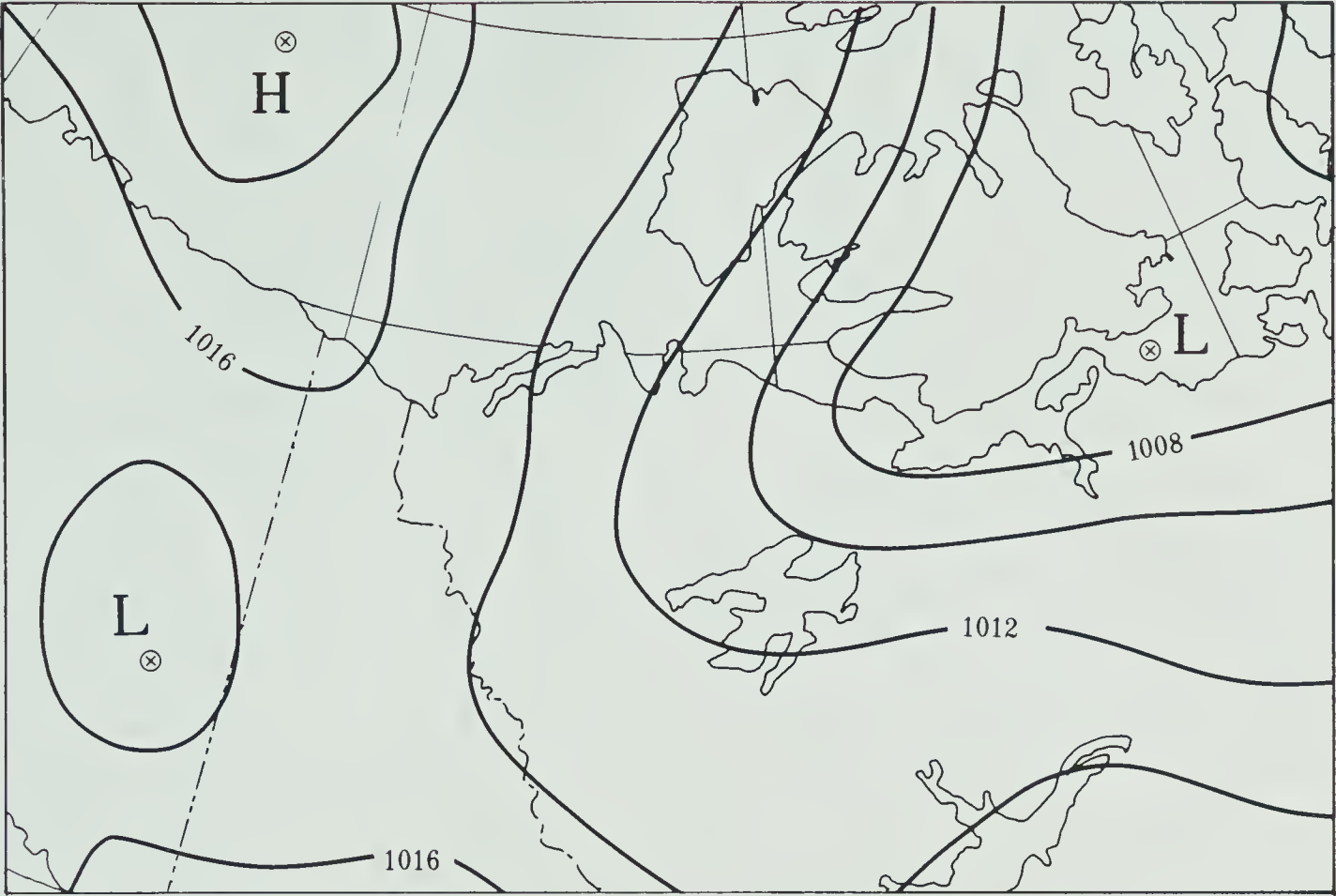


FIGURE 5.14 BAB surface map: July 29, 1977, 1800 GMT.

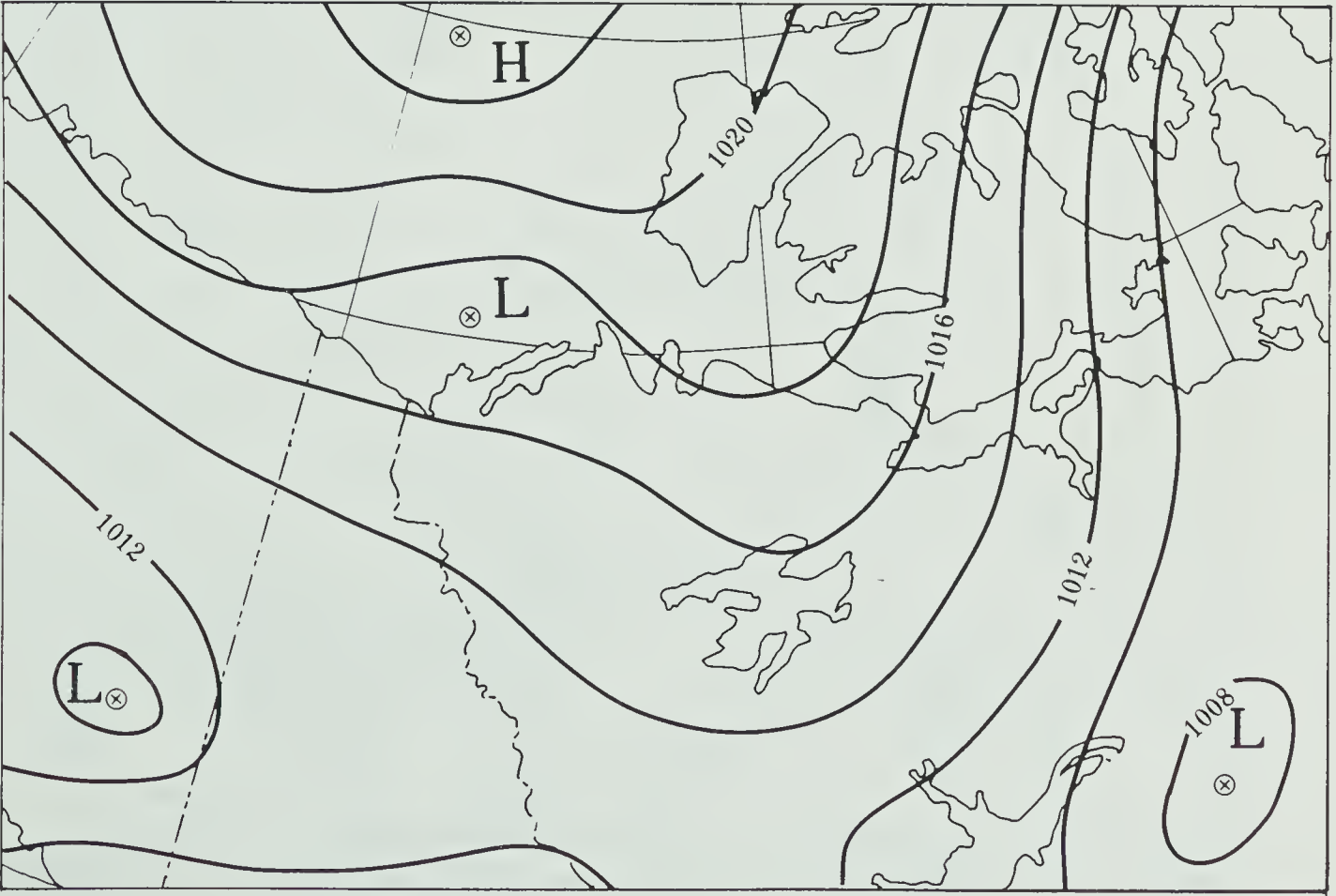


FIGURE 5.15 BAB surface map: July 30, 1977, 1800 GMT.

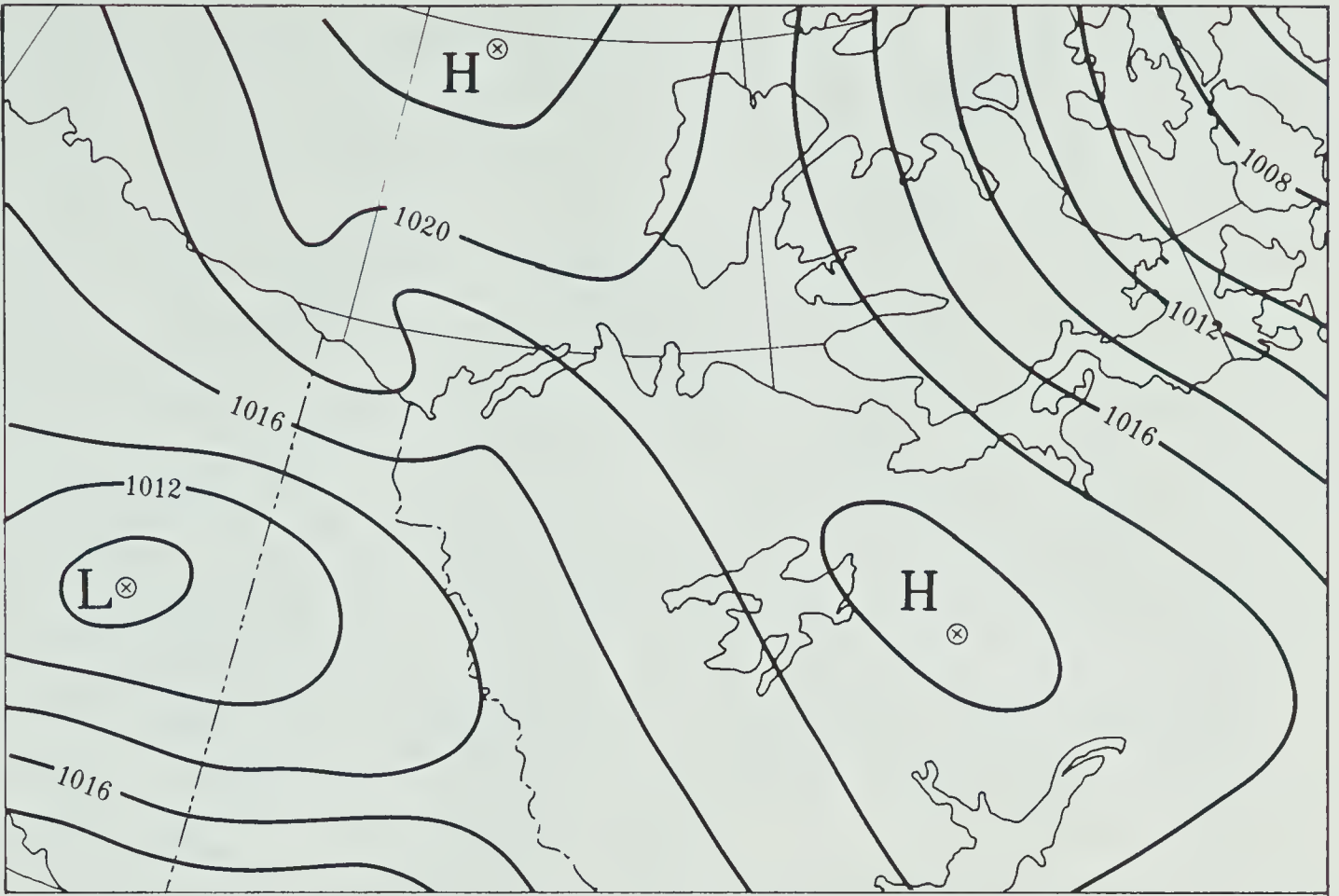


FIGURE 5.16 BAB surface map: July 31, 1977, 1800 GMT.

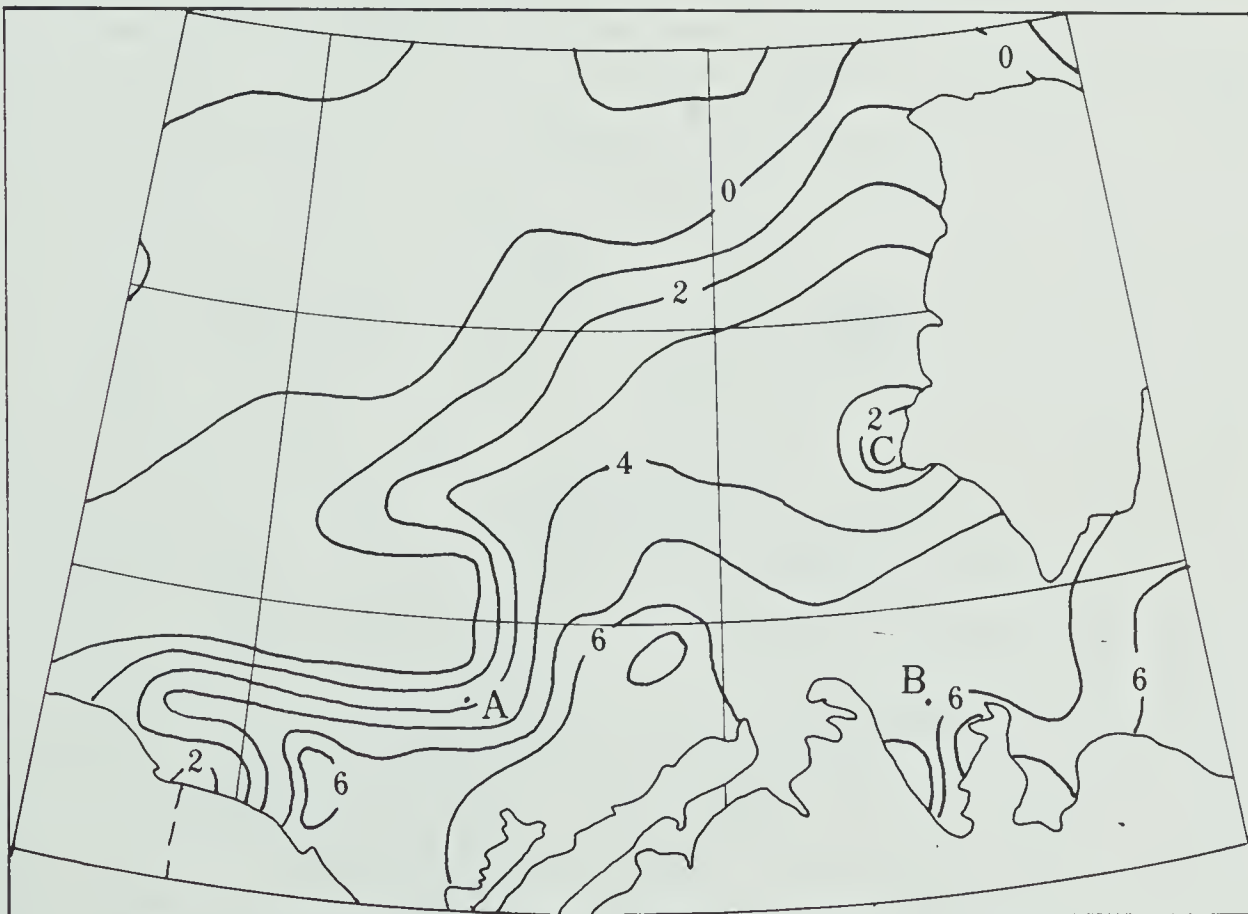


FIGURE 5.17 Composite isotherm analysis: July 27-29, 1977, Orbits 4495, 4507 and 4519.

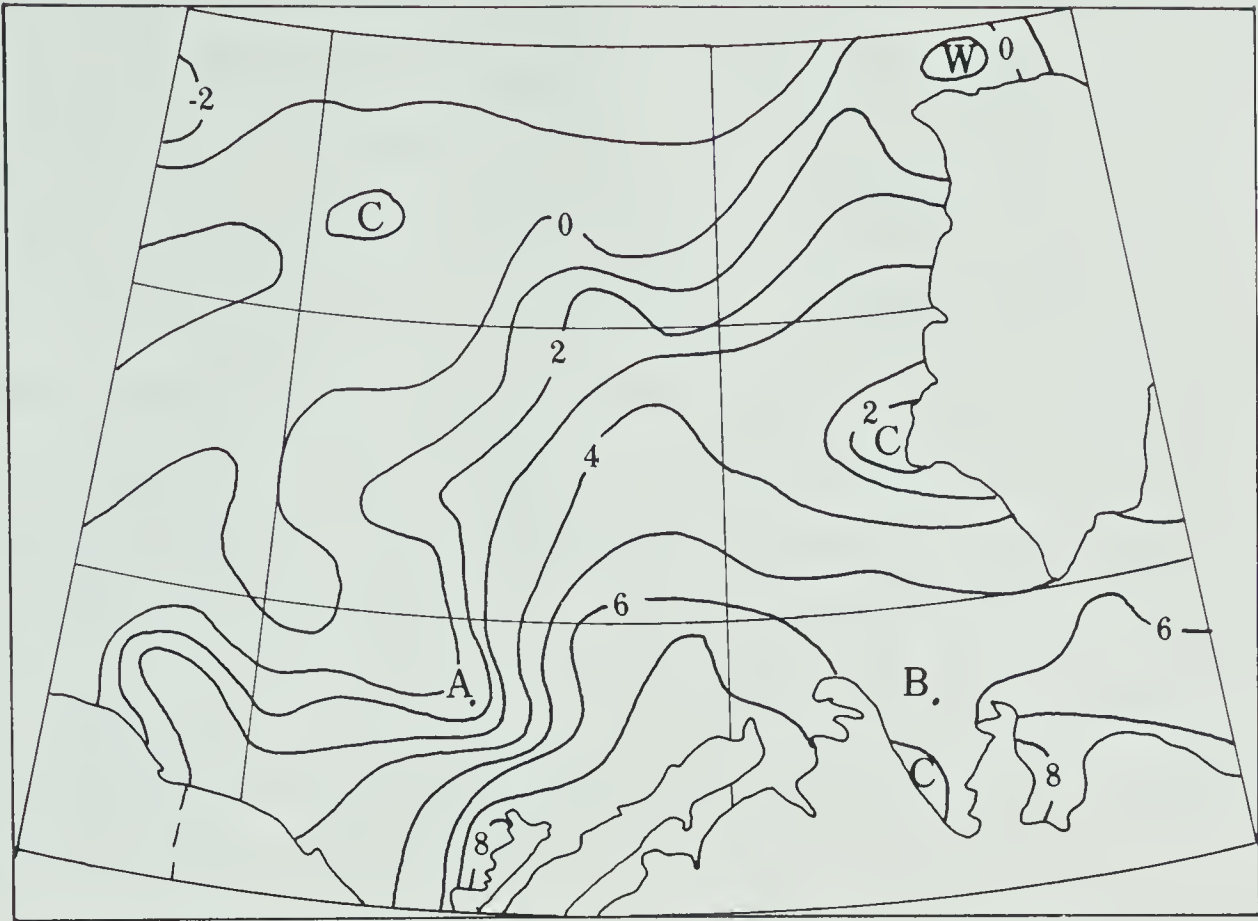


FIGURE 5.18 Composite isotherm analysis: July 28-30, 1977, Orbits 4507, 4519 and 4532.

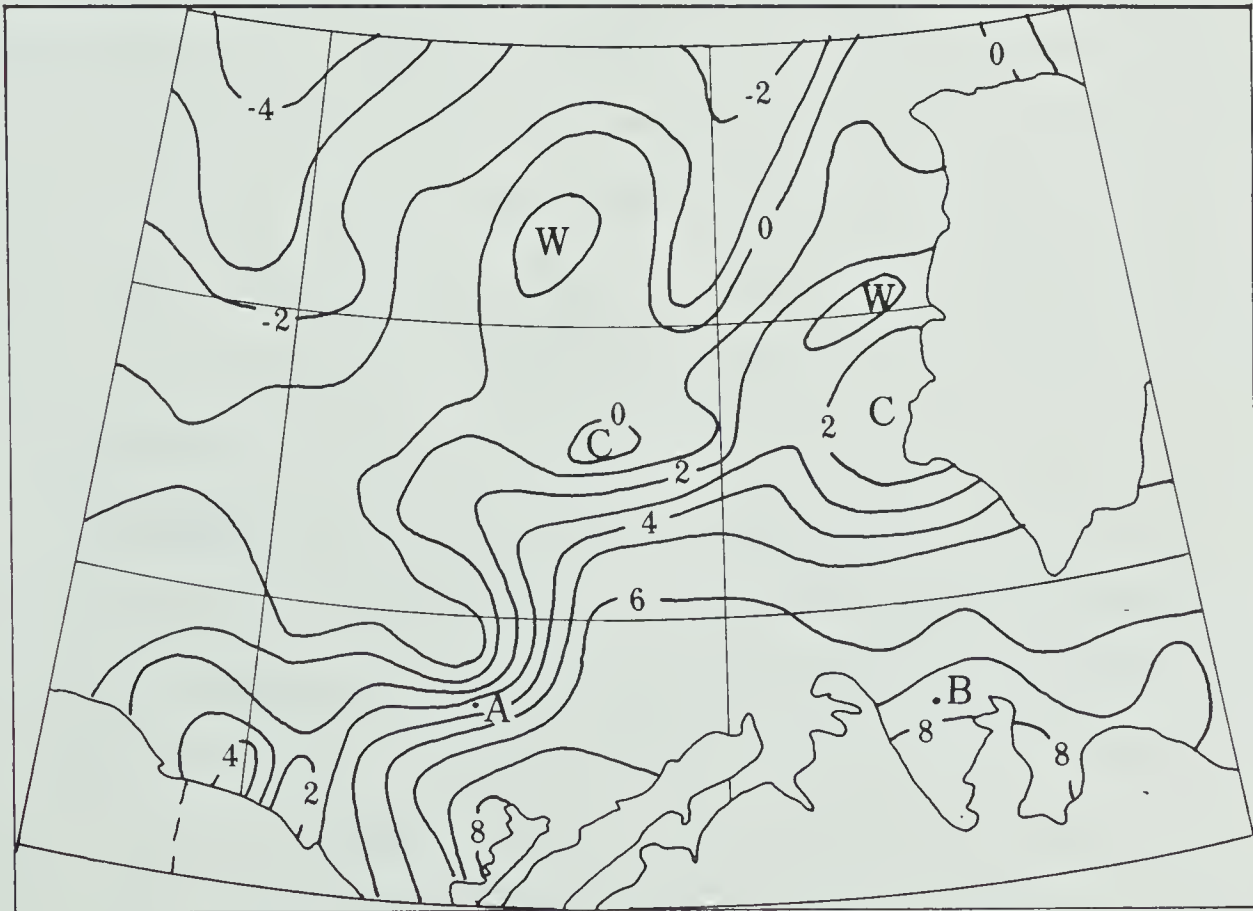


FIGURE 5.19 Composite isotherm analysis: July 29-31, 1977, Orbits 4519, 4532 and 4544.

two later composite charts. Variations in surface temperature atop the ice belt are likely due to unequal freezing and melting. If a comparison of Figure 5.17 is made to the one-day temperature analyses for July 27 and 28 in Chapter IV, areas of high gradient do not match particularly well, while consistencies are evident over the main ice pack. The rapidly changing nature of the surface temperature regime is apparent.

In terms of satellite imagery, Figures 4.2a, 4.2b, 4.4a and 4.4b as well as Figure 5.21a, the IR image for Orbit 4532 and Figure 5.21b, the visible image for Orbit 4533, show many features identifiable from the composites. In addition to the discussion given in Chapter IV, the edge of the ice in the Archipelago is reproduced well in all composites (just northeast of Banks Island).

The images for July 29 show two main cloud bands, one near 70°N 140°W, and the other across the centre of the study area in a northwest to southeast line. These are displayed in Figures 5.20a and 5.20b, and are from Orbit 4520. The major ice edge shows little change in shape from the previous visible image (4508), except that the ice belt in the south appears to be undergoing some modifications. Along the major ice edge in the centre of the study area, a large floe or ice island appears to be separating from the main ice pack.

The imagery from July 30 allows further examination of suspected changes. The ice island appears to have moved toward the southwest, while indentations on either side of the ice belt appear more pronounced. Low cloud or fog lies along the mainland coast near the Yukon-Alaska border. On the IR image a band of cloud across the central study area in a north to south line hampers interpretation. Slightly warmer water

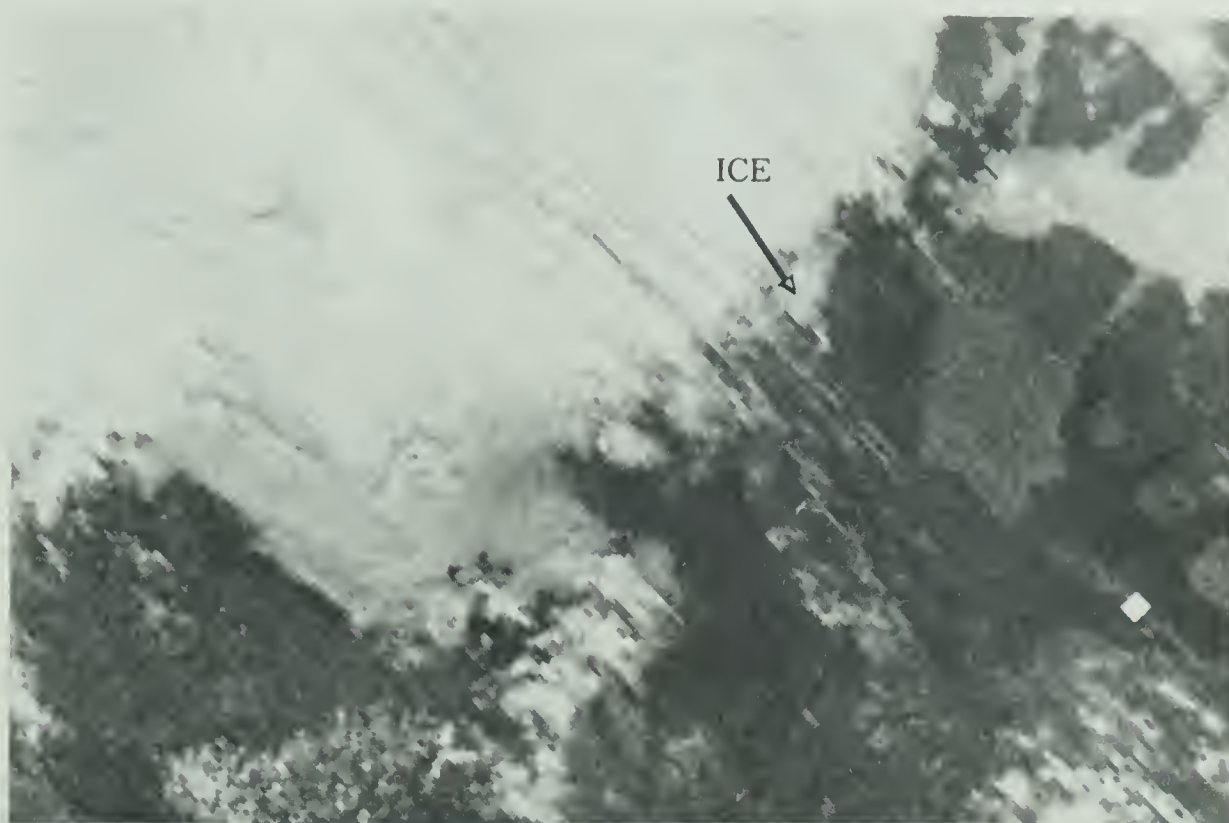


FIGURE 5.20a Visible image, July 29, 1977, Orbit 4520.

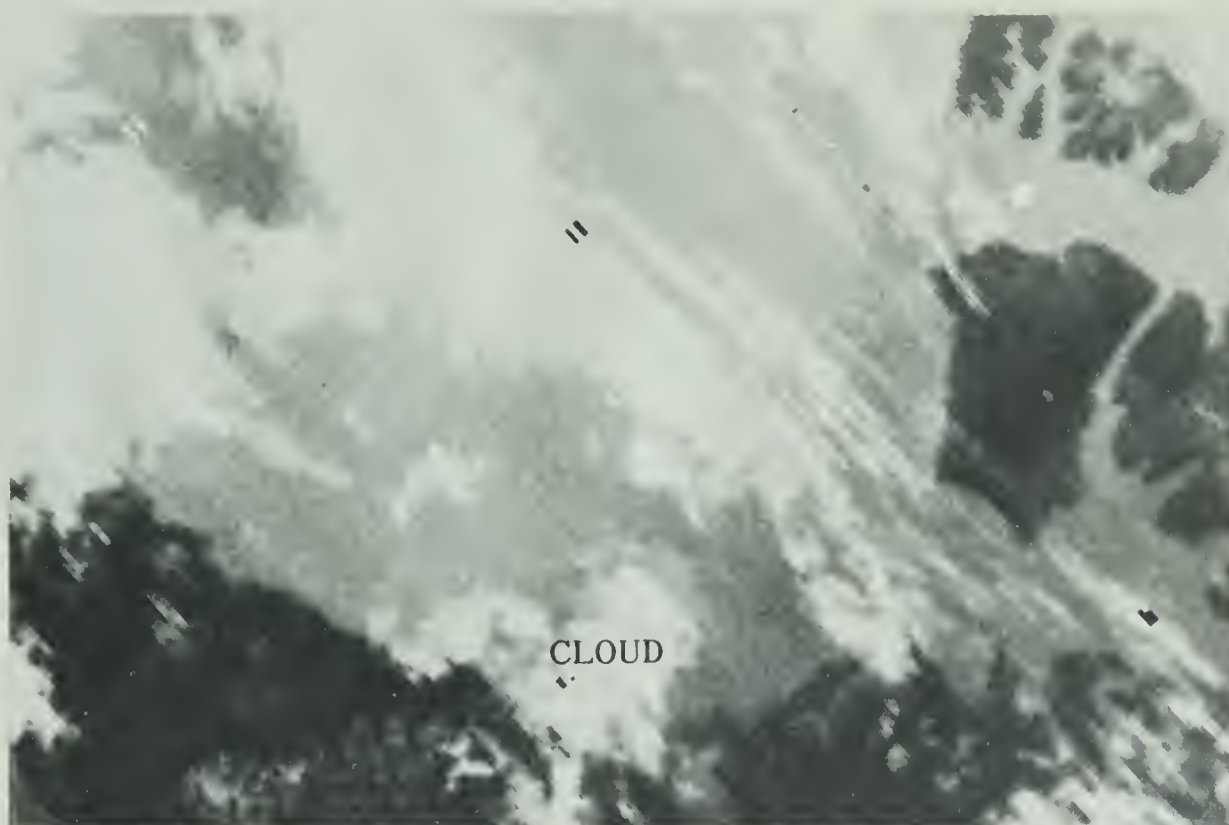


FIGURE 5.20b IR image, July 29, 1977, Orbit 4520.

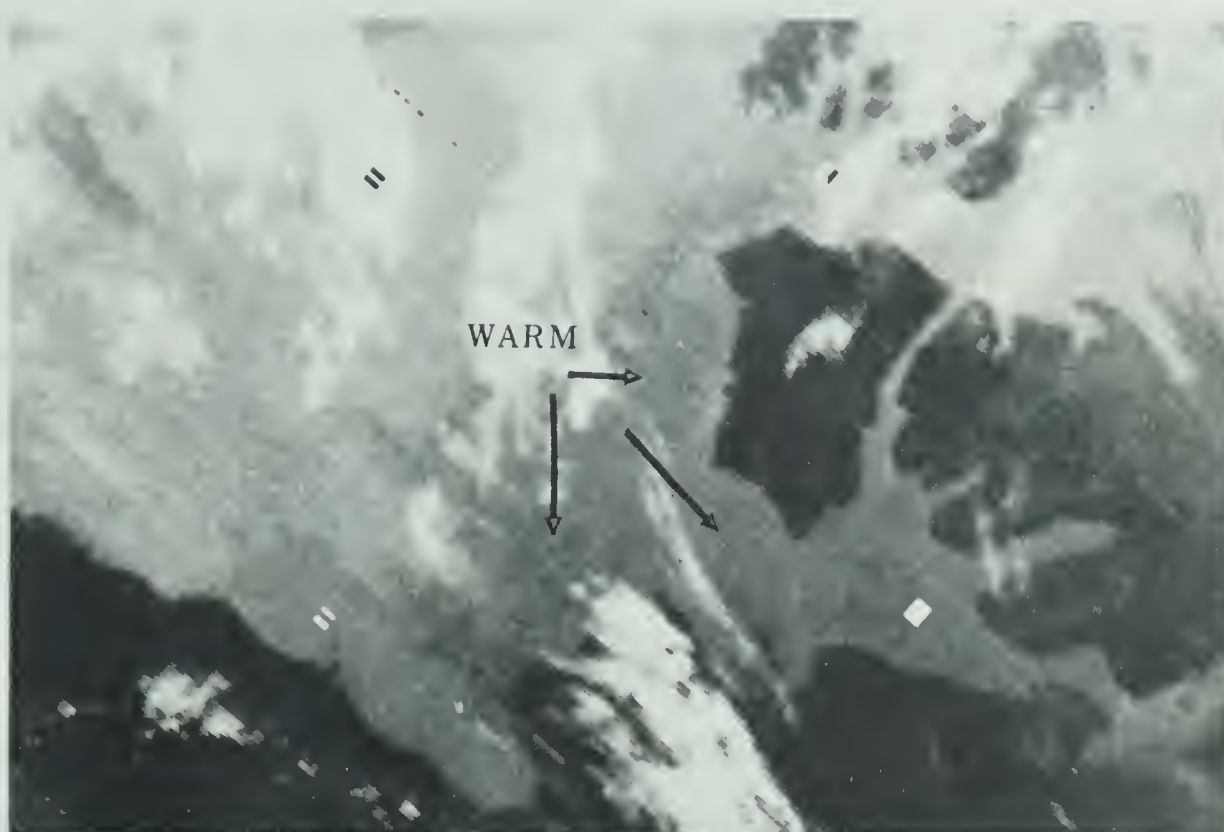


FIGURE 5.21a IR image, July 30, 1977, Orbit 4532.

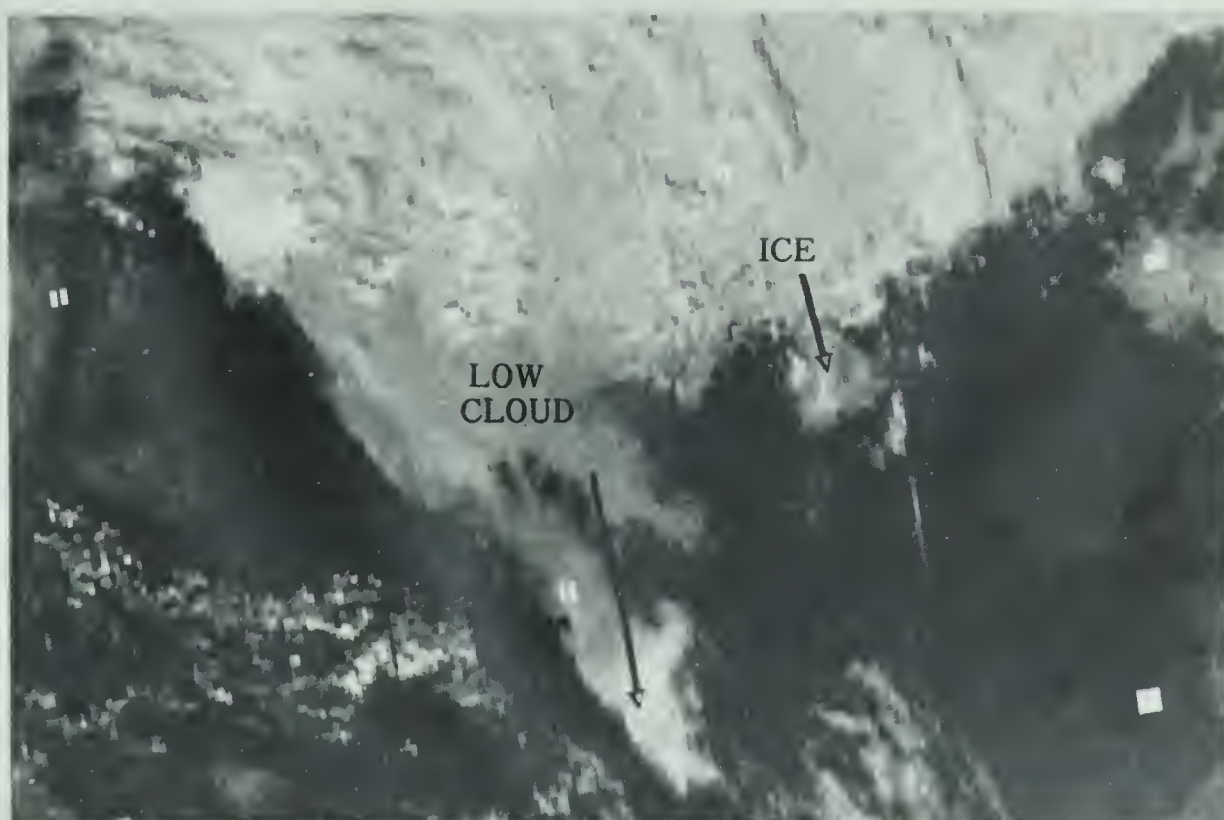


FIGURE 5.21b Visible image, July 30, 1977, Orbit 4533.

areas are identifiable along the mainland coast due south of Sachs Harbour, along a north to south line about 50 to 100 kilometers west of Banks Island, and along the mainland coast north of Tuktoyaktuk.

The imagery for July 31 is not reproduced here, since it is too cloud-contaminated to allow useful interpretation.

The features described above are well-defined on the composite analyses, with the exception of the areas near the Yukon-Alaska border, and at Sachs Harbour, where cloud contamination is the probable error source.

With reference to the central portion of the study area, the suspected motion of the "breakaway" ice island is identifiable. The "wake" of cooler water behind may be related to cloud contamination described previously. In addition, a pocket of warm water has moved northward to lie north of the ice island on Figure 5.19. If all three composites are studied, the motion of this feature is quite regular, although it is not discernible on the satellite imagery. This warm eddy has a consistent movement toward the north of roughly one meter per second.

In terms of ground-truth data, several measurements available for consideration are summarized in Table 5.3. The location of drill site Kopanoar is marked by point A on the composites; that of supply ship Pandora 2 by point B. It is apparent that Kopanoar is located in a high temperature gradient area; and, judging from the sequence of reported sea temperatures, the temperatures observed in its vicinity are by no means constant or uniform. Because of local weather conditions the only reasonable agreements to be anticipated are for July 29 and 30. The agreement observed of conventional with satellite-

derived measurements on these dates is either remarkable or highly suspect. The poor agreement for the Pandora 2 data in a relatively uniform temperature field, may be due to ship-board measurement error.

TABLE 5.3

Ground-Truth Information Versus Satellite-Derived
Temperatures, Case 2, July 27-31, 1977

Kopanoar - 70°23'N 135°06'W				
*Pandora 2 - 70°15'N 126°00'W				
Date	Hour (GMT)	Temp. (°C)	Weather	Computed Temp./ Std. Dev. (°C)
July 27	1200	5	Fog	
July 27	2400	6	Fog	3.2 / 2.04
July 28	1800	8	4/10 High Cloud	3.7 / .65
July 29	1800	3	1/10 Mid Cloud	3.5 / 2.07
July 30	1800	3	1/10 Low Cloud	2.5 / 2.49
July 31	1800	11	10/10 Low Cloud	Not Calculable
*July 29	1800	9	2/10 High Cloud	5.3 / 1.07

5.4.3 Statistical Summary

The analysis statistics for Case 2 are given in Tables 5.4 and 5.5. Of note is the performance (statistically) of the two-day compositing period, which may not be strictly valid since all but one day in this

TABLE 5.4
Statistical Summary of Compositing,
Case 2, July 27-31, 1977.

# Days of Data	1	2	3	4	5
Areas Recovered (/208)	194 181 114 71 162	177 149 141 152	154 150 140	141 151	138
Recovery Efficiency (%)	69.4	74.4	71.1	70.2	66.8
Mean Std. Dev. (M.S.D.) (°C)	.91 .98 1.28 1.10 1.31	1.23 1.08 1.21 1.27	1.22 1.27 1.32	1.25 1.30	1.29
Mean of M.S.D. (°C)	1.17	1.20	1.27	1.28	1.29

TABLE 5.5
Compositing Over Land- or Water- Covered Areas, Case 2.

Interval	Number Recovered		
	Water Only (/124)	Other (/84)	All (/208)
July 27 - 29	110	44	154
July 28 - 30	103	47	150
July 29 - 31	90	50	140

case were basically cloud-free. The statistics for this case are in general not as encouraging as those for the previous case, presumably due to rapidly changing features in the study area. The compositing period must be kept as short as possible.

5.5 Case 3, August 13-16, 1977

5.5.1 Synoptic Situation

A north to south ridge of high pressure dominated the eastern study area on August 13 and 14, while a low pressure centre was situated near 70°N 138°W on the 14th. By August 16 a low, which had formed near this location overnight on August 15, moved into the central study area, posing a potential cloud contamination threat for the final day. Figures 5.22 to 5.25 display the corresponding surface synoptic conditions.

This case examines the reliability of the compositing technique in a somewhat more cloudy situation. In view of the apparently transient nature of much of the cloud formations on the days in question, two concurrent studies, separated by one satellite orbit, are conducted; in this manner the direct effect of cloud contamination will hopefully be discerned.

5.5.2 Verification

Figures 5.26 to 5.29 depict the relevant composite analyses. The information analysed is from Orbits 4705, 4717, 4730 and 4742 of NOAA-5 for the "early" study, and from Orbits 4706, 4718, 4731 and 4743 for the "late" study.

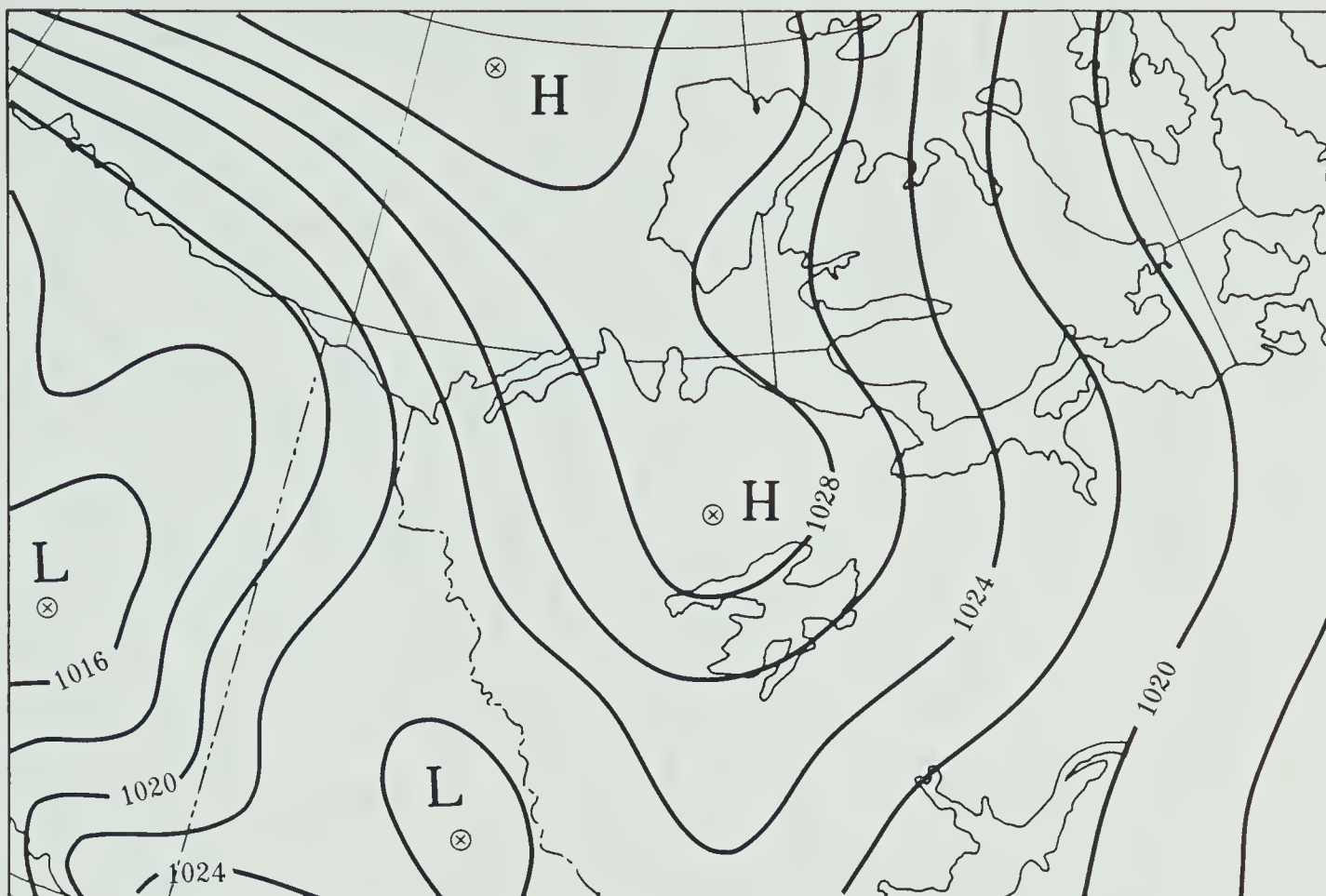


FIGURE 5.22 BAB surface map: August 13, 1977, 1800 GMT.

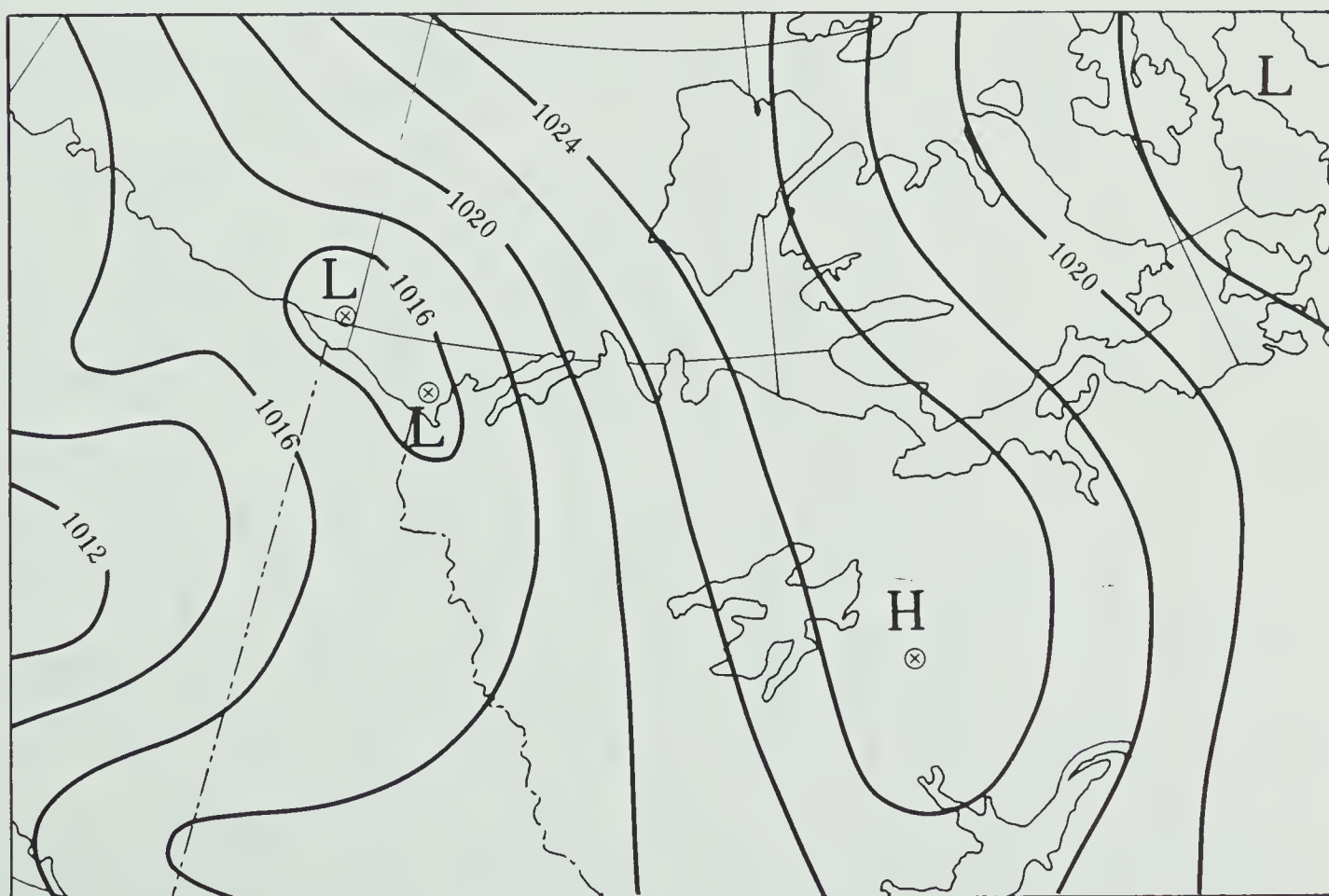


FIGURE 5.23 BAB surface map: August 14, 1977, 1800 GMT.

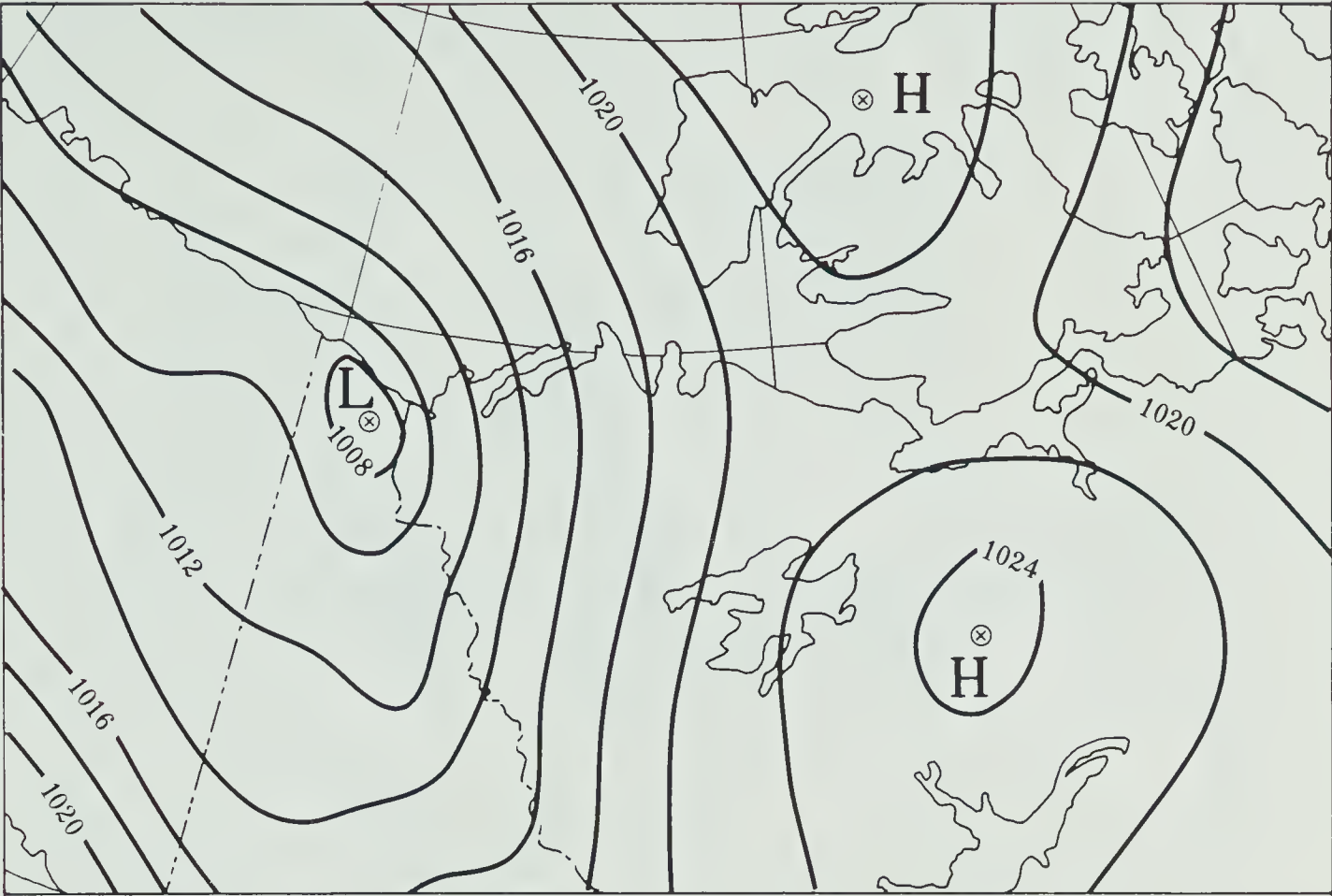


FIGURE 5.24 BAB surface map: August 15, 1977, 1800 GMT.

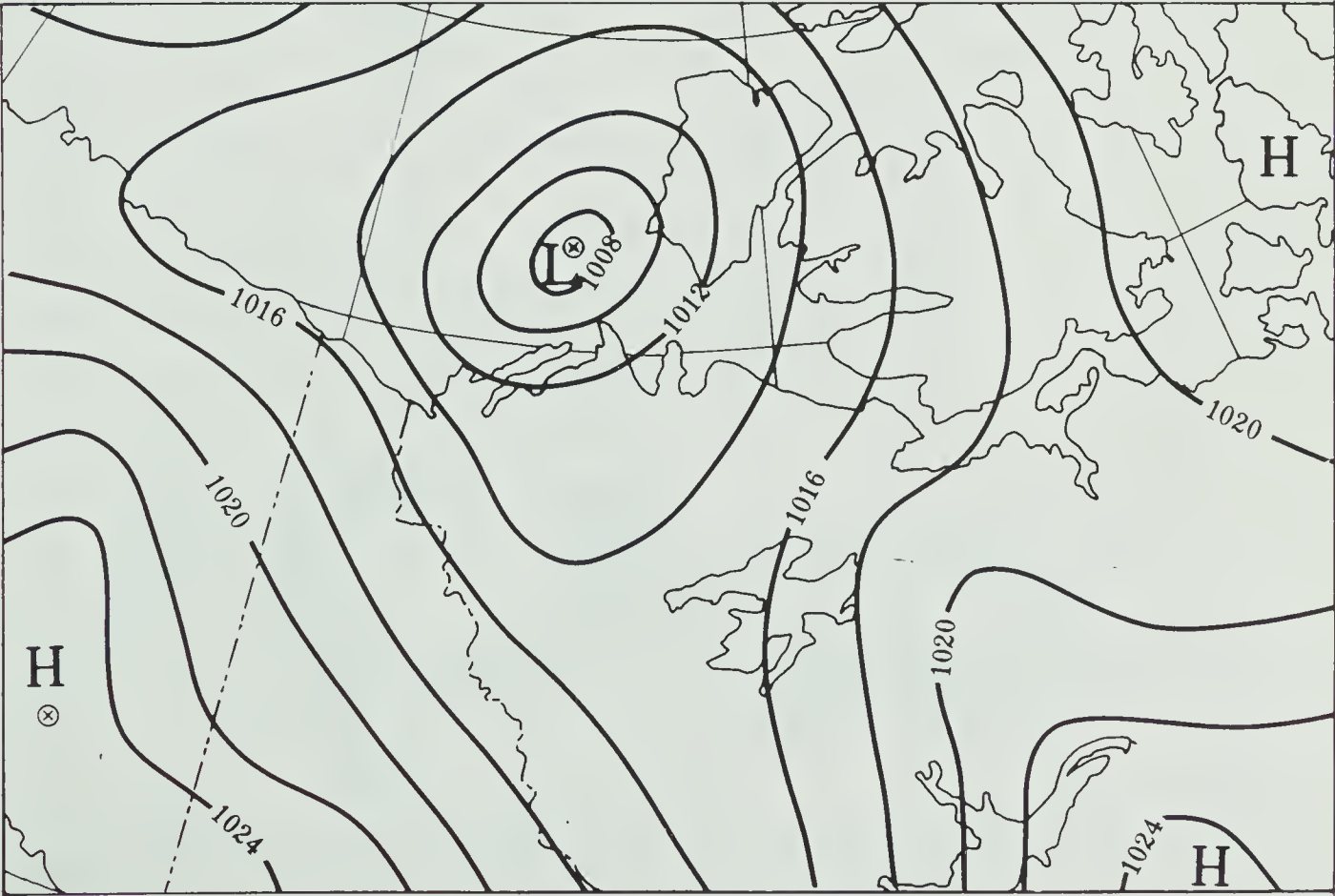


FIGURE 5.25 BAB surface map: August 16, 1977, 1800 GMT.

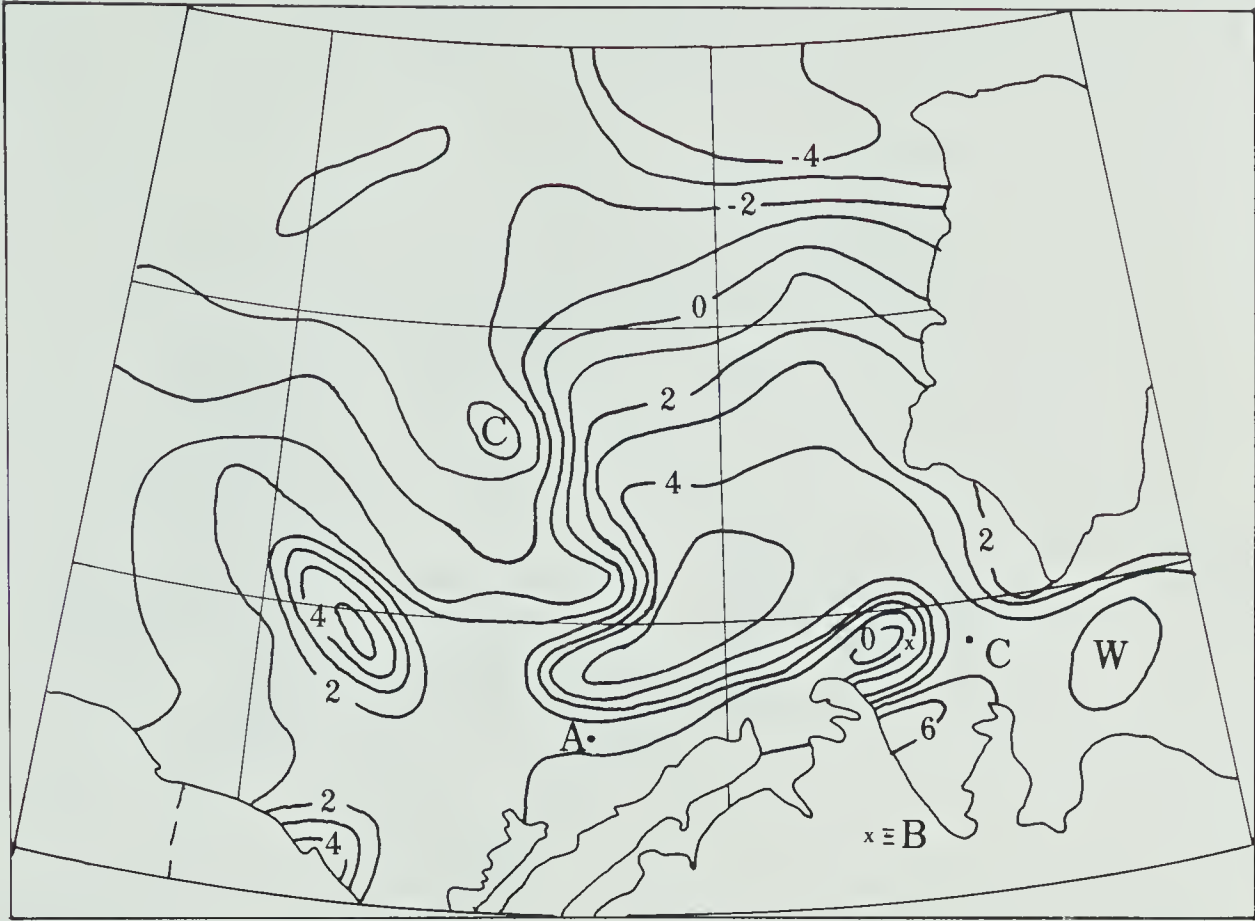


FIGURE 5.26 Composite isotherm analysis: August 13-15, 1977, Orbits 4705, 4717 and 4730.

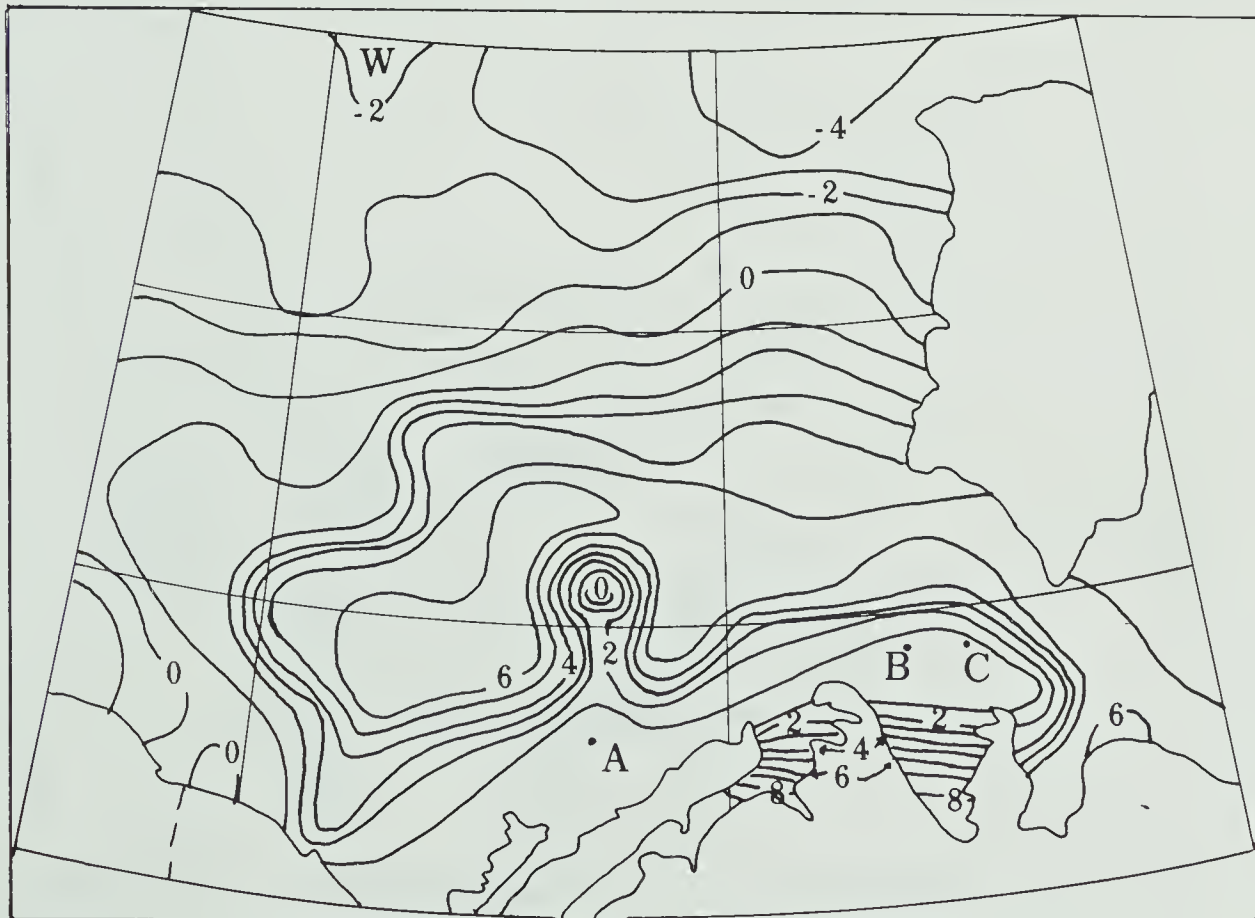


FIGURE 5.27 Composite isotherm analysis: August 13-15, 1977, Orbits 4706, 4718 and 4731.

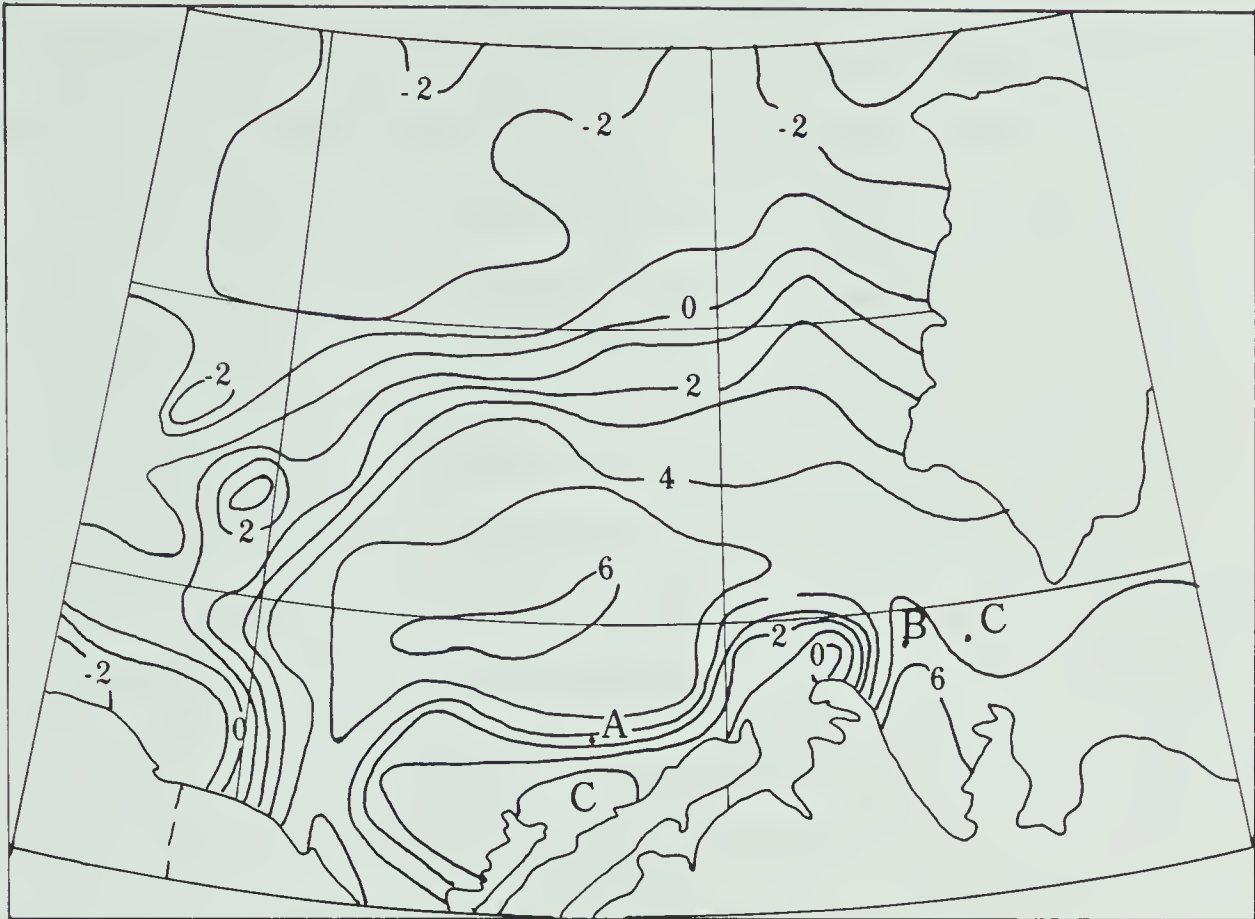


FIGURE 5.28 Composite isotherm analysis: August 14-16, 1977, Orbits 4717, 4730 and 4742.

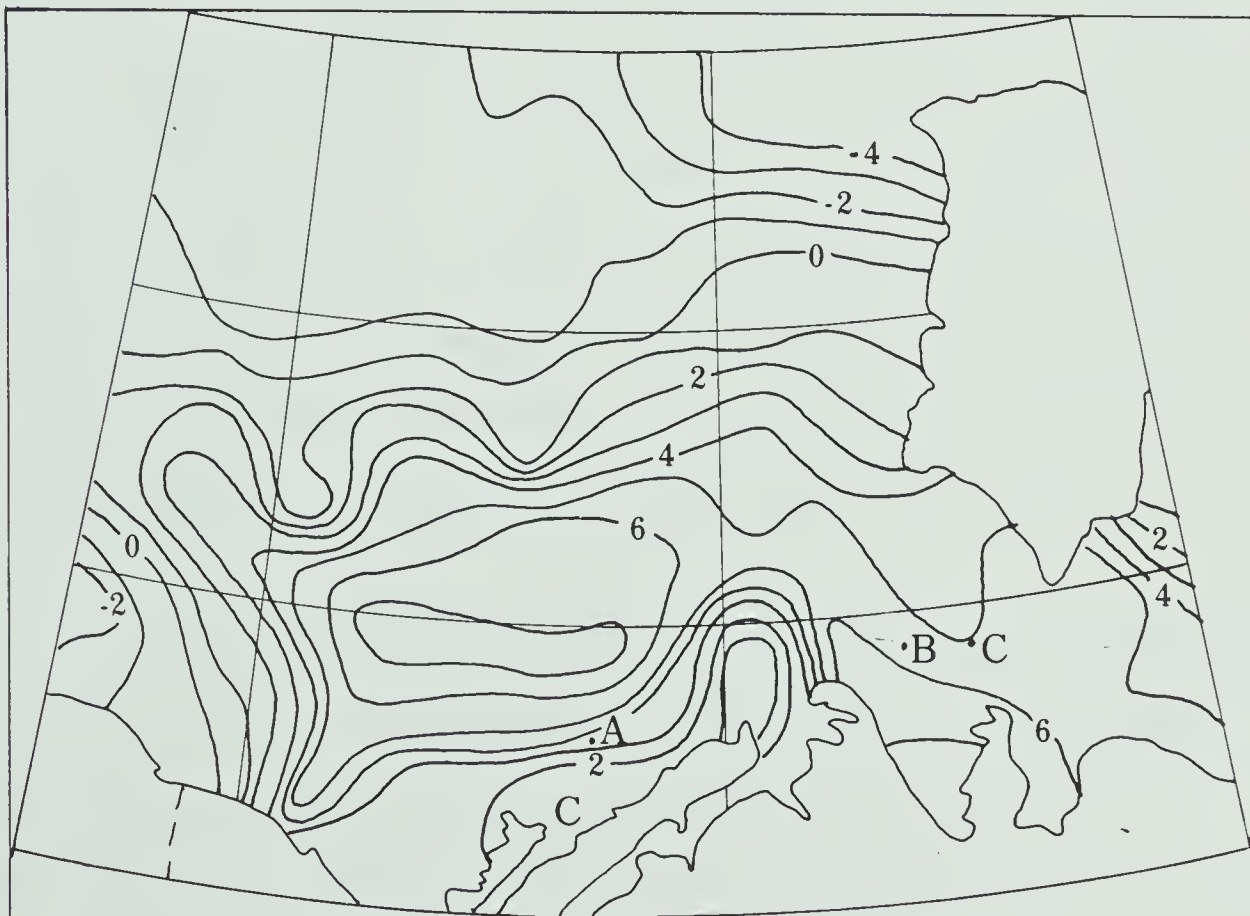


FIGURE 5.29 Composite isotherm analysis: August 14-16, 1977, Orbits 4718, 4731 and 4743.

In terms of ice information (Overlay 2), all four composite charts separate close and open pack ice using the -1°C isotherm. Cloud contamination affects Figure 5.26 in central areas, and both Figures 5.26 and 5.27 in the vicinity of the Yukon-Alaska border. Temperatures between -1°C and $+1^{\circ}\text{C}$ delineate very open pack and open pack ice conditions fairly well in Figure 5.27, while above zero temperatures correspond to open water and ice-free areas in Figure 5.28 and 5.29. On these two charts cloud contamination affects western areas.

Satellite imagery for this case show the relatively large amount of cloud contamination present, particularly in the earlier set of orbits. Figure 5.30a shows the IR image for Orbit 4705, and Figure 5.30b the visible imagery for Orbit 4706. On this IR image a bright (cold) area in the central Beaufort Sea is identifiable, and also what appears to be low cloud over much of the water area northwest of Tuktoyaktuk. This cloudiness is also apparent, to a lesser degree, on the visible image for Orbit 4706. On August 14, cloud contamination is less severe. From the IR image for Orbit 4717, Figure 5.31, cool areas along the central mainland coast are distinguishable. Upon examination of Figure 1.2, the visible image for Orbit 4718, this area may be identified as relatively cool water. The cool area to the west of the Yukon-Alaska border is probably low cloud, since no ice is reported in the vicinity.

The visible and IR imagery for August 15, Orbit 4731, is shown in Figures 5.32a and 5.32b, respectively. The area of interest along the central mainland coast is indeed cool water, possibly the result of an upwelling episode. On the IR image this area extends well into the



FIGURE 5.30a IR image, August 13, 1977, Orbit 4705.

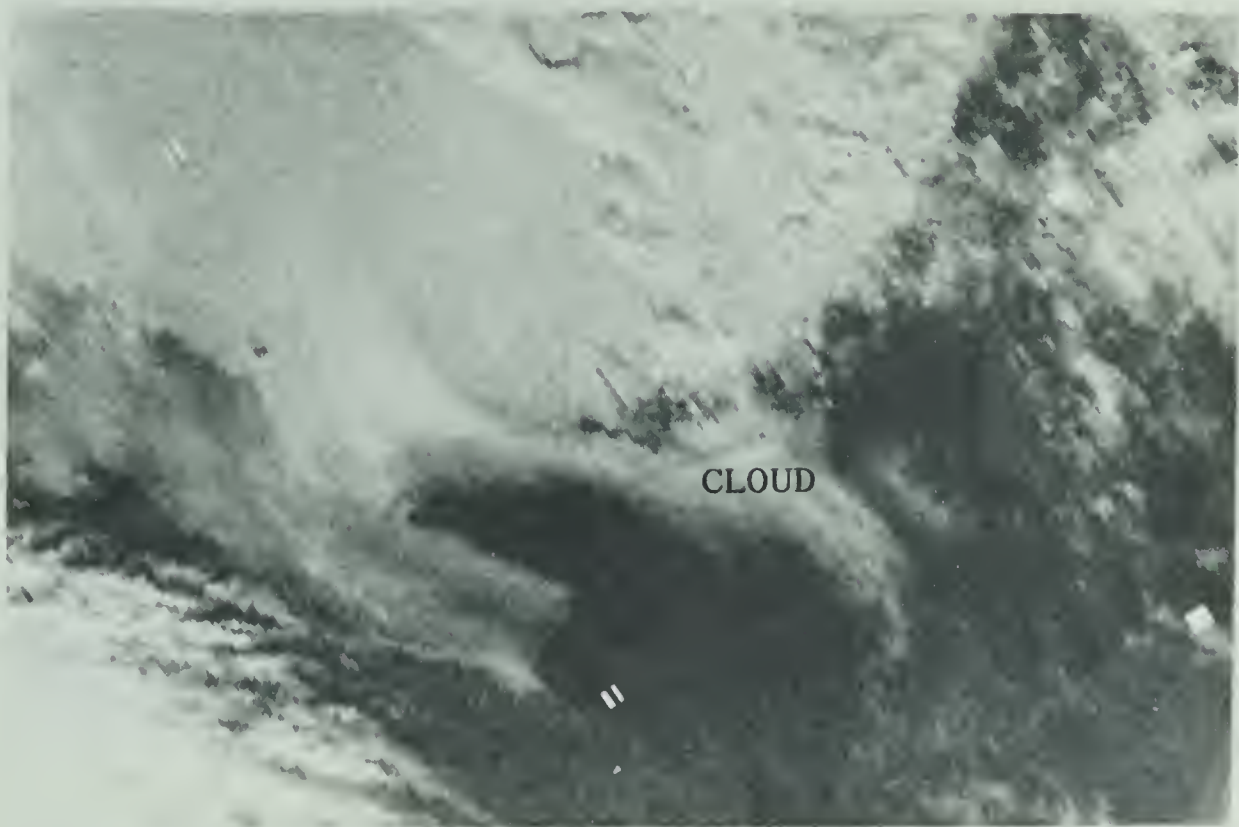


FIGURE 5.30b Visible image, August 13, 1977, Orbit 4706.

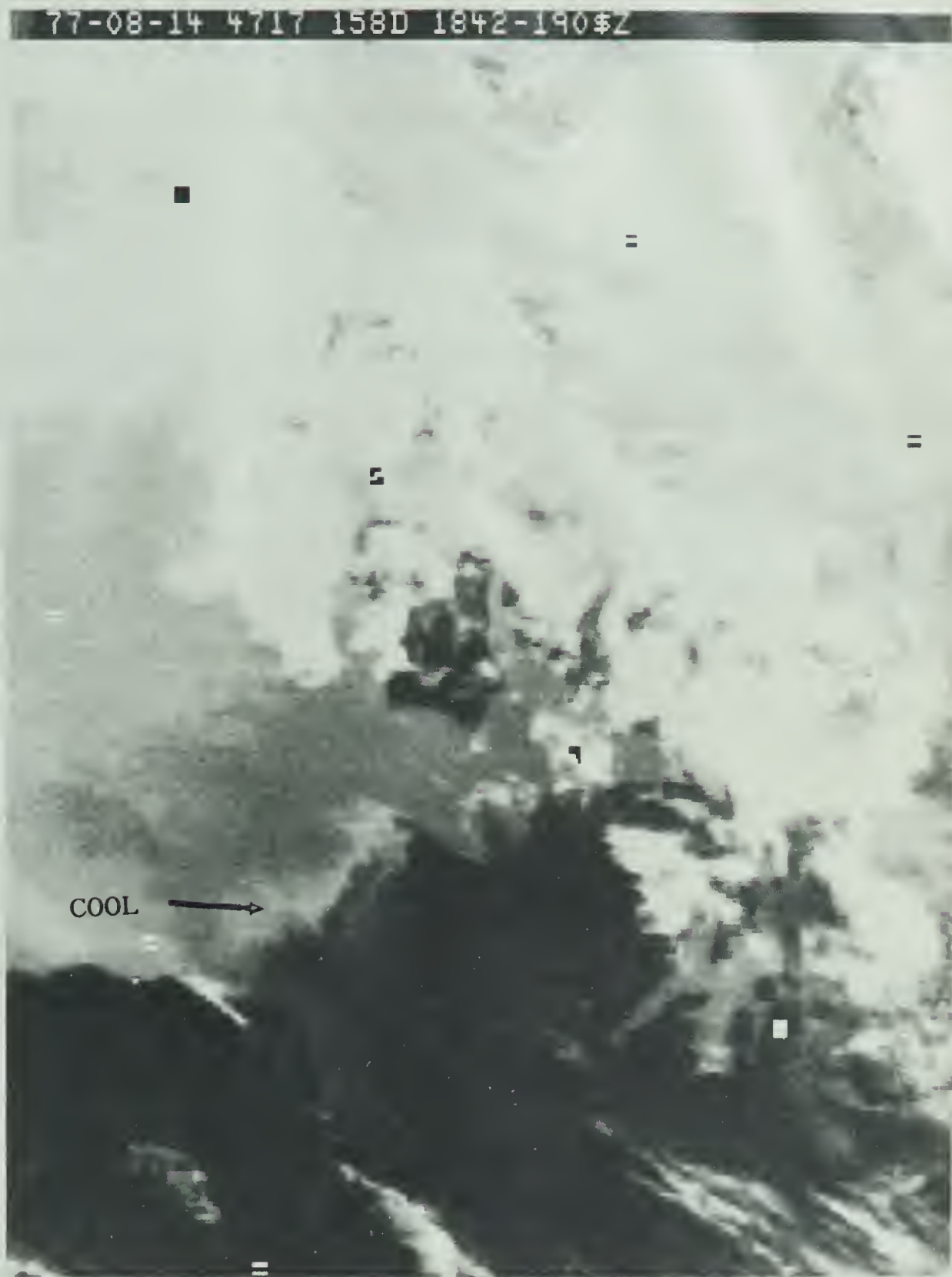


FIGURE 5.31 IR image, August 14, 1977, Orbit 4717.

MacKenzie Delta. Figure 5.32a shows persistent cloud at the coast near the Yukon-Alaska border.

The August 16 satellite imagery is not included since a great deal of middle- and high- level cloud covered much of the study area.

A comparison of the imagery to the detail present in the composite analyses yields much information of interest. The suspected low cloud discernible northwest of Tuktoyaktuk on Orbit 4705 affects Figure 5.26 but not Figure 5.27, as the low cloud there presumably dissipated between the times of passes 4705 and 4706. Cloud contamination is less severe in Figure 5.27 in the central study area near the ice edge. The coastal upwelling area shown in Figure 5.27, however, appears to extend too far to the east. The wave-like ice features identifiable on the infra-red imagery for August 14 are much better-resolved in Figure 5.27 than in Figure 5.26. The net effect of the low cloud and its subsequent dissipation on August 13 is quite dramatic.

The thermal details resolved by Figures 5.28 and 5.29 are quite different. The wave-like features along the ice edge are only discernible on the later composite, while the coastal upwelling areas are analysed quite differently east of the MacKenzie Delta. Persistent cloud affects both analyses in the vicinity of the Yukon-Alaska border, as it does northwest of Banks Island in Figure 5.28. Again the effect on the temperature fields produced when low cloud dissipates is readily apparent.

The ground-truth data used in Case 3 are listed with the corresponding calculations in Table 5.6. One calculation listed below was done for August 14 in Chapter III. The Ukalerk drill site is marked A on the composites, while Pandora 2's location is denoted Bor C. As in

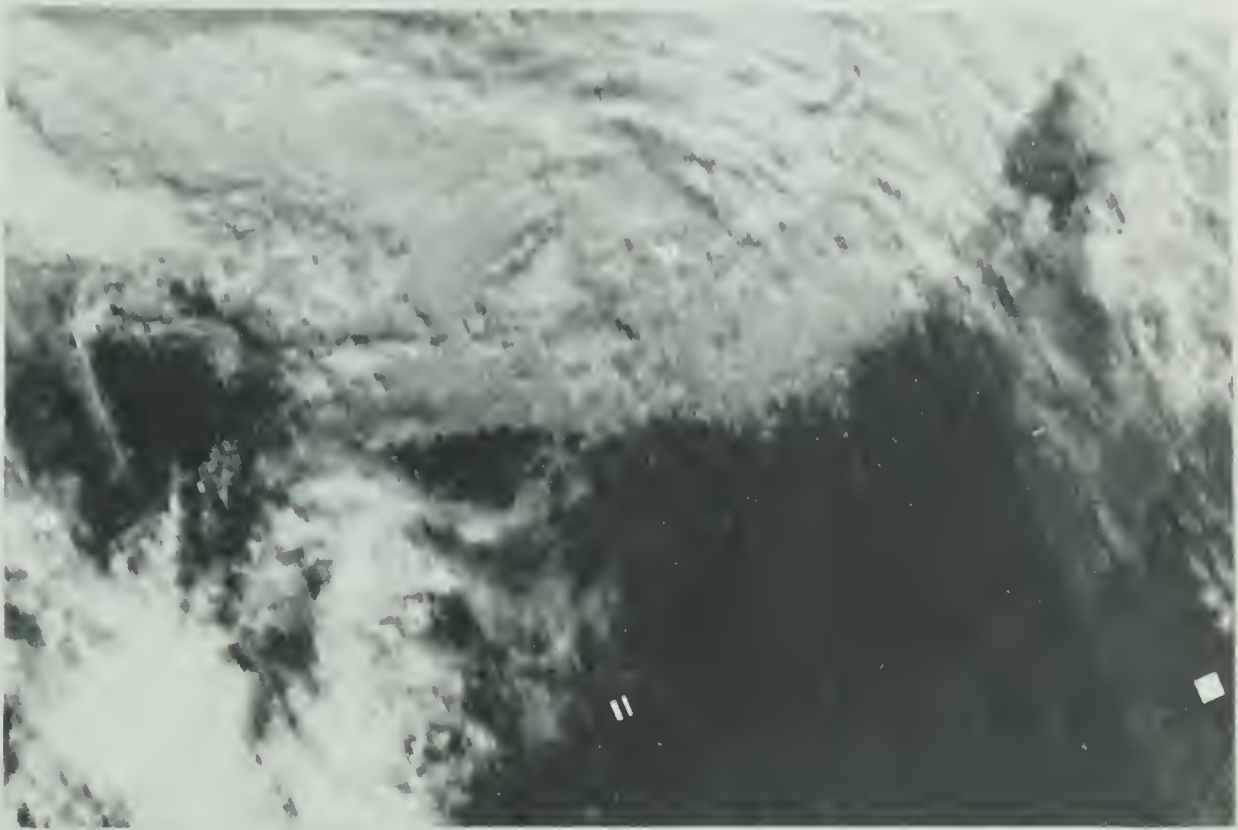


FIGURE 5.32a Visible image, August 15, 1977, Orbit 4731.

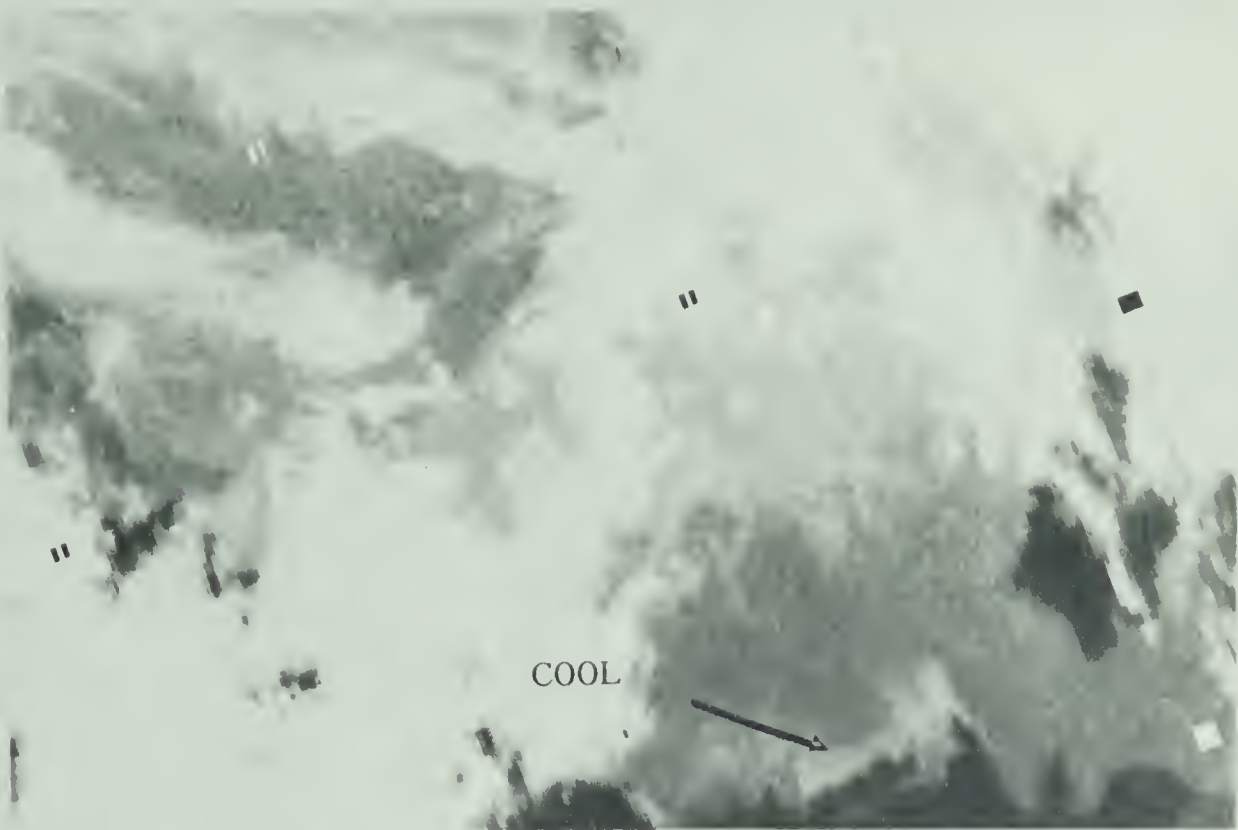


FIGURE 5.32b IR Image, August 15, 1977, Orbit 4731.

Case 2, the former is located in an area of high temperature gradient while the latter apparently is not. Reported weather suggests that superior correlations between surface and satellite-derived temperatures are likely for August 14 and 15. On these dates, a similar non-agreement for Pandora 2 measurements with the satellite information to that found in Case 2 is noted. Note how satellite-derived temperatures for Ukalerk increase during the day in all three possible situations; whether this effect is a spurious one, a function of internal calibration, or one associated with solar heating effects, is unknown.

TABLE 5.6

Ground-Truth Information Versus Satellite-Derived
Temperatures, Case 3, August 13-16, 1977

Ukalerk position: 70°09'N 132°48'W (A)						
*Pandora 2 position: 70°45'N 126°30'W (B)						
**Pandora 2 position: 70°45'N 125°10'W (C)						
Date	Hour GMT	Temp. (°C)	Weather	Computed Temp./Std.Dev.(°C)		
				Early Pass	Late Pass	
August 13	1800	4.5	1/10 Low Cloud	.6 / 1.72	.7 / .96	
August 14	1800	5.2	10/10 High Cloud	3.3 / 1.60	4.6 / 1.74	
*August 14	1800	8	1/10 Cloud	5.0 / .77	5.7 / .83	
August 15	1200	4.7	2/10 High Cloud	4.9 / 1.47	6.2 / 2.08	
August 15	2400	5.5	1/10 High Cloud			
**August 15	1800	8	2/10 Cloud	5.0 / .84	4.8 / .69	
August 16	1800	5.7	2/10 Mid Cloud 10/10 High Cloud	- Not Computed -		

5.5.3 Statistical Summary

Table 5.7 shows the recovery and mean standard deviation summary for the two cases. Note the improvement using data one orbit later in the day. In both situations a two-day compositing interval appears optimal from the standpoint of recovery efficiency; however, the stability of recovery values is somewhat superior for three-day compositing periods.

Table 5.8 shows areas recovered over land and water for both sets of orbits. The improvement in recovery for the later set of passes is evident. Despite excessive cloud in Case 3, better than 80 per cent of all purely water/ice areas are recovered over a three-day interval.

TABLE 5.8

Compositing Over Land- or Water- Covered Areas,
Case 3.

Interval	Number Recovered		
	Water Only (/124)	Other (/84)	Other (/208)
August 13-15	96	32	128
August 14-16 Early	98	39	137
August 13-15	107	29	136
August 14-16 Late	102	46	148

TABLE 5.7

Statistical Summary of Compositing,
Case 3, August 13-16, 1977.

1. Early Passes

# Days of Data	1	2	3	4
Areas	155	123	128	113
Recovered	149	152	137	
(/208)	76	136		
	96			
Recovery Efficiency (%)	57.2	65.9	63.7	54.3
Mean Std. Dev.	1.29	1.27	1.31	1.40
(M.S.D.)	1.07	1.21	1.31	
(°C)	1.15	1.28		
	1.35			
Mean of M.S.D. (°C)	1.22	1.25	1.31	1.40

2. Late Passes

# Days of Data	1	2	3	4
Areas	114	134	136	132
Recovered	170	159	148	
(/208)	144	139		
	96			
Recovery Efficiency (%)	62.9	69.2	68.3	63.4
Mean Std. Dev.	1.33	1.27	1.31	1.35
(M.S.D.)	1.05	1.19	1.28	
(°C)	1.19	1.29		
	1.30			
Mean of M.S.D. (°C)	1.22	1.25	1.30	1.35

5.6 Information in the Composite Analyses

From study of Case 1, the effect of large-scale melting and puddle formation is detectable. Depending on cloud cover and associated solar heating differences, the surface temperature in these areas may fluctuate by as much as one degree per day.

The movement of large ice islands may be traced in the second case study. Judging from the motion of this feature and the warm water pocket nearby, surface currents are of the order of one meter per second. During this episode the surface winds were variable in direction, although generally from the east; this condition may or may not have significantly influenced the movement of the ice island.

Examination of the final case illustrates the effect on surface temperatures of an upwelling episode. The water in this coastal area is likely less than fifty meters deep, and the upwelling effect is substantial, considering that adjacent shallow inlets to the east display a surface temperature about five degrees warmer than that in the area in question. Presumably the water in the affected area would have warmed rapidly again under normal insolation conditions. The northern edge of the upwelling effect may also define the edge of influence of the Mackenzie River outflow, suspected to flow as shown in Figure 5.33 (Walker, 1977).

5.7 Compositing - Statistical Summary

A statistical summary of all cases considered in this Chapter is presented in Table 5.9. It is evident that for these cases a two or



FIGURE 5.33 Surface water currents in the Arctic,
as summarized by Collin (1963).

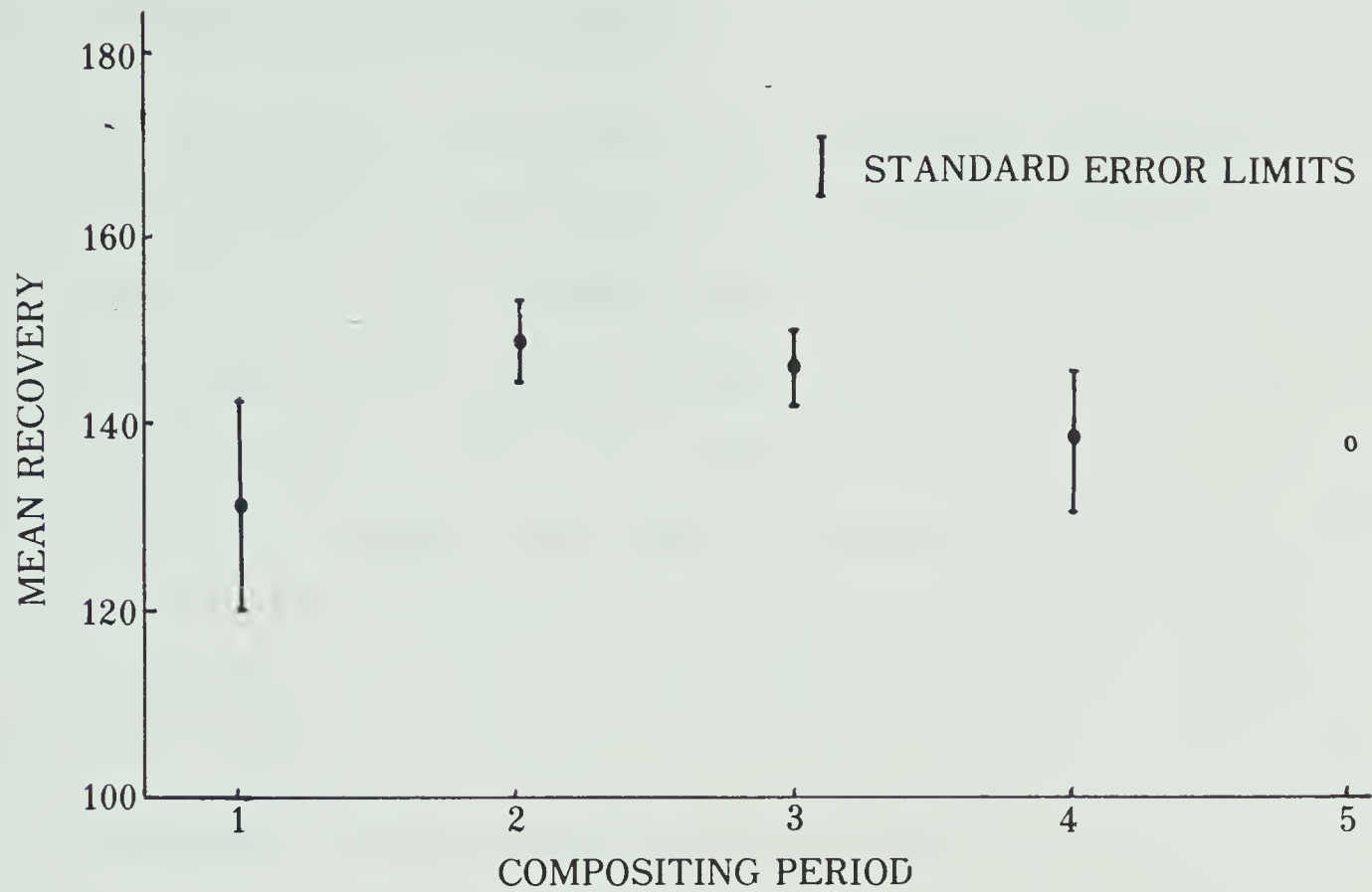
three-day compositing interval is optimal in terms of recovery efficiency and statistical stability (standard error). These results are shown graphically in Figure 5.34.

TABLE 5.9
Statistical Summary of All Compositing Cases

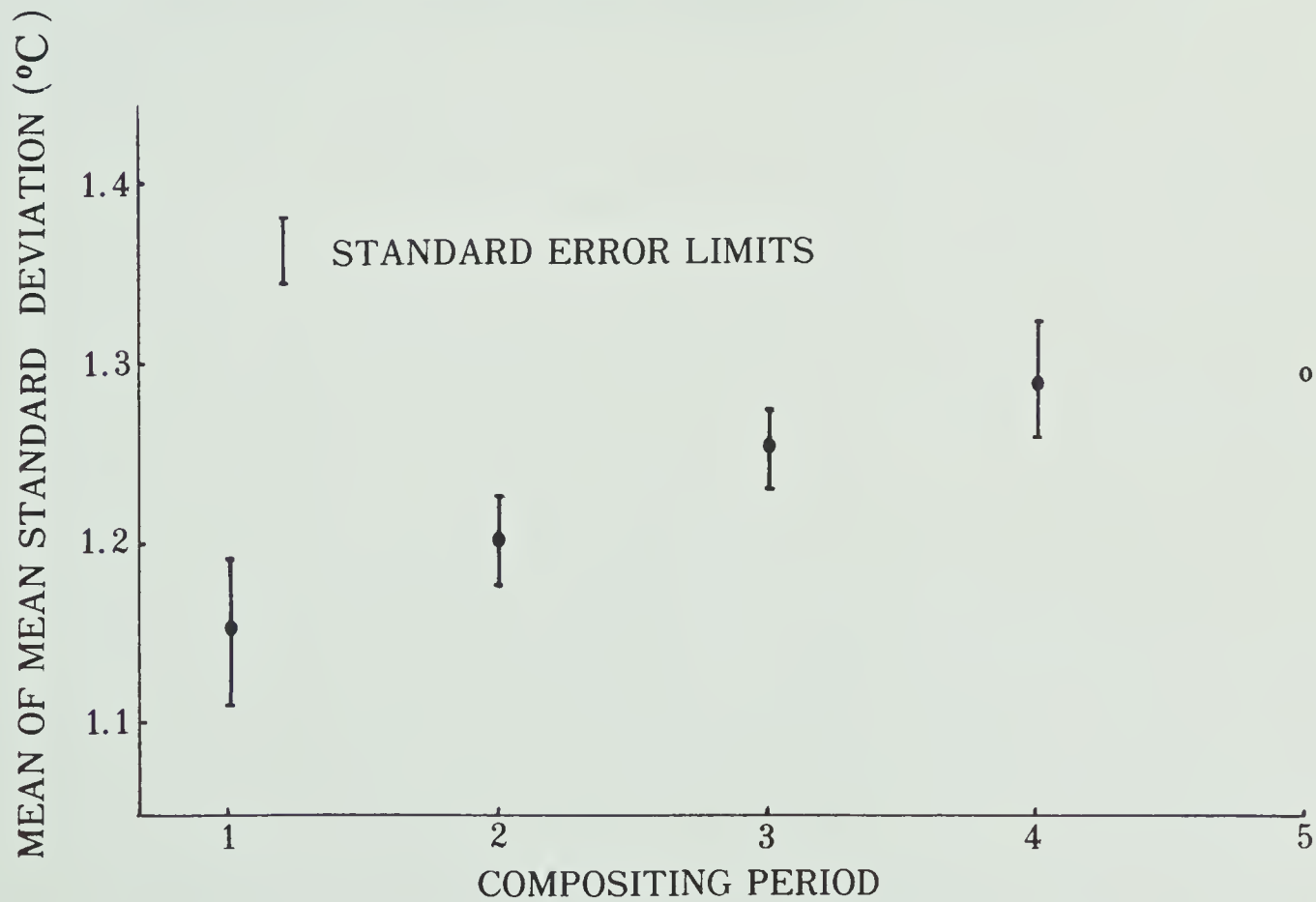
# Days of Data	1	2	3	4	5
Mean Recovery (/208)	131.6	149.8	147.1	140.0	139.0
Std. Dev. of Recovery	47.0	14.8	12.4	17.0	-
Std. Error of Recovery	11.6	4.1	4.1	7.6	-
Mean of M.S.D.'s (°C)	1.154	1.204	1.259	1.298	1.290
Std. Dev. of M.S.D.'s (°C)	.143	.085	.065	.074	-
Std. Error of M.S.D.'s (°C)	.035	.024	.022	.033	-
No. of Cases Used	17	13	9	5	1

In terms of recovery efficiency of land and water areas for all three-day composite charts, a mean efficiency of 83.8% occurred for water/ice areas, and 51.7% of all areas were recovered, in the mean, over land-contaminated squares.

FIGURE 5.34 Compositing summary, all cases



(a) Mean recovery versus compositing period.



(b) Mean of mean standard deviation versus compositing period.

5.8 External Calibration - Summary

The differences between ground-truth sea-surface temperature measurements and the corresponding satellite-derived temperatures are plotted on the scatter diagram, Figure 5.35. Situations representing excessive cloud contamination are circled. (This separation was based on weather reports.) The mean discrepancy is 1.59°C for twelve "reliable" reports. The Pandora 2 measurements are high in the mean by 3.04°C ; while all others are high by an average of 0.56°C . The discrepancy in the case of Pandora 2 is quite consistent, adding support to the idea that a bias error is present in those reports. It is reasonable to suspect that the attenuation of the infra-red radiation between earth and the satellite is generally less than one degree, for the small zenith angles and the Arctic summertime atmospheres examined here.

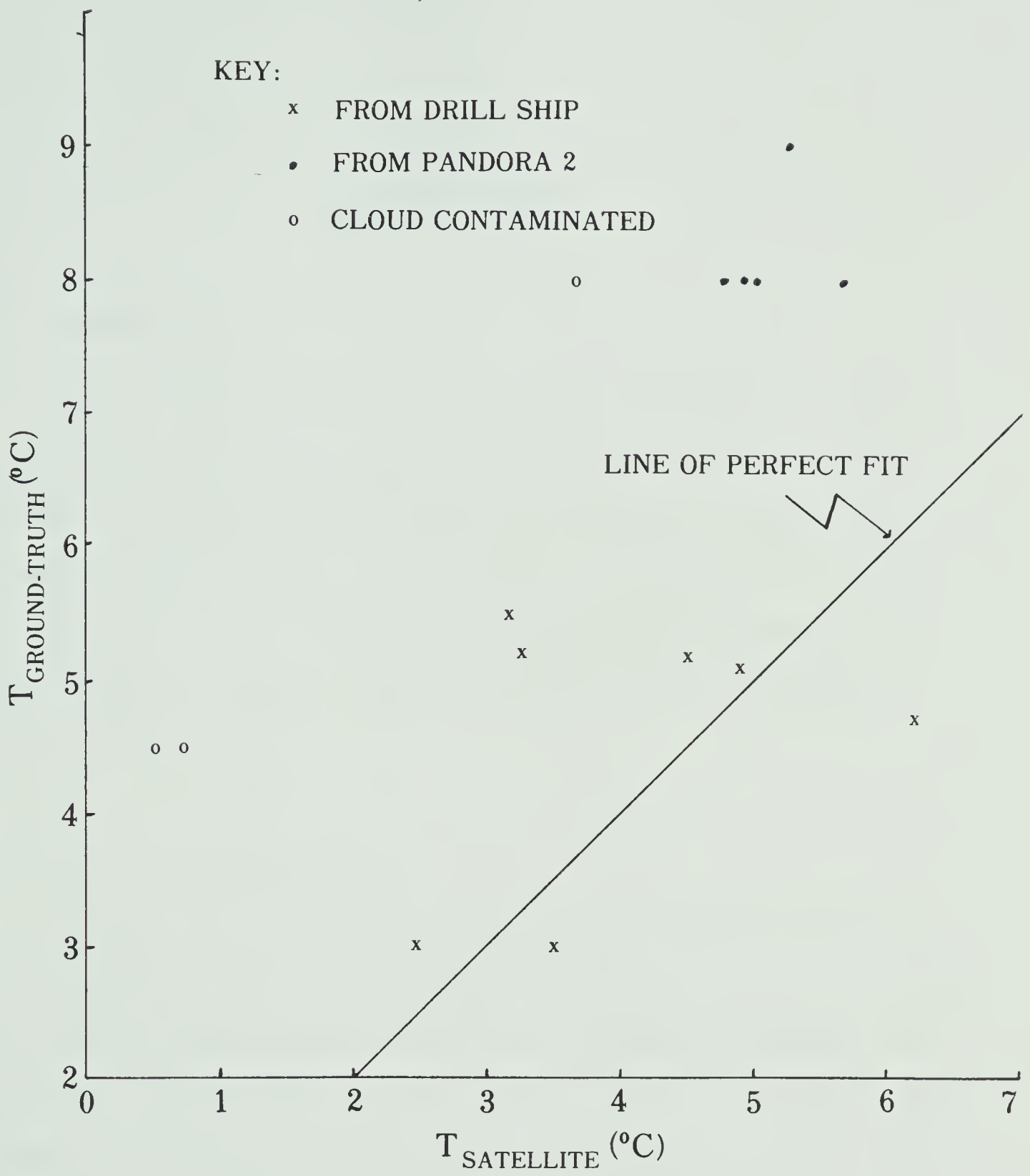


FIGURE 5.35 Ground-truth versus satellite-derived temperature, all cases.

CHAPTER VI

SUMMARY OF RESULTS

6.1 Introduction

It is fitting that the questions posed in Chapter II, on the subject of deriving sea-surface temperatures in the Beaufort Sea using a histogram analysis technique, be answered, as adequately as possible, in this Chapter. Subsequently, an overview of the experimentation as it relates to the meteorology and oceanography of the Western Arctic is given. Finally, recommendations for future work are put forth.

6.1.1 Optimum Grid Size

In terms of a compromise of the need for statistical stability (population size), the constancy of surface temperature in the relevant area, and the reproduceability of satellite grey-shade imagery, one-half degree latitude squares are optimal bin sizes. If synoptic-scale detail were required, a coarser mesh would perhaps be feasible, while if finer-scale resolution were desired, data sensed by a radiometer capable of better resolution would be necessary before the mesh could be made denser.

6.1.2 Daton Averaging

Near the subsatellite point the grouping together of digital values is suggested by the data overlap situation. Nearer the satellite viewing horizons less averaging is appropriate. Over a small region near the subpoint, however, an averaging of three consecutive datons smoothes the histograms while reducing dispersion, with no noticeable loss in physical detail.

6.1.3 Ice Conditions

Correlations between horizontal temperature gradients and ice conditions, mostly in regions of multi-year ice, are identifiable. The delineation between open water and very open pack ice is found at or near the locus of maximum gradient. In some instances the first relative maximum on the "iceward" side of the absolute temperature gradient maximum may be used, since gradients over open water and ice-free areas have in practice been found to behave in a somewhat erratic manner.

The division between open pack and close pack multi-year ice generally corresponds to a gradient of 1.0 to 1.5 °C/°L. Variability in this correlation value is likely due to inhomogeneity of reported or analysed ice conditions in this transitional region.

6.1.4 External Calibration

Presuming that bias error is largely responsible for differences of about three degrees between reported and satellite-derived surface temperatures at Pandora 2, the amount of attenuation present in the

SR data used here is likely less than one degree. Consistency of temperature correlations with ice conditions also suggests this to be so. Much of the data used is taken at small scan angles; thus atmospheric attenuation in the Arctic may on the average be somewhat larger than that reported here.

6.1.5 Cloud Filtering

Judging from the few situations studied, cloud filtering is possible through the use of composite histograms, in spite of persistent clouds in some instances. A maximum compositing limit of two or three days must be imposed in summer to avoid drastic surface temperature changes. This period needs to remain quite short even in more cloudy situations since wind action, surface currents and convective overturn are additional sun-independent mechanisms of temperature change.

6.1.6 Resolution Near Coastlines

A mean recovery of just over 50% is noted for land-contaminated squares, a figure which suggests that relevant surface temperature information may be obtained even along coastlines as irregular as the Arctic coast of Canada and Banks Island. Warm areas of 6°C to 8°C in shallow coastal bays, and cool coastal upwelling episodes are identifiable. Chunks of shore-fast ice near Banks Island of one grid square size are also distinguishable.

The cold-mode scanning routine is one probable reason for some of the resolution recovered in coastal areas. Choosing satellite passes near the time of maximum solar insolation permits a potentially large

thermal differentiation of land and water areas.

Using a "warm-mode" scanning method of scanning might not be feasible since the day-to-day inhomogeneity of land temperatures may cause a number of extraneous modes to be chosen. From which temperature should scanning begin?

6.2 A Study of the Beaufort Sea

Many features regarding the surface temperature distribution of the Beaufort Sea are distinguishable. Ice melt may be quite rapid, wheather along the major ice edge, or atop the ice, in the case of puddling. Puddling on multi-year ice has been detected to be not nearly as extensive as on first-year ice, presumably since first-year ice has a characteristically thinner cover of insulating snow.

Surface currents of the order of one meter per second are discernible near the major ice edge. The effect of surface winds on the drifting of large ice islands is not obvious in the cases presented.

Upwelling episodes in shallow coastal waters can be dramatic (as much as 5° or 6°C), while temperatures of 6° to 8°C are not uncommon in the shallow bays and inlets along the Arctic coast in late summer.

Perhaps the most striking detail of the surface temperature regime of the Beaufort Sea is its dramatically and rapidly changing nature during the Arctic summer season, one in which the sun and clouds compete incessantly for control.

6.3 Suggestions For Future Studies

The need for further case studies is evident, in terms of cloud-filtering technique requirements, and correlation studies between temperature gradients and ice conditions.

The atmospheric attenuation problem has only briefly been considered here. A more comprehensive study on the usefulness of ground-truth data and their relation to satellite-derived surface temperatures, using the scanning radiometer, would be useful.

Depending on the type of information required, the resolution obtainable through use of the histogram technique will allow study of synoptic and sub-synoptic scale features including distributions of clouds as well as surface temperatures.

The use of infra-red satellite data allows the techniques tried herein to be applied at night, and especially during the long periods of winter darkness in the polar regions. While surface-ice thermal contrasts may be smaller in winter, the compositing period can be made longer since large-scale surface temperature changes would likely not be as large as in summer.

The histogram technique offers a convenient method of archiving "grid-point" surface temperature data over what has historically been a data-sparse area. Such data could easily be incorporated into climatic and heat budget models, and also provide a systematic record for cause-and-effect studies of polar regions and the manner in which they interact with temperate and tropical regions.

REFERENCES

- Anderson, R.K. 1973. The use of satellite pictures in weather analysis and forecasting. W.M.O. Technical Note, No. 124, 275 pp.
- Anon. 1978. Manual of Standard Procedures and Practices for Ice Reconnaissance (MANICE). Atmospheric Environment Service, Environment Canada, Downsview. 60 pp.
- Barnes, J.C., D.T. Chang and J.H. Willand. 1972. Image enhancement techniques for improving sea ice depiction in satellite infra-red data. J. Geophys. Res., 77, pp. 453-462.
- Breaker, L., J. Klein and M. Pitts. 1978. Quantitative measurements of sea surface temperatures at several locations using the NOAA-3 very high resolution Radiometer. NOAA Technical Mem., NESS 98. 28 pp.
- Brooks, C.E.P. and N. Carruthers. 1953. Handbook of Statistical Methods in Meteorology, London. 412 pp.
- Collin, A.E. 1963. Waters of the Canadian Arctic Archipelago. In Proceedings of the Arctic Basin Symposium 1962, Arctic Institute of N. America, Washington. 313 pp.
- Fortuna, J.J. and L.N. Hambrick. 1974. The operation of the NOAA polar satellite system. NOAA Tech. Mem., NESS 60. 127 pp.
- Greaves, B. 1979. Personal communication, based on Uncompleted Masters Thesis, University of Alberta, Edmonton.
- Green, B.C. 1977. An Investigation of Thermal Fields and Secondary Circulations in the Canadian Western Arctic. Unpublished M.Sc. Thesis, University of Alberta, Edmonton. 166 pp.
- Hussey, W.J. 1977. The TIROS-N polar orbiting environmental satellite system. National Environmental Satellite Service, Washington. 20 pp. (Presented at Tenth Session of the ESCAP/W.M.O. Typhoon Committee, Tokyo.)

- Koffler, R., A.G. De Cotiis and P.K. Rao. 1973. A procedure for measuring cloud amount and height from satellite infra-red radiation data. Mon. Wea. Rev., 101, pp. 240-243.
- Langleben, M.P. 1972. The decay of an annual cover of sea ice. J. Glaciol., 11, pp. 337-344.
- LeSchack, L.A. 1975. Potential use of satellite IR data for ice thickness mapping. Final Report on NOAA/NESS Contract No. 3-35384. 33 pp.
- Maykut, G.A. and N. Untersteiner. 1971. Some results from a time dependent thermodynamic model of sea ice. J. Geophys. Res., 76, pp. 550-575.
- McClain, E.P. 1973. Quantitative use of satellite vidicon data for delineating sea ice conditions. Arctic, 26, pp. 44-57.
- _____. 1975. Potential value of earth satellite measurements to oceanographic research in the southern ocean. NOAA Technical Mem., NESS 61. 18 pp.
- _____. 1978. Sea ice observations by NOAA's National Environmental Satellite Service. In Glaciological Data, Report GD-2, Part 1, Institute of Alpine and Arctic Research, Boulder, Colorado. 262 pp.
- _____ and D.R. Baker. 1969. Experimental large-scale snow and ice mapping with composite minimum brightness charts. ESSA Technical Mem., NESCTM-12. 19 pp.
- _____ and M.D. Baliles. 1971. Sea ice surveillance from earth satellites. Mariner's Weather Log, 15, pp. 1-4.
- Poulin, A.O. 1975. Significance of surface temperature in IR Sensing of Sea Ice. J. Glaciol., 15, pp. 277-283.
- Rao, P.K. 1970. Estimating cloud amount and height from satellite infra-red radiation data. ESSA Technical Rep. NESCTR-54, 11 pp.
- _____, W.L. Smith and R. Koffler. 1972. Global sea-surface temperature distribution determined from an environmental satellite. Mon. Wea. Rev., 100, pp. 10-14.
- Reinelt, E.R., P. Hof, D. Oracheski and J. Broszkowski. 1975. Research studies of numerical enhancement of APT scanning radiometer data for application to Arctic weather and ice prediction. Final Report, DDS(AES) Contract OSV4-0183, University of Alberta, Edmonton. 204 pp.

- Reynolds, D.W. and T.H. Vonder Haar. 1977. A bispectral method of cloud parameter determination. Mon. Wea. Rev., 105, pp. 446-457.
- Sater, J.E. (ed.). 1963. The Arctic Basin. Arctic Institute of North America, Washington. 319 pp.
- Smith, W.L., P.K. Rao, R. Koffler and W.R. Curtis. 1970. Determination of sea-surface temperature from satellite high resolution infra-red window radiation measurements. Mon. Wea. Rev., 98, pp. 604-611.
- Vonder Haar, T.H. and V.E. Suomi. 1969. Satellite observations of the earth's radiation budget. Science, 163, pp. 667-669.
- Vowinckel, E. 1965. The inversion over the polar ocean. Arctic Meteor. Res. Group, Scientific Report 14, McGill University, Montreal. 21 pp.
- Vowinckel, E. and S. Orvig. 1976. Experiments with the surface heat and water budgets of the Canadian middle north. Tellus, XXVIII, pp. 442-450.
- Vukovich, F.M. 1971. Detailed sea-surface temperature analysis utilizing nimbus HRIR data. Mon. Wea. Rev., 99, pp. 812-817.
- Walker, E.R. 1977. Aspects of Oceanography in the Archipelago. Unpublished, Institute of Ocean Sciences, Patricia Bay, Victoria. 186 pp.
- Wendler, G. 1973. Sea ice observations by means of satellite. J. Geophys. Res., 78, pp. 1427-1448.
- Wiesnet, D.R. 1974. The role of satellites in snow and ice measurements. NOAA Tech. Mem., NESS 58. 12 pp.

APPENDIX A

HISTOGRAM COMPILATION ROUTINE

In this Appendix is listed the program used to assimilate the histograms used in surface temperature computations. Use is made of a "scan by scan" gridding algorithm (Reinelt, et al., 1975).

A major feature of this program is the variable specification of bin sizes in both latitudinal and longitudinal senses. Longitudinal demensions may be altered at several latitude locations, such that bin sizes may remain nearly constant, especially at high latitudes. Table A.1 lists this program.

Table A.2 lists sample input parameters for HIST, and Table A.3 lists sample histogram output.

TABLE A.1

```

C      PROGRAM HIST      ***HISTOGRAM COMPILATION PROGRAM***
C      MAY BE USED FOR VIS OR IR
C*****DEVICES USED IN PROGRAM ARE AS FOLLOWS:
C
C*****UNIT 1
C      INPUT (FORMATTED) OF GROUND TRUTH DATA (IF AVAILABLE)
C      (MAY ALSO BE USED TO DETERMINE SCAN/POSITION LIMITS OF STUDY AREA)
C
C*****UNIT 2
C      INPUT OF INTERNAL CALIBRATION DATA (FORMAT-FREE) IN FORM OF
C      SIX DATA VALUES AND SIX CORRESPONDING TEMPERATURES
C
C*****UNIT 3
C      INPUT OF FORMAT-FREE SATELLITE DATA (FILE OR MAG TAPE)
C
C*****UNIT 4
C      *FORMAT-FREE INPUT OF PROGRAM PARAMETERS
C          KINP = INPUT TYPE
C              KINP=0  IR DATA FROM FILE
C              KINP=1  VISIBLE DATA FROM FILE
C              KINP=3  IR DATA FROM MAG TAPE
C              KINP=4  VISIBLE DATA FROM MAG TAPE
C          NSKIP= NUMBER OF SCANS OF INPUT TO BE SKIPPED (FOR USE WITH MAG
C                  TAPE INPUT ONLY. FOR FILE INPUT, PROGRAM WILL READ EACH
C                  SCAN OF DATA, AND BEGIN OUTPUT WHEN BSCAN IS REACHED)
C          BSCAN= SCAN NUMBER TO BEGIN PROCESSING
C          ESCAN= SCAN NUMBER TO END PROCESSING
C                  (PROCESSING IS ESCAN-BSCAN+1 SCANS LONG)
C          MNDAT  FIRST POSITION TO BE PROCESSED
C          MXDAT  LAST POSITION TO BE PROCESSED
C          NSTOP=  0  DO NOT WRITE SCAN PARAMETERS;EXECUTE PRGM
C                  1  WRITE SCAN PARAMETERS; NO EXECUTION
C                  2  WRITE SCAN PARAMETERS;EXECUTE PROGRAM
C                  3  FIND EXTERNAL CAL. PTS.; NO EXECUTION
C          NGND=  0  NO GROUND TRUTH DATA AVAILABLE
C                  1  OTHERWISE (UP TO FIVE ALLOWED)
C      *GRIDDING INCREMENTS
C          DLATP  =LATITUDINAL INCREMENT
C          DLONGP(N)=LONGITUDINAL INCREMENTS
C          NAVG   NUMBER OF CONSECUTIVE DATONS AVERAGED TOGETHER
C          IATM   =0  LOCAL ZENITH ANGLE OF UP TO 90 DEG. ALLOWED
C                  =1  LOCAL ZENITH ANGLES LIMITED TO 65 DEG. OR LESS
C      *FREQUENCY TABLE PARAMETERS
C          MNLT,MXLT  DENOTE LATITUDE RANGE
C          MNLN,MXLN  DENOTE LONGITUDE RANGE
C          KMIN,KMAX  DENOTE TEMPERATURE OR BRIGHTNESS LIMITS
C      *ORBITAL DATA FOR CURRENT ORBIT
C          NYR  = YEAR OF ORBIT
C          NMO  = MONTH OF ORBIT
C          NDY  = DAY OF ORBIT
C          NSAT = SATELLITE NUMBER (04 = NOAA 4)
C          NORBIT = NUMBER OF ORBIT
C          IGRID = NUMBER OF SCANS BETWEEN EQUATOR CROSSING AND
C                  ARRIVAL OF SATELLITE
C          NPAR = SUBPOINT POSITION(DATON NUMBER)
C      *ORBITAL DATA FOR REFERENCE ORBIT
C          RORBIT = NUMBER OF REFERENCE ORBIT
C          RQ     = QUADRANT OF REFERENCE ORBIT EQUATOR CROSSING
C              RQ=0 (5)  0 TO 90 DEGREES LONGITUDE WEST
C              RQ=1 (6)  90 TO 180 DEGREES LONGITUDE WEST
C              RQ=2 (7)  90 TO 180 DEGREES LONGITUDE EAST
C              RQ=3 (8)  0 TO 90 DEGREES LONGITUDE EAST
C              0,1,2,3 ARE QUADRANTS FOR NORTHERN HEMISPHERE
C              5,6,7,8 ARE QUADRANTS FOR SOUTHERN HEMISPHERE
C          RLONG  = 'LONGITUDE' OF REFERENCE ORBIT EQUATOR CROSSING
C              RQ AND RLONG ARE CODED VALUES READ DIRECTLY FROM T-BUS.
C              THE PROGRAM CALCULATES RLONGC FROM THESE VALUES BY ASSUMING
C              RIGHT ASCENSION OF THE ORBIT, THAT IS, LONGITUDE IS TAKEN
C              TO BE POSITIVE TO EAST AND NEGATIVE TO WEST (T-BUS CODE
C              ASSUMES 0 TO 180 DEGREES BOTH EAST AND WEST)
C          RHR   = HOUR OF REFERENCE ORBIT (GMT)
C          RMIN  = MINUTE OF REFERENCE ORBIT
C          RSEC  = SECOND OF REFERENCE ORBIT

```



```

C      *SATELLITE PARAMETERS
C
C      PT      = ORBITAL PERIOD IN MINUTES
C      PL      = LONGITUDINAL DISPLACEMENT PER ORBIT IN DEG LONG TO WEST
C      H       = HEIGHT OF SATELLITE AT FIRST SCAN IN KM
C      ORIN    = INCLINATION OF SATELLITE AT FIRST SCAN IN DEGREES
C                (PROGRAM USES ORIN-90.)
C
C      *OUTPUT PARAMETER
C      NWRITE=  0  OUTPUT FORMATTED HISTOGRAMS ONLY
C                1  OUTPUT FORMATTED AND UNFORMATTED HISTOGRAMS
C                2  OUTPUT UNFORMATTED HISTOGRAMS ONLY
C
C*****UNIT 5
C      OUTPUT OF UNFORMATTED HISTOGRAMS (FOR STATISTICAL EVALUATION)
C
C*****UNIT 6
C      OUTPUT OF SCAN INFORMATION, INTERNAL AND EXTERNAL CALIBRATION
C      INFORMATION
C
C*****UNIT 7
C      OUTPUT OF FORMATTED HISTOGRAMS
C
C*****
C      LOGICAL*1 LFMT(1) /'*/
C      LOGICAL*1 LA(920)
C      REAL*8 IR,VISIBL,IROV,EAST,WEST,QUAD,TMULP
C      REAL DLONGP(8),INFO(5,4),T(46),RMN(8),RMX(8),X(6),FOFX(6)
C      INTEGER*2 ID(920),NSUM1(768),NCNT(100,45,20),NSUM(45)
C      INTEGER*2 HSCAN,BSCAN,ESCAN,NCAL(11,5)
C      INTEGER RORBIT,RQ,RHR,RMIN,RSEC,KFAC(10),ISHP(5,4)
C      DATA IR/8H      IR /,VISIBL/8H VISIBLE/,EAST/5H EAST/,WEST/5H WEST/
C
C*****CONSTANTS REQUIRED
C      DATA DIGF/2400./,SRPM/48./,PI/3.14159/,C1/.01745333/,R/6368./
C      RT=PI/2.
C      TMULP=DIGF*60./(360.*SRPM)
C      C2=1./C1
C      READ(4,LFMT) KINP,NSKIP,BSCAN,ESCAN,MNDAT,MXDAT,NSTOP,NGND
C      READ(4,LFMT) DLATP,(DLONGP(N),N=1,8),NAVG,IATM
C      READ(4,LFMT) MNLT,MXLT,MNLN,MXLN,KMIN,KMAX
C      READ(4,LFMT) NYR,NMO,NDY,NSAT,NORBIT,IGRID,NPAR
C      READ(4,LFMT) RORBIT,RQ,RLONG,RHR,RMIN,RSEC
C      READ(4,LFMT) PT,PL,H,ORIN
C      READ(4,LFMT) NWRITE
C*****CONVERT INPUT LONGITUDE TO PROGRAM FORM
C      IF(RQ.EQ.0.OR.RQ.EQ.5) RLONGC=360.-RLONG
C      IF((RQ.EQ.1.OR.RQ.EQ.6).AND.RLONG.GE.90.) RLONGC=360.-RLONG
C      IF((RQ.EQ.1.OR.RQ.EQ.6).AND.RLONG.LT.90.) RLONGC=360.-RLONG-100.
C      IF((RQ.EQ.2.OR.RQ.EQ.7).AND.RLONG.LT.90.) RLONGC=RLONG+100.
C      IF((RQ.EQ.2.OR.RQ.EQ.7).AND.RLONG.GE.90.) RLONGC=RLONG
C      IF(RQ.EQ.3.OR.RQ.EQ.8) RLONGC=RLONG
C*****CONVERT TO REAL LONGITUDE FOR OUTPUT ONLY
C      QUAD=EAST
C      RLONGR=RLONGC
C      IF(RLONGC.LE.180.0) GO TO 7
C      QUAD=WEST
C      RLONGR=360.-RLONGC
C*****CALCULATE LAST EQUATOR CROSSING FROM REFERENCE LONG
C      7 RL=RLONGC-(NORBIT-RORBIT)*PL
C      RL=AMOD(RL,360.)
C      IF(RL.LT.0.) RL=RL+360.
C      RRL=RL*C1
C      RI=(ORIN-90.)*C1
C      CI=COS(RI)
C      SI=SIN(RI)
C      RTIME=RHR*60.+RMIN+RSEC/60.
C      STIME=RTIME+(NORBIT-RORBIT)*PT+IGRID/SRPM
C      SHR=AMOD(STIME,1440.0)
C      NHR=SHR/60.
C      SMIN=SHR-NHR*60.
C      NMIN=SMIN

```



```

SSEC=SMIN-NMIN
NSEC=SSEC*60.
IROV=IR
IF(KINP.EQ.1.OR.KINP.EQ.4) IROV=VISIBL
REF=1500-NPAR
C*****CHECK INPUT DATA
WRITE(6,531) IROV,NORBIT,NSAT,NMO,NDY,NYR,NHR,NMIN,NSEC,IGRID,
1 NORBIT,RLONGR,QUAD,RHR,RMIN,RSEC,PT,PL,H,R,ORIN,SRPM
WRITE(6,532) BSCAN,ESCAN
531 FORMAT(1H1,5X,A8,' INFORMATION FROM ORBIT',16,2X,'OF NOAA',13,
1 5X,'ON ',13,1H/,12,1H/,14,5X,'TIME:',13,1H:,12,1H:,12,' GMT',
2 //,15X,15,' SCANS PASSED SINCE LAST EQUATOR CROSSING',//,5X,
3 'REFERENCE ORBIT',16,5X,'CROSSED EQUATOR AT LONGITUDE',F7.2,
4 ' DEGREES',A5,5X,'TIME:',13,1H:,12,1H:,12,' GMT',//,5X,
5 'ORBITAL PERIOD =',F10.5,' MIN',5X,'LONGITUDINAL INCREMENT =',
6 F6.2,' DEGREES TO WEST',//,5X,'HEIGHT OF SATELLITE AT EQUATOR =',
7 F6.0,' KM',5X,'RADIUS OF EARTH =',F6.0,' KM',//,5X,
8 'ORBITAL INCLINATION =',F7.2,' DEG',5X,'SCANNING RATE =',
9 F4.0,' SCANS PER MINUTE')
532 FORMAT(1H0,4X,'SCANNING BEGINS AT',16,2X,'AND ENDS AT',16)
WRITE(6,533) NPAR
533 FORMAT(1H0,4X,'SUBPOINT POSITION AT DATON NUMBER',14)
IF(NSTOP.EQ.1) STOP
IF(NSTOP.EQ.3)GO TO 191
C
C*****INITIALIZE APPROPRIATE DATA REGISTERS TO ZERO
C*****AND CHECK LAT/LONG AND TEMPERATURE RANGES
JX=0
IF(MXLT.LE.88)GO TO 20
MXLT=MAX0(MNLT,88)
JX=1
20 I1=MNLT/DLATP
R1=FLOAT(I1)*DLATP
I2=MXLT/DLATP+.99
R2=FLOAT(I2)*DLATP
JJJ=IFIX((R2-R1)/DLATP)+JX
IF(JJJ.LE.20)GO TO 19
JJJ=20
R2=R1+20.*DLATP
IF(R2.GT.88)R2=90.
WRITE(6,14) R1,R2
14 FORMAT(1H0,'***ERROR ON LATITUDE RANGE INPUT***',/,1X,
1 'MINIMUM LATITUDE WILL BE',F5.2,' DEGREES, MAXIMUM LATITUDE',
2 ' WILL BE',F5.2,' DEGREES')
19 IF((KMAX-KMIN+1).LE.100)GO TO 16
KMIN=KMAX-99
WRITE(6,11) KMIN,KMAX
11 FORMAT(1H0,'***ERROR ON HISTOGRAM RANGE INPUT***',/,' MINIMUM',
1 ' VALUE WILL BE',14,' MAXIMUM VALUE WILL BE',14)
16 KKK=KMAX-KMIN+1
DO 15 N=1,8
I1=MNLN/DLONGP(N)
RMN(N)=FLOAT(I1)*DLONGP(N)
I2=MXLN/DLONGP(N)+.99
RMX(N)=FLOAT(I2)*DLONGP(N)
15 CONTINUE
RX=R1+DLATP
N=NSIZE(RX)
MMM=IFIX((RMX(N)-RMN(N))/DLONGP(N))
IF(MMM.LE.45)GO TO 17
MMM=45
- RMX(N)=RMN(N)+45.*DLONGP(N)
MXLN=RMX(N)
WRITE(6,18) RMN(N),RMX(N)
18 FORMAT(1H0,'***ERROR ON LONGITUDE RANGE INPUT***',/,1X,'FOR',
1 ' LATITUDE RANGE NEAREST EQUATOR, MINIMUM LONGITUDE WILL BE',
2 F6.2,' DEGREES',/,37X,'MAXIMUM LONGITUDE WILL BE',F6.2,' DEGREES')
17 DO 10 J=1,JJJ
DO 10 M=1,MMM
DO 10 K=1,KKK
NCNT(K,M,J)=0
10 CONTINUE
IF(IROV.EQ.VISIBL)GO TO 196

```



```

C
C*****INTERNAL CALIBRATION
C
C*****FIND CALIBRATION VALUES FOR DATON SUMS
  READ(2,LFMT) (X(N),N=1,6)
  READ(2,LFMT) (FOFX(N),N=1,6)
  NCALC=256*NAVG
  DO 60 JJM=1,NCALC
    JJ=JJM-1
    SUM=JJ/FLOAT(NAVG)
C*****ORDER CAL. PTS. IN INCREASING DISTANCE FROM CURRENT DATON VALUE
  DO 90 II=1,6
    J=7-II
    DO 90 M=2,J
      IF(ABS(SUM-X(M)).GT.ABS(SUM-X(M-1)))GO TO 90
      A=X(M-1)
      X(M-1)=X(M)
      X(M)=A
      B=FOFX(M-1)
      FOFX(M-1)=FOFX(M)
      FOFX(M)=B
  90 CONTINUE
C*****USE FIVE CLOSEST PTS. IN CURVE-FITTING (NEWTON POLYNOMIAL)
  FTOT=0.
  DO 56 NN=1,5
    FX=0.
    YPROD=1.
    DO 27 M=1,NN
      XPROD=1.
      DO 30 L=1,NN
        IF(L.EQ.M)GO TO 30
        XPROD=XPROD*(X(M)-X(L))
  30 CONTINUE
      FX=FX+(FOFX(M)/XPROD)
      IF(M.EQ.NN)GO TO 27
      YPROD=YPROD*(SUM-X(M))
  27 CONTINUE
      FTOT=FTOT+(FX*YPROD)
  56 CONTINUE
      NSUM1(JJM)=IFIX(FTOT+.5)
  60 CONTINUE
      IF(NGND.EQ.0)GO TO 196
C
C*****READ EXTERNAL CALIBRATION DATA
  191 NSHPS=1
  300 READ(1,100,END=200) (INFO(NSHPS,I),I=1,4)
  NSHPS=NSHPS+1
  100 FORMAT(4X,F6.2,F7.2,F5.1,F4.1)
  GO TO 300
  200 NSHPS=NSHPS-1
  WRITE(6,400)
  400 FORMAT(1H1,2X,'SHIP OBSERVATIONS AVAILABLE FOR TEMPERATURE ',
    1'ADJUSTMENT',/,2X,'SHIP',2X,'LATITUDE',2X,'LONGITUDE',2X,
    2'TEMP(C)',2X,'CLOUD COVER FRACTION')
  REWIND 1
  800 READ(1,500,END=600) F1,F2,F3,F4,F5,F6
  500 FORMAT(2(A2),F6.2,F7.2,F5.1,F4.1)
  WRITE(6,700) F1,F2,F3,F4,F5,F6
  700 FORMAT(1H0,2(A2),4X,F6.2,4X,F7.2,4X,F5.1,10X,F4.1)
  GO TO 800
  600 CONTINUE
C*****CONVERT DATA LOCATIONS TO USEABLE FORM (DECIMAL DEGREES)
  DO 8 J=1,NSHPS
    DO 6 I=1,2
      M=INFO(J,I)
      Q=INFO(J,I)-FLOAT(M)
      S=Q*100./60.
      INFO(J,I)=(FLOAT(M)+S)*C1
  6 CONTINUE
      IF(INFO(J,2).LE.0.)INFO(J,2)=INFO(J,2)+2.*PI
      ISHP(J,1)=999
  8 CONTINUE

```



```

C*****INITIALIZE REGISTERS FOR EXTERNAL CALIBRATION
DO 4 L=1,NSHPS
DO 4 M=1,11
NCAL(M,L)=0
4 CONTINUE
C
C*****DETERMINE SCAN ANGLES FOR FIRST AND SECOND HORIZONS
196 RETAH=ARSIN(R/(R+H))
ETAH=RETAH*C2
RGAMH=PI*.5-RETAH
GAMH=90.-ETAH
SIGH1=180.-ETAH
SIGH2=180.+ETAH
KB=SIGH1*TMULP+.99-REF
KE=SIGH2*TMULP+.01-REF
IF(KB.LT.2)KB=2
IF(KE.GT.919)KE=919
IF(NSTOP.EQ.0)GO TO 1310
WRITE(6,1301) KB,KE
1301 FORMAT(1H0,'FIRST HORIZON AT DATON NO.',I3,
1' SECOND HORIZON AT DATON NO.',I4)
1310 IF(IATM.EQ.0)GO TO 195
C*****FIND MAXIMUM ALLOWABLE SCANNING DISTANCE FROM SUBPOINT
C***** (ALLOWING FOR A LOCAL ZENITH ANGLE OF 65 DEGREES)
RALPH=ARSIN(R*.9063/(R+H))
ALPH=RALPH*C2
AAA=TMULP*ALPH
XPAR=FLOAT(NPAR)
KB=IFIX(XPAR-AAA+.5)
KE=IFIX(XPAR+AAA+.5)
IF(NSTOP.EQ.0)GO TO 195
WRITE(6,1308) KB,KE
1308 FORMAT(1H0,'FORESHORTENING DATON LIMITS: FIRST',I3,' LAST',I4)
C*****ADJUST SCAN DATA FOR AVERAGING SCHEME
195 IF(MNDAT.EQ.0)GO TO 194
KB=MAX0(MNDAT,KB)
KE=MIN0(MXDAT,KE)
194 JAV=MOD((KE-KB+1),NAVG)
IF(NAVG.EQ.1.OR.JAV.EQ.0)GO TO 107
IF(NAVG.EQ.2.OR.JAV.EQ.2)GO TO 104
KE=KE+1
104 KB=KB-1
107 NF=IFIX(KB/FLOAT(NAVG)+.5)
NL=NF+(KE-KB+1)/NAVG
WRITE(6,1391) NF,NL
1391 FORMAT(1H0,'FIRST USEABLE POSITION:',I3,', ',
1' FINAL USEABLE POSITION:',I4)
IIL=ESCAN-BSCAN+1
ICNT=0
IF(NGND.EQ.0)GO TO 197
C
C*****SEARCH FOR SCAN/POSITION OF GROUND TRUTH INFORMATION
N0=12/(NAVG+1)
CSI=COS(ORIN*C1)
SSI=SIN(ORIN*C1)
PX=PL/360.
CA=1.-PX*CSI
CD=PX-CSI
CC=3000./(2.*PI)
DO 166 J=1,NSHPS
CB=COS(INFO(J,1))
SB=SIN(INFO(J,1))
THETZ=RRL-INFO(J,2)
ST=THETZ-PX*INFO(J,1)
S0=ATAN2(SSI*SB-CSI*CB*SIN(ST),CB*COS(ST))
IF(S0.LT.0..AND.INFO(J,1).GT.RT)S0=S0+2.*PI
SP=S0
DO 177 JX=1,10
ST=THETZ-PX*S0
CT=COS(ST)
ST=SIN(ST)
CSO=COS(S0)

```



```

      SSO=SIN(S0)
      SP=S0-(CB*(SSO*CT+CSI*CSO*ST)-SSI*SB*CSO)/
1    (CB*(CA*CSO*CT+CD*SSO*ST)+SSI*SB*SSO)
      ST=CSI*SB+SSI*CB*SIN(THETZ-PX*SP)
      IF(ABS(SP-S0).LT.1E-6)GO TO 167
      S0=SP
177  CONTINUE
      WRITE(6,178) J
178  FORMAT(1H0,'NO CONVERGENCE FOR POINT #',I3)
      GO TO 166
167  YY=ATAN(R*ST/(H+R*(1.-SQRT(1.-ST*ST))))
      N5=IFIX((NPAR+(CC*YY))/FLOAT(NAVG)+.5)
      NSCAN=IFIX(.5+SRPM*SP*PT/(2.*PI))-IGRID
      N3=N5-N0
      N4=N5+N0
      IF(N3.GT.NL.OR.N4.LT.NF)GO TO 31
      ISHP(J,3)=MAX0(NF,N3)
      ISHP(J,4)=MIN0(NL,N4)
      N1=NSCAN-3
      N2=NSCAN+3
      IF(N1.GT.ESCAN.OR.N2.LT.BSCAN)GO TO 31
      ISC=BSCAN
      ISHP(J,1)=MAX0(N1,ISC)
      ISC=ESCAN
      ISHP(J,2)=MIN0(N2,ISC)
      KFAC(J)=IFIX(INFO(J,3)-5.)
      KFAC(J+5)=IFIX(INFO(J,3)+5.)
      WRITE(6,33) J,NSCAN,N5
33   FORMAT(1H0,'SHIP #',I2,' LOCATION:  SCAN',I4,' POSITION',I4)
      ICNT=ICNT+1
      GO TO 166
31   WRITE(6,34) J,NSCAN,N5
34   FORMAT(1H0,'SHIP #',I2,' OUTSIDE ALLOWABLE SCANNING RANGE'
1     1,/, ' SCAN',I4,' POSITION',I4)
166  CONTINUE
      IF(NSTOP.EQ.3)STOP
C
C*****COMMENCE SCAN-BY-SCAN GRIDDING PROCEDURE
C
197  IF(KINP.NE.3.AND.KINP.NE.4)GO TO 5
      CALL SKIP(0,NSKIP,3,&993)
5     I=0
2     IF(I.EQ.IIL)GO TO 998
      READ(3) HSCAN,LA
      IF(HSCAN.LT.BSCAN)GO TO 2
      I=I+1
C*****DETERMINE LAT/LONG (PHI/THET) OF SUBPOINT
      DEGAM=(IGRID+HSCAN)*360./(SRPM*PT)
      RDEGAM=DEGAM*C1
      RPHI=ARSIN(SIN(RDEGAM)*C1)
      X1=SI*SIN(RDEGAM)
      X2=COS(RDEGAM)
      RDLONG=ATAN2(X1,X2)
C*****ADJUST LONGITUDE TO ROTATING EARTH
      RTHET=RRL-RDLONG-(IGRID+HSCAN)*C1/(4.*SRPM)
      IF(RTHET.LT.0.)RTHET=RTHET+2.*PI
C*****DETERMINE AZIMUTH OF HEADING LINE AT SUBPOINT
      X1=SI/C1
      X2=-COS(RDEGAM)
      RIS=ATAN2(X1,X2)
      PHI=RPHI*C2
      THET=RTHET*C2
C*****DETERMINE WHETHER SATELLITE IS SOUTH (D=1.) OR
C*****NORTH (D=2.) BOUND
      D=1.
      IF(RIS.GT.RT)D=2.
C*****DETERMINE LAT/LONG OF HORIZONS
C*****FIRST HORIZON (PHIH1/THETH1)
      RPHIH1=ARSIN(SIN(RPHI)*COS(RGAMH)+COS(RPHI)*SIN(RGAMH)
1     1*SIN(RIS))
      X1=SIN(RGAMH)*COS(RIS)*COS(RPHI)
      X2=COS(RGAMH)-SIN(RPHIH1)*SIN(RPHI)

```



```

      FUD=ATAN2(X1,X2)
      RTHTH1=RTHET-FUD
      THETH1=RTHTH1*C2
      PHIH1=RPHIH1*C2
C*****SECOND HORIZON (PHIH2/THETH2)
      RPHIH2=ARSIN(SIN(RPHI)*COS(RGAMH)-COS(RPHI)*SIN(RGAMH)
1*SIN(RIS))
      X1=-X1
      X2=COS(RGAMH)-SIN(RPHIH2)*SIN(RPHI)
      FUD=ATAN2(X1,X2)
      RTHTH2=RTHET-FUD
      THETH2=RTHTH2*C2
      PHIH2=RPHIH2*C2
      IF(NSTOP.EQ.0)GO TO 1340
      WRITE(6,1341) HSCAN,PHIH1,THETH1,PHIH2,THETH2,PHI,THET
1341 FORMAT(1H0,'SCAN#',I4,'HORIZON 1:',4X,'LAT',F6.2,3X,'LONG',F6.2,
1/,1X,'HORIZON 2:',3X,'LAT',F6.2,3X,'LONG',F6.2,/,1X,'SUBPOINT:',
29X,'LAT',F6.2,3X,'LONG',F6.2)
C*****DETERMINE IF SCAN CROSSES SAME LATITUDE TWICE
1340 LCHK=1
      RGAMM=ATAN(SI/SIN(RPHI))
      IF(RGAMM.LT.RGAMH)LCHK=2
C*****DETERMINE MAXIMUM LATITUDE CROSSING FOR CURRENT SCAN (PHIM)
C*****AND MAXIMUM GRIDDED LATITUDE CROSSING (PHIG)
      RPHIM=ARSIN(SIN(RPHI)/COS(RGAMM))
      PHIM=RPHIM*C2
      NFLAG=0
      IF(LCHK.EQ.2)GO TO 62
      IF(PHIH1.GT.PHIH2)GO TO 61
      AMX=PHIH2/DLATP
      GO TO 85
61 AMX=PHIH1/DLATP
      NFLAG=1
      GO TO 85
62 AMX=PHIM/DLATP
85 MX=AMX
      PHIG=FLOAT(MX)*DLATP
      IF(PHIG.GT.88.)PHIG=88.
      IF(NSTOP.EQ.0)GO TO 1370
      WRITE(6,444) PHIG
444 FORMAT(1H0,5X,'MAXIMUM LATITUDE CROSSING IS',F5.1,' DEGREES')
1370 IF(PHIG.LT.R1.AND.ICNT.EQ.0)GO TO 2
      RPHIG=PHIG*C1
C*****DO DATON AVERAGING ALONG SCAN
      NX=NF
      DO 109 IX=KB,KE,NAVG
      IE=MIN0(KE,IX+NAVG-1)
      NS=0
      DO 140 J=IX,IE
      ID(J)=IBYTE(LA(J))
      NS=NS+ID(J)
140 CONTINUE
      IF(IROV.EQ.IR)GO TO 175
      ID(NX)=IFIX(NS/FLOAT(NAVG)+.5)
      GO TO 174
175 ID(NX)=NSUM1(NS+1)
174 NX=NX+1
109 CONTINUE
      NL=NX-1
      IF(ICNT.EQ.0)GO TO 210
C*****PLACE EXTERNAL CAL. DATA IN APPROPRIATE REGISTERS (IF NECESSARY)
      DO 209 J=1,NSHPS
      IF(ISHP(J,1).EQ.999)GO TO 209
      IF(ISHP(J,1).GT.HSCAN.OR.ISHP(J,2).LT.HSCAN)GO TO 209
      KK1=ISHP(J,3)
      KK2=ISHP(J,4)
      DO 208 K=KK1,KK2
      IF(ID(K).LT.KFAC(J).OR.ID(K).GT.KFAC(J+5))GO TO 208
      KTMP=ID(K)-KFAC(J)+1
      NCAL(KTMP,J)=NCAL(KTMP,J)+1
208 CONTINUE
209 CONTINUE

```



```

C
C*****DETERMINE FIRST LATITUDE CROSSING IN SCAN
C***** (INTERROGATE SCAN BEGINNING FROM FIRST HORIZON)
C
210 IF(PHIG.LT.R1)GO TO 2
    NN1=NF
    IF(NFLAG.EQ.1)GO TO 72
    ANXT=(PHIH1+DLATP)/DLATP
    NXT=ANXT
    PHIC=FLOAT(NXT)*DLATP
    GO TO 71
72 PHIC=PHIG
71 THETC=THETH1
73 RPHIC=PHIC*C1
C*****DETERMINE LONGITUDE INCREMENT
    PH=PHIC
    IF(NFLAG.EQ.1)PH=PH+DLATP
    IF(PH.LE.R1.AND.NFLAG.EQ.1)GO TO 2
    APH=(PH-R1)/DLATP
    JP=APH
    N=NSIZE(PH)
C*****DETERMINE GREAT CIRCLE ARC LENGTH FOR LATITUDE CROSSING
    RGAMP=ARCOS(SIN(RPHIC)/SIN(RPHIM))
    IF(NFLAG.EQ.1)GO TO 75
    RGAMG=-RGAMP-RGAMM
    GO TO 76
75 RGAMG=RGAMP-RGAMM
76 RETAG=ATAN(R*SIN(RGAMG)/(H+R*(1.-COS(RGAMG))))
    ETAG=RETAG*C2
    SIGG=ETAG+180.
    AJ3=(SIGG*TMULP-REF)/FLOAT(NAVIG)
    JJ=IFIX(AJ3+.5)
C*****CHECK SIGN OF LONGITUDE INCREMENT RELATIVE TO POLAR SCAN CROSSING
    IF(D.EQ.2..AND.DLONGP(N).GT.0.)DLONGP(N)=-DLONGP(N)
    IF(D.EQ.1..AND.DLONGP(N).LT.0.)DLONGP(N)=-DLONGP(N)
C*****DETERMINE APPROPRIATE LONGITUDE CROSSING
    NVAL=THETC/DLONGP(N)
    VAL=NVAL
    AVAL=VAL*DLONGP(N)
    IF(AVAL.EQ.0.)GO TO 142
41 IF(D.EQ.2..AND.AVAL-DLONGP(N).GE.THETC)GO TO 142
    IF(D.EQ.2..AND.AVAL-DLONGP(N).LT.THETC)GO TO 143
    IF(AVAL.LT.THETC)AVAL=AVAL+DLONGP(N)
    GO TO 142
143 AVAL=AVAL-DLONGP(N)
    GO TO 41
142 RR=AVAL
    IF(RMX(N).GT.360..AND.RR.LT.180.)RR=RR+360.
    IF(RMX(N).LE.360.)RR=AMOD(AVAL,360.)
    JTHETC=ABS(RR/DLONGP(N))
    IF(D.EQ.2.)JTHETC=JTHETC+1
    RTHETC=AVAL*C1
    RDTHET=RTHET-RTHETC
    CSALFA=SIN(RIS)*COS(RDTHET)-COS(RIS)*SIN(RDTHET)*
1SIN(RPHI)
    Y=COS(RDEGAM)
    SNALFA=SIGN(1.,Y)*SORT(1.-CSALFA*CSALFA)
    RGAMG=ARSIN(SIN(RDTHET)*COS(RPHI)/SNALFA)
    RETAG=ATAN(R*SIN(RGAMG)/(H+R*(1.-COS(RGAMG))))
    ETAG=RETAG*C2
    SIGG=ETAG+180.
    AJ3=(SIGG*TMULP-REF)/FLOAT(NAVIG)
    KK=IFIX(AJ3+.5)
    LL=MIN0(KK,JJ)
    IF(LL.LT.NN1)GO TO 42
    IF(LL.GT.NL)LL=NL

```



```

C*****ASSIGN RADIATION DATA TO APPROPRIATE REGISTER
  JT=JTHETC-ABS(RMN(N)/DLONGP(N))
  JTP=ABS(RMX(N)/DLONGP(N))
  IF(JT.LE.0.OR.JTHETC.GT.JTP)GO TO 40
  IF(N.EQ.8.AND.R2.GT.88)JP=JJJ
  IF(JP.LE.0.OR.JP.GT.JJJ)GO TO 40
  DO 38 K=NN1,LL
  IF(ID(K).LT.KMIN.OR.ID(K).GT.KMAX)GO TO 38
  K2=ID(K)-KMIN+1
  NCNT(K2,JT,JP)=NCNT(K2,JT,JP)+1
38 CONTINUE
C*****ADJUST LATITUDE AND/OR LONGITUDE CROSSINGS
  IF(LL.EQ.NL)GO TO 2
40 NN1=LL+1
42 IF(JJ.LE.KK)GO TO 101
  THETC=AVAL
  AVAL=AVAL+DLONGP(N)
  GO TO 142
101 IF(PHIC.LT.PHIG.AND.NFLAG.NE.1)GO TO 106
  IF(PHIC.EQ.PHIG.AND.NFLAG.NE.1)GO TO 105
  PHIC=PHIC-DLATP
  GO TO 73
106 PHIC=PHIC+DLATP
  GO TO 73
105 NFLAG=1
  GO TO 73
998 IF(ICNT.EQ.0)GO TO 116
C
C*****COMPUTE EXTERNAL CALIBRATION ADJUSTMENT
C
  JCNT=0
  TADJ=0.
  DO 110 J=1,NSHPS
  IF(ISHP(J,1).EQ.999)GO TO 110
  SUM=0.
  TOT=0.
  DO 111 K=1,11
  K1=K+KFAC(J)-1
  SUM=SUM+NCAL(K,J)
  TOT=TOT+NCAL(K,J)*K1
111 CONTINUE
  IF(SUM.LT.10.)GO TO 118
  AVG=TOT/SUM
  VAR=0.
  DO 112 K=1,11
  S1=K+KFAC(J)-1
  VAR=VAR+NCAL(K,J)*(S1-AVG)*(S1-AVG)
112 CONTINUE
  VAR=VAR/SUM
  STD=SQRT(VAR)
  IF(STD.GT.2.)GO TO 113
  TADJ=TADJ+(INFO(J,3)-AVG)
  JCNT=JCNT+1
  GO TO 114
113 WRITE(6,117) J,AVG,STD
117 FORMAT(1H0,'SHIP',12,' NOT USED IN ADJUSTMENT, TEMP=',F6.2,
1' C, STD. DEV=',F5.2,'C')
  GO TO 110
118 WRITE(6,119) J
119 FORMAT(1H0,'SHIP',12,' NOT USED IN ADJUSTMENT, INSUFFICIENT DATA')
  GO TO 110
114 WRITE(6,115) J,INFO(J,3),AVG,STD,SUM
115 FORMAT(1H0,'SHIP',12,' REPORTED',F5.1,' C COMPUTED',F6.2,' C',/,
15X,'STANDARD DEVIATION=',F5.2,' C POPN=',F4.0)
110 CONTINUE
  IF(JCNT.EQ.0)GO TO 116
  TADJ=TADJ/FLOAT(JCNT)
  KMIN=KMIN+IFIX(TADJ+.5)
  KMAX=KMAX+IFIX(TADJ+.5)
  WRITE(6,120) TADJ,JCNT
120 FORMAT(1H0,'///','FINAL ADJUSTMENT:',F5.1,' DEG USING',12,' SHIPS')

```



```

C
C*****OUTPUT DATA IN FREQUENCY TABLE FORMAT
C
116 IF(NWRITE.EQ.2)GO TO 58
DO 50 J=1,JJJ
P1=R1+(J-1)*DLATP
P2=P1+DLATP
N=NSIZE(P2)
IF(N.EQ.8)P2=90.
IF(IROV.EQ.VISIBL)GO TO 622
WRITE(7,123) P1,P2
123 FORMAT(1H1,15X,'FREQUENCY TABLES OF RADIATION TEMPERATURES',///,
15X,'LATITUDINAL RANGE',F5.1,' DEGREES TO',F5.1,' DEGREES',//,
215X,'***LONGITUDINAL RANGES (DEG. EAST)***')
GO TO 623
622 WRITE(7,122) P1,P2
122 FORMAT(1H1,15X,'FREQUENCY TABLES OF BRIGHTNESS VALUES',///,
15X,'LATITUDINAL RANGE',F5.1,' DEGREES TO',F5.1,' DEGREES',//,
215X,'***LONGITUDINAL RANGES (DEG. EAST)***')
623 IF(DLONGP(N).LT.0.)DLONGP(N)=-DLONGP(N)
MP=((RMX(N)-RMN(N))/DLONGP(N))+1
DO 51 M=1,MP
T(M)=RMN(N)+(M-1)*DLONGP(N)
51 CONTINUE
MPP=MP-1
DO 49 M=1,MPP
NSUM(M)=0
DO 49 K=1,KKK
NSUM(M)=NSUM(M)+NCNT(K,M,J)
49 CONTINUE
M1=1
M2=MIN0(MPP,12)
55 WRITE(7,124) (T(M),M=M1,M2)
124 FORMAT(1H0,5X,12F7.1)
WRITE(7,124) (T(M+1),M=M1,M2)
IF(IROV.EQ.VISIBL)GO TO 728
WRITE(7,128)
128 FORMAT(1H0,'TEMP(C)')
GO TO 727
728 WRITE(7,127)
127 FORMAT(1H0,'VALUE')
727 DO 52 K=1,KKK
K1=K+KMIN-1
WRITE(7,125) K1,(NCNT(K,M,J),M=M1,M2)
125 FORMAT(1H ,14,12I7)
52 CONTINUE
WRITE(7,126) (NSUM(M),M=M1,M2)
126 FORMAT(/,1X,'TOTAL',12(16,1X))
IF(MPP.EQ.M2)GO TO 50
M1=M2+1
M2=MIN0(M2+12,MPP)
IF(IROV.EQ.VISIBL)GO TO 923
WRITE(7,123) P1,P2
GO TO 55
923 WRITE(7,122) P1,P2
GO TO 55
50 CONTINUE
58 IF(NWRITE.EQ.0)GO TO 91
C
OUTPUT OF UNFORMATTED DATA
WRITE(5) KMIN,KMAX,(((NCNT(K,M,J),K=1,KKK),M=1,MMM),J=1,JJJ)
GO TO 91
993 WRITE(6,1993)
1993 FORMAT(1H0,10X,'***ERROR ON SCAN SKIP***')
91 STOP
END

```



```
C
C      CONVERT ONE BYTE NUMBER INTO TWO BYTES
C
      FUNCTION IBYTE(NUM)
      LOGICAL*1 NUM,INT(2)
      INTEGER*2 I/O/
      EQUIVALENCE (I,INT)
      INT(2)=NUM
      IBYTE=I
      RETURN
      END

C
C      CALCULATE LONGITUDE INCREMENT PARAMETER
C
      FUNCTION NSIZE(ABC)
      NSIZE=1
      IF(ABC.GT.55.)NSIZE=2
      IF(ABC.GT.65.)NSIZE=3
      IF(ABC.GT.70.)NSIZE=4
      IF(ABC.GT.75.)NSIZE=5
      IF(ABC.GT.80.)NSIZE=6
      IF(ABC.GT.85.)NSIZE=7
      IF(ABC.GT.88.)NSIZE=8
      RETURN
      END
```


TABLE A.2

Sample List of Parameters for HIST.

KINP	3	NAVG	3	RHR	19
NSKIP	0	IATM	1	RMIN	42
BSCAN	420	MNLT	70	RSEC	37
ESCAN	535	MXLT	75	PT	116.336
MNDAT	50	MNLN	216	PL	29.0842
MXDAT	850	MXLN	231	H	1525.
NSTOP	0	KMIN	-7	ORIN	102.11
NGND	1	KMAX	12	NPAR	454
DLATP	.5	NYR	77	NWRITE	0
DLONGP(1)	.5	NMO	08		
DLONGP(2)	.75	NDY	15		
DLONGP(3)	1.	NSAT	05		
DLONGP(4)	1.5	NORBIT	4731		
DLONGP(5)	2.	RORBIT	4693		
DLONGP(6)	2.5	RQ	3		
DLONGP(7)	4.	RLONG	14.28		
DLONGP(8)	45.	IGRID	1042		

TABLE A.3

Sample Output from HIST, Orbit 4718.

FREQUENCY TABLES OF RADIATION TEMPERATURES

LATITUDINAL RANGE 72.0 DEGREES TO 73.0 DEGREES

TEMP (C)	***LONGITUDINAL RANGES (DEG. EAST)***							
	216.0	219.0	222.0	225.0	228.0	231.0	234.0	237.0
	219.0	222.0	225.0	228.0	231.0	234.0	237.0	240.0
-7	0	0	0	0	0	0	1	0
-6	0	0	0	0	0	1	3	1
-5	0	0	0	0	0	2	2	0
-4	0	0	0	0	0	1	2	1
-3	0	0	0	0	0	8	5	0
-2	9	7	0	0	0	6	2	3
-1	25	19	3	4	1	5	1	2
0	41	65	25	23	15	20	19	7
1	31	31	21	37	16	22	14	5
2	27	17	28	24	23	24	4	6
3	11	13	33	19	35	22	6	14
4	11	5	27	15	34	26	2	9
5	4	2	20	27	27	15	3	15
6	0	0	3	8	4	1	2	9
7	0	0	0	0	0	0	2	6
8	0	0	0	0	0	0	7	12
9	0	0	0	0	0	0	3	7
10	0	0	0	0	0	0	7	9
11	0	0	0	0	0	0	3	7
12	0	0	0	0	0	0	6	14
13	0	0	0	0	0	0	2	6
14	0	0	0	0	0	0	17	8
15	0	0	0	0	0	0	19	5
16	0	0	0	0	0	0	5	3
17	0	0	0	0	0	0	0	1
18	0	0	0	0	0	0	0	0
19	0	0	0	0	0	0	0	0
20	0	0	0	0	0	0	0	0
TOTAL	159	159	160	157	155	153	137	150

APPENDIX B

INTERNAL CALIBRATION OF THE RADIOMETER

In the transformation of satellite data from digital values to equivalent black-body temperatures, an "internal calibration" must be performed. The general function to be approximated in this procedure is shown in Figure B.1. This is an example of the response curve of radiation versus black body temperature for the scanning radiometer, generated before the satellite is launched.

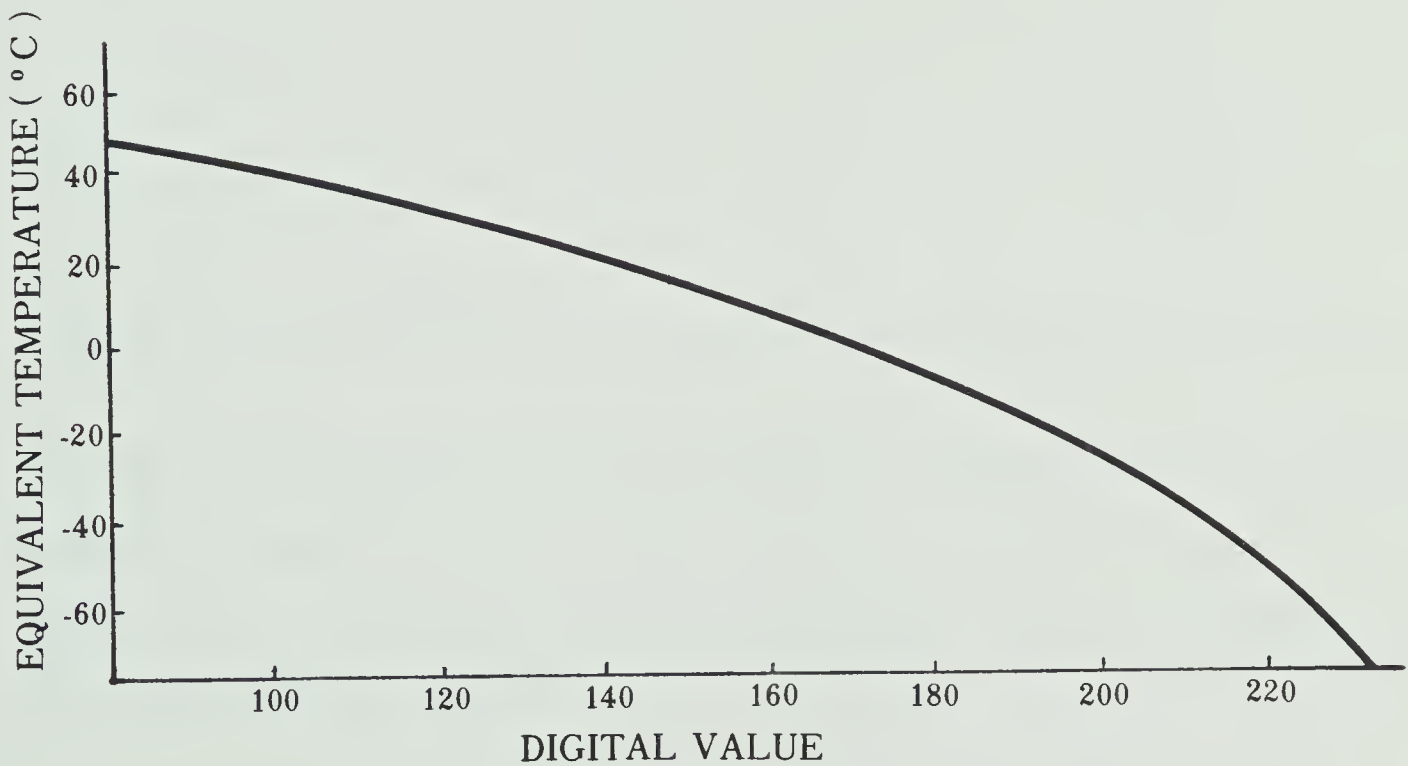


FIGURE B.1 IR response curve for Scanning Radiometer. (NOAA-4)

From the calibration pulses available in digital form in the scan data, a set of calibration points is extracted (Greaves, 1979). A sample of such points is shown in Table B.1. It remains, then, to evaluate the response curve at unknown points using the given set of data. Commonly, an interpolating polynomial is used.

TABLE B.1

Sample calibration points for NOAA-5, Orbit 9433.

Level	Digital Value	Equivalent Temperature (°C)
1	47.06	49.52
2	90.72	31.52
3	133.24	10.76
4	173.84	-15.24
5	212.92	-52.00
6	231.93	-86.00

The interpolating polynomial used here is the Newton form. If $T_n(X)$ denotes the temperature to be derived using a polynomial of degree n , X the particular digital value to be converted and the X_j the calibration point digital values, then

$$T_n(X) = \sum_{i=0}^n f[X_0, X_1, \dots, X_i] \prod_{j=0}^{i-1} (X - X_j) \quad (\text{B.1})$$

Here $f[X_0, X_1, \dots, X_i]$ is the n th "divided difference" of $T_n(X)$, such that

$$f[X_0, X_1, \dots, X_k] = \sum_{i=0}^n \frac{T_i(X)}{(X_i - X_0)(X_i - X_1) \dots (X_i - X_k)}, \quad i \neq k \quad (\text{B.2})$$

where $T_i(X)$ are the calibration point temperatures.

In practice one is uncertain as to how many calibration points to use. Using the Newton form of the interpolating polynomial, one may calculate $T_0(X)$, $T_1(X)$ and so on, increasing the number of points used until a satisfactory approximation to $T_n(X)$ has been made. In the region near 0°C , the response curve is seen to be quite flat; fewer calibration points would be needed here than in the region, say, near -60°C .

Use of the other interpolative polynomials (for example, the Lagrange form) may not make use of previously calculated $T_i(X)$ in calculating the final order of the polynomial. The Newton method allows one to study the effect of each point as it is added to the approximation to $T_n(X)$. The user is afforded the option of determining how much accuracy is necessary by choosing as many or as few points as desired.

In this research it has been found that, by ordering the calibration points with increasing distance from the digital value of interest, the nearest five points give a residual (size of sixth term), of less than $.25^\circ\text{C}$. Since integer temperature values are required, only the five nearest points are used in the interpolation scheme.

APPENDIX C

EXTERNAL CALIBRATION OF DATA

C.1 Limb-Darkening Correction

As discussed in Chapter II, data collected at large local zenith angles are subject to limb-darkening and are of very low resolution. Data near the viewing horizons may be eliminated from use in the analysis program by omitting all datons in the scan which fall outside local zenith angles of 65° . This value may seem arbitrary; however, it in fact defines the data contiguity point for successive orbits crossing the equator.

If the radiometer scan rate is 48 per minute, and the digitizing frequency is 2400 per second, then there are $8 \frac{1}{3}$ datons produced for each degree of scan by the radiometer

From Figure C.1,

$$\sin A = \frac{R (\sin 65^\circ)}{R + H} \quad (C.1)$$

Similarly,

$$\sin B = \frac{R}{R + H} \quad (C.2)$$

Thus, $(B - A) \cdot 8 \frac{1}{3}$ datons near each horizon are removed from the analysis procedure if the data used are restricted to zenith angles of 65° or less. This option is available in the program listed in Appendix A.

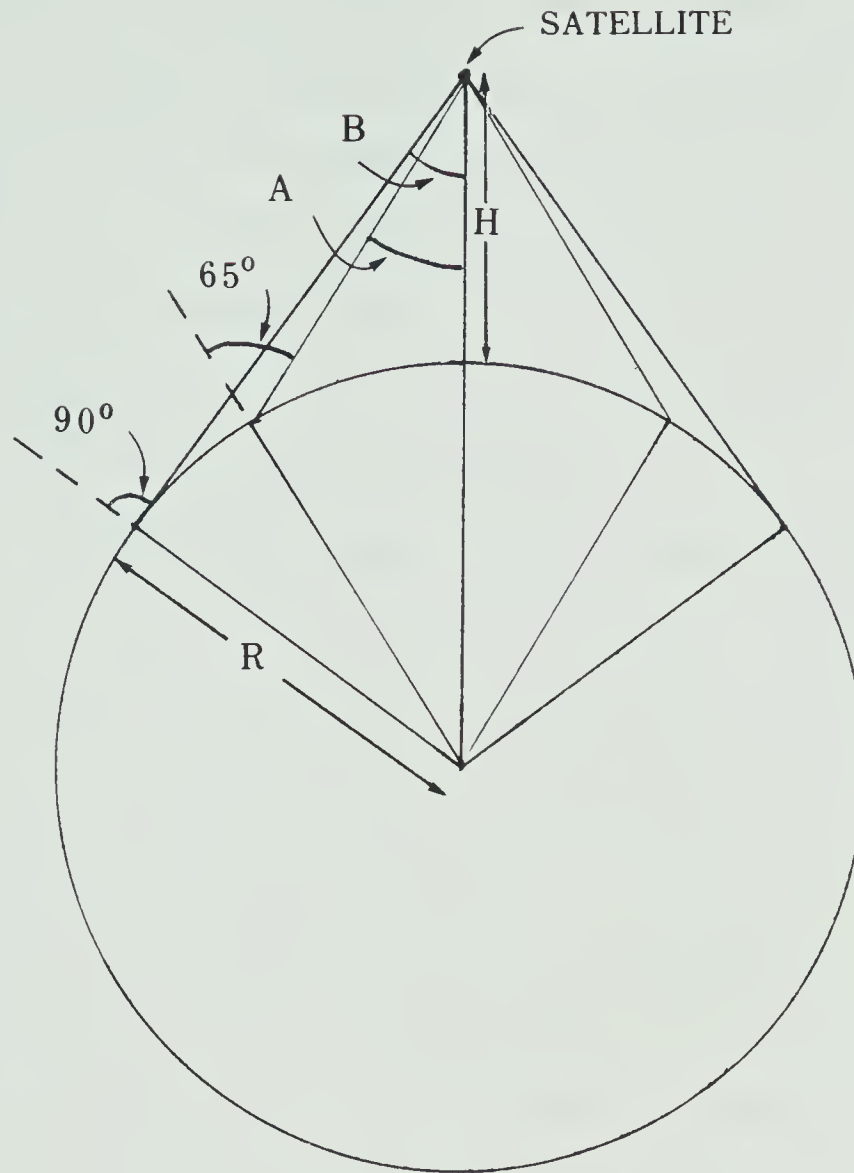


FIGURE C.1 Depiction of data zenith angle calculation.

C.2 Ground-truth Calibration

To correct for atmospheric effects, ground-truth temperature data may be employed as a comparison and correction to satellite-derived temperatures. If the position of the surface observation is known, its location in terms of satellite scan data may be computed using a point-by-point gridding procedure (Reinelt, et al., 1975).

Depending on the daton averaging scheme employed, all data comprising an area approximately one-half of one latitude degree square, centred at the surface observation location, are collected in histogram form. An array 7 scans wide and $((\text{NDAT} \cdot 2) + 1)$ averaged datons long is used, where

$$\text{NDAT} = 12 / (\text{NAVG} + 1), \quad (\text{C.3})$$

NAVG being the number of datons averaged.

For small zenith angles, Barnes (1972), points out that attenuation effects should be small for the scanning radiometer. With this in mind, a ten degree window, centred at the reported surface temperature (represented as a truncated integer), is used as the cut-off for acceptable entries in the above histogram. In this manner it is believed that mean and standard deviation calculations will suffer from a minimal amount of cloud contamination. If contamination is severe, few values are likely to fall inside the window, except in the case of cloud tops near the surface temperature. If less than ten entries are collected, no use of the surface data is made. Similarly, if the dispersion is too large the surface observation may be rejected.

To reduce bias errors, the mean value of all useable corrections is used as final attenuation correction.

APPENDIX D

SAMPLE OUTPUT FROM HISTOGRAM ANALYSIS PROGRAM

The square by square surface temperature values used in production of Figure 3.2a are for Orbit 4222, July 5, 1977, and listed below as a sample of the output from the histogram analysis program (which has not been included). Note that "99" is used to denote unacceptable surface temperatures.

TABLE D.1

Surface Temperature Retrievals, Low Resolution,
Orbit 4222, July 5, 1977.

STATISTICS FOR SURFACE TEMPERATURE RETREIVALS

TOTAL NUMBER OF PASSES USED = 1

LATITUDE	LONGITUDE (EAST)	POP.N	MODE (C)	MEAN (C)	STD.DEV (C)	SST (C)
69.0-70.0	216.0-218.0	64.	0.	-0.4	1.8	99.0
69.0-70.0	222.0-224.0	108.	-1.	-1.1	1.4	-1.1
69.0-70.0	224.0-226.0	111.	0.	0.3	1.2	0.3
69.0-70.0	226.0-228.0	113.	0.	-0.1	0.9	-0.1
69.0-70.0	228.0-230.0	116.	12.	12.7	1.7	99.0
69.0-70.0	230.0-232.0	120.	15.	15.7	1.6	99.0
69.0-70.0	232.0-234.0	120.	18.	16.8	1.2	16.8
69.0-70.0	234.0-236.0	125.	15.	15.4	1.7	99.0
69.0-70.0	236.0-238.0	120.	0.	1.0	1.4	1.0
69.0-70.0	238.0-240.0	128.	2.	1.7	1.3	1.7
70.0-71.0	216.0-219.0	127.	-3.	-3.2	1.4	-3.2
70.0-71.0	222.0-225.0	136.	-2.	-2.7	1.2	-2.7
70.0-71.0	225.0-228.0	157.	-2.	-1.8	1.1	-1.8
70.0-71.0	228.0-231.0	165.	0.	-0.7	1.0	-0.7
70.0-71.0	231.0-234.0	171.	0.	0.5	0.9	0.5
70.0-71.0	234.0-237.0	174.	0.	-0.4	0.8	-0.4
70.0-71.0	237.0-240.0	173.	0.	0.3	1.3	0.3
71.0-72.0	216.0-219.0	121.	-2.	-2.7	0.9	-2.7
71.0-72.0	219.0-222.0	100.	-3.	-3.8	1.4	-3.8
71.0-72.0	225.0-228.0	110.	-3.	-3.5	1.4	-3.5
71.0-72.0	228.0-231.0	147.	-2.	-2.2	1.1	-2.2
71.0-72.0	231.0-234.0	159.	0.	-0.2	0.7	-0.2
71.0-72.0	234.0-237.0	164.	0.	0.5	0.8	0.5
71.0-72.0	237.0-240.0	166.	15.	15.3	1.7	99.0
72.0-73.0	216.0-219.0	57.	-3.	-4.1	1.4	-4.1
72.0-73.0	225.0-228.0	75.	-3.	-4.2	1.4	-4.2
72.0-73.0	228.0-231.0	141.	-1.	-1.3	1.1	-1.3
72.0-73.0	231.0-234.0	146.	0.	0.5	0.7	0.5
72.0-73.0	234.0-237.0	153.	0.	0.7	0.9	0.7
72.0-73.0	237.0-240.0	159.	14.	14.4	1.7	99.0
73.0-74.0	216.0-219.0	102.	-2.	-2.5	1.0	-2.5
73.0-74.0	219.0-222.0	112.	-3.	-2.8	1.0	-2.8
73.0-74.0	222.0-225.0	117.	-3.	-2.9	1.0	-2.9
73.0-74.0	225.0-228.0	124.	-3.	-2.6	0.8	-2.6
73.0-74.0	228.0-231.0	129.	0.	-1.0	1.0	-1.0
73.0-74.0	231.0-234.0	137.	0.	0.6	0.9	0.6
73.0-74.0	234.0-237.0	143.	1.	0.9	0.9	0.9
73.0-74.0	237.0-240.0	141.	0.	0.6	1.5	0.6
74.0-75.0	216.0-219.0	96.	-2.	-2.4	1.0	-2.4
74.0-75.0	219.0-222.0	101.	-2.	-2.1	0.9	-2.1
74.0-75.0	222.0-225.0	107.	-2.	-2.2	0.7	-2.2
74.0-75.0	225.0-228.0	114.	-2.	-2.5	0.5	-2.5
74.0-75.0	228.0-231.0	118.	-2.	-2.0	0.8	-2.0
74.0-75.0	231.0-234.0	126.	0.	-0.7	0.9	-0.7
74.0-75.0	234.0-237.0	126.	0.	-0.1	0.9	-0.1
74.0-75.0	237.0-240.0	130.	-3.	-3.1	2.0	99.0

STATISTICAL RECOVERY OF 39 VALUES FROM 52 GRIDDED REGIONS
RECOVERY EFFICIENCY= 75.0 PER CENT FOR DAY 1
AVG. STD. DEVIATION = 1.15 DEG. C. (46. ACCEPTABLE AREAS)

APPENDIX E

ICE NOMENCLATURE

Some relevant ice characteristics that are observed and reported are described in this Appendix.

Sea-Ice: Any form of ice originating from the freezing of water.

First-Year Ice: Sea ice of not more than one winter's growth; thickness from .3 meters to 2 meters or more.

Old Ice: Sea ice which has survived at least one summer's melt. Most topographic features are smoother than on first-year ice. May be subdivided into second-year ice and multi-year ice.

Multi-Year Ice: Old ice up to 3 meters or more thick which has survived at least 2 summers. The ice is almost salt-free. Melt pattern consists of large interconnecting, irregular puddles and a well-developed drainage system.

Fast Ice: Sea ice which forms and remains fast along the coast.

Pack Ice: Term used to include, in a wide sense, any accumulation of sea ice other than fast ice, no matter what form it takes or how disposed.

Ice Cover: The ratio of any area of ice of any concentration to the total area of sea surface within some large geographic locale; this locale may be global, hemispheric, or prescribed by some specific geographic entity, such as the Beaufort Sea.

Concentration: The ratio in eighths or tenths of the sea surface actually covered by ice to the total area of sea-surface; both ice-covered and ice-free, at a specific location or over a defined area.

Compact Pack Ice: Pack ice in which the concentration is 10/10; no water is visible.

Consolidated Pack Ice: Pack ice in which the concentration is 10/10 and floes are frozen together.

Very Close Pack Ice: Pack ice in which the concentration is 9/10 to less than 10/10.

Close Pack Ice: Pack ice in which the ice concentration is 7/10 through 8/10 composed of floes mostly in contact.

Open Pack Ice: Pack ice in which the ice concentration is 4/10 through 6/10 with many leads, and the floes are generally not in contact with one another.

Very Open Pack Ice: Pack ice in which the ice concentration is 1/10 through 3/10 and water preponderates over ice.

Open Water: A large area of freely navigable water in which the sea ice is present in concentration less than 1/10.

Ice-Free: No sea ice present. There may be some ice of land origin.

Floe: Any relatively flat piece of sea ice 20 meters across or more. Floes are subdivided according to horizontal extent, with maximum size being 10 kilometers (5NM).

Ice Field: Area of pack ice consisting of any size of floes, which is greater than 10 kilometers (5NM) across.

Large Ice Field: An ice field over 20 kilometers (10NM) across.

Ice Edge: The demarcation at any given time between the open sea and sea ice of any kind, whether fast or drifting.

Belt: A large feature of pack ice arrangement, longer than it is wide; from 1 kilometer to more than 100 kilometers in width.

Bight: An extensive crescent-shaped indentation in the ice edge formed by wind or current.

Ice Boundary: The demarcation at any given time between fast ice and pack ice, or between areas of pack ice of different concentrations.

Concentration Boundary: A line approximating the transition between two areas of pack ice with distinctly different concentrations.

Puddle: An accumulation of melt water on the ice, mainly due to melting snow but in the more advanced stages also to the melting of ice. Initial stage consists of patches of melted snow.

Rotten Ice: Sea ice which has become honeycombed and which is in an advanced state of disintegration.

APPENDIX F

ICE INFORMATION OVERLAYS

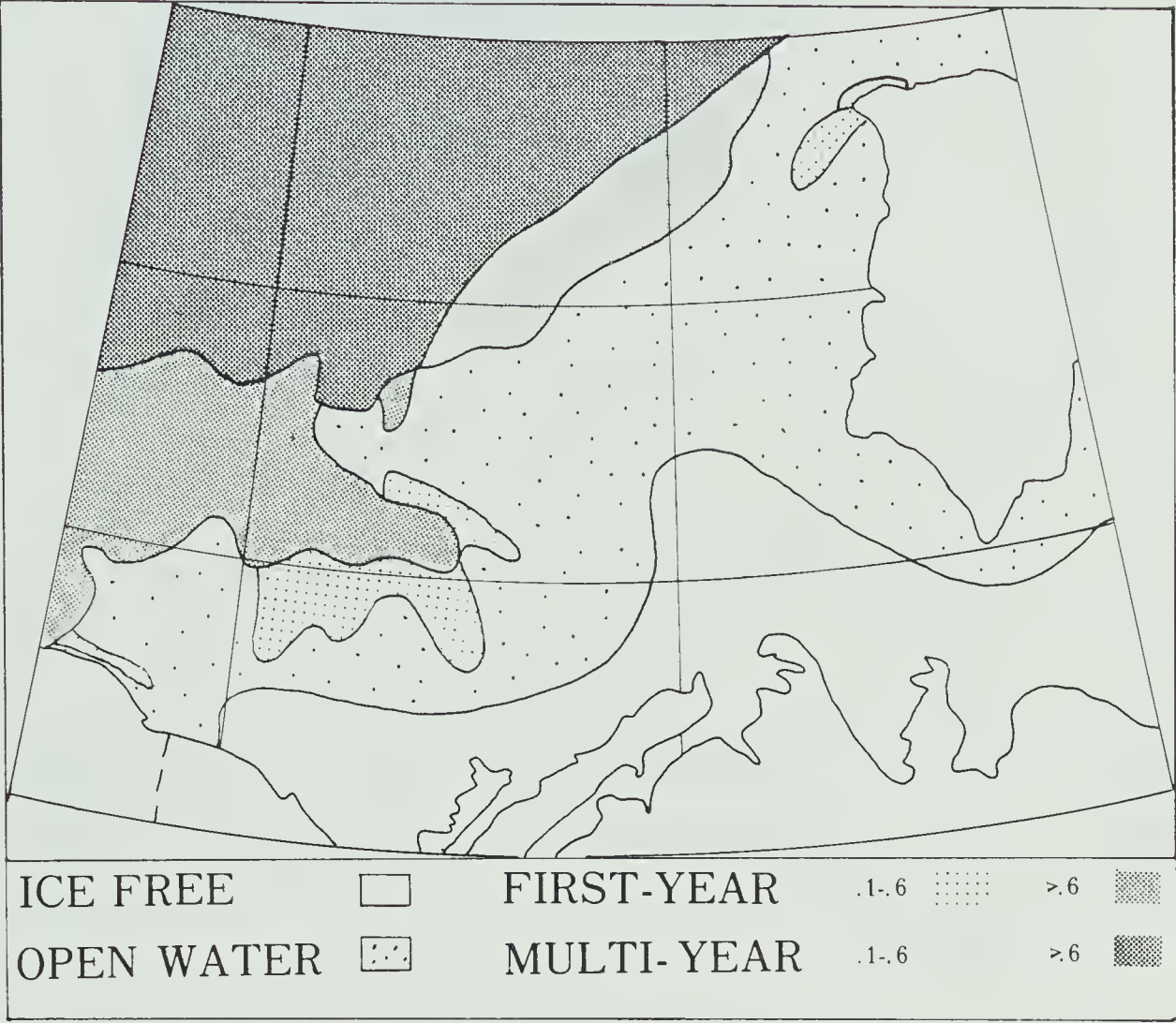


FIGURE F.1 Overlay 1: Mean ice conditions for week ending July 29, 1977.

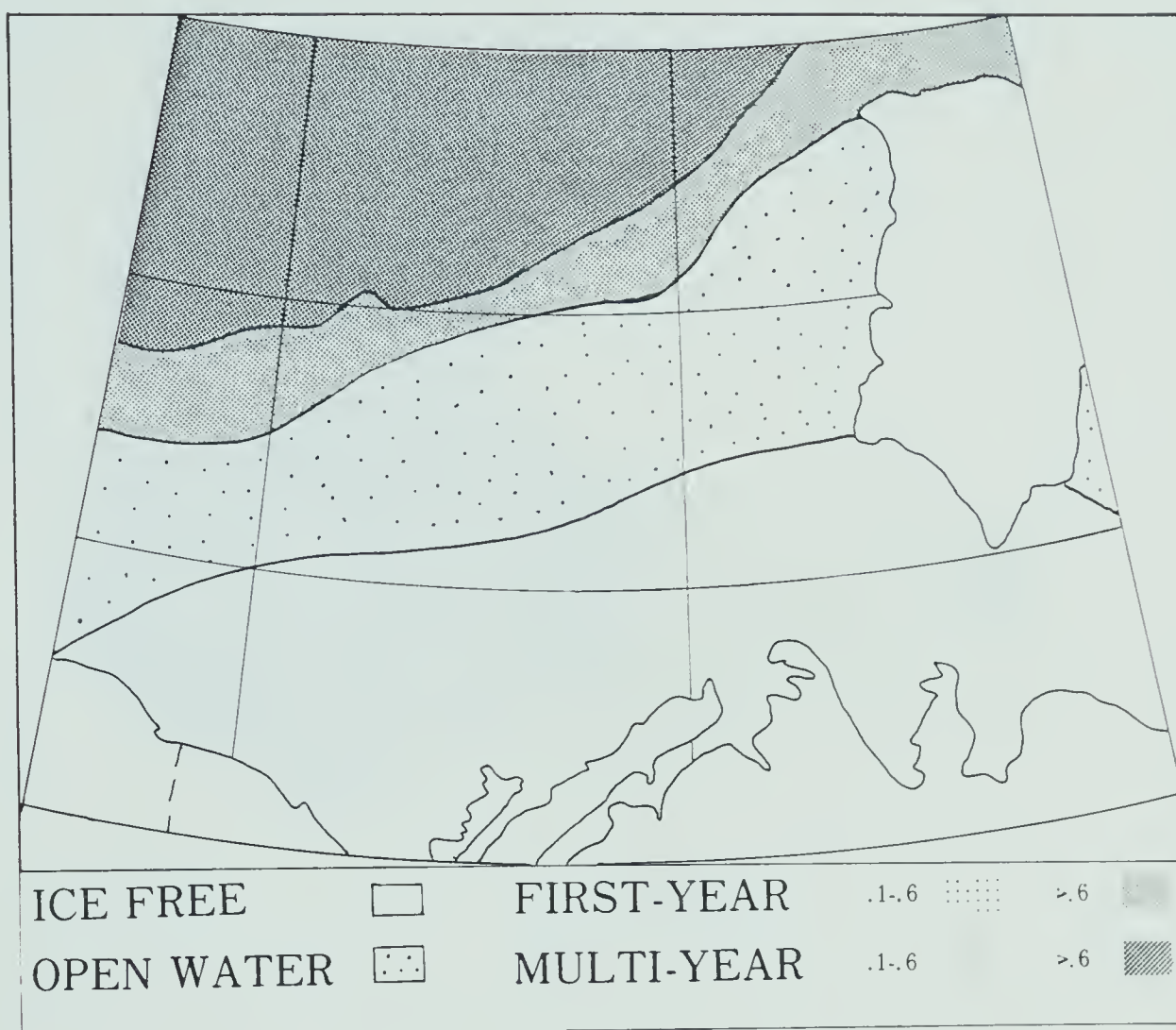


FIGURE F.2 Overlay 2: Mean ice conditions for week ending August 12, 1977.

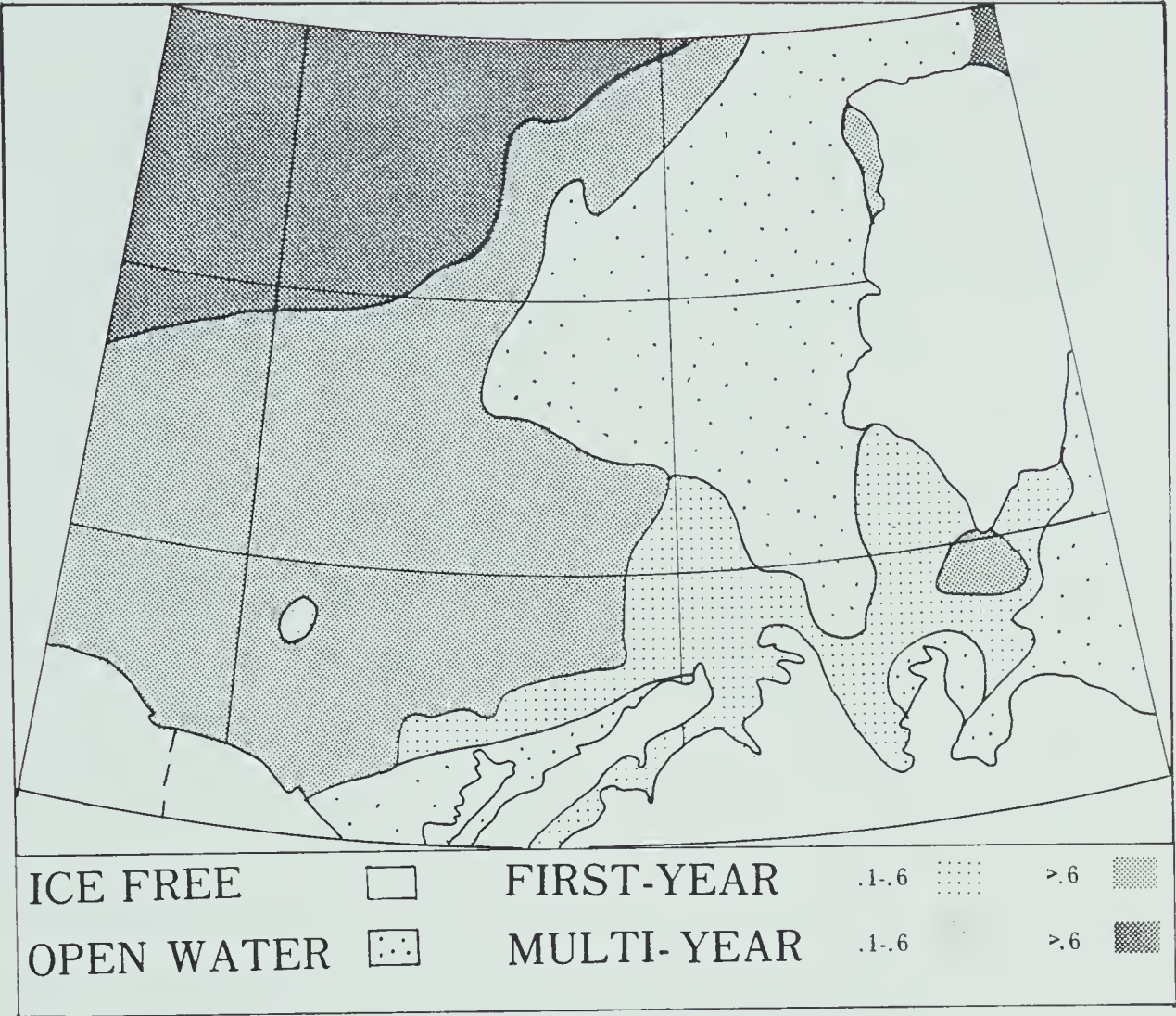


FIGURE F.3 Overlay 3: Mean ice conditions for week ending July 8, 1977.

B30248